UNIVERSITÀ DEGLI STUDI DELL'INSUBRIA
Ph.D. PROGRAM IN EXPERIMENTAL AND TRANSLATIONAL MEDICINE

Metabolic reprogrammed primary skin fibroblasts as patient specific cellular models for Parkinson's disease

Supervisor: **Prof. Tiziana Alberio**
Co-supervisor: **Dr. Marta Lualdi**

Thesis by: **Martina Brughera**
Matriculation number: **719737**
Cycle: XXXVII

Index

Abstract

Mitochondria are crucial organelles which undergo fusion and fission processes responsible for mitochondrial network rearrangements. Once mitochondria are damaged, they are selectively degraded by mitophagy. Collectively, these processes are referred to as mitochondrial dynamics, and dysregulations that hamper their function are often associated with neurodegenerative diseases like Parkinson's disease (PD). Mutations in mitophagy-related *PRKN* gene, which encodes the E3 ubiquitin ligase Parkin, have been linked to autosomal recessive juvenile PD. Recently, molecular players of the endosomal-lysosomal pathway such as Rab proteins, have been linked to the mitophagic pathway, indeed, mutations in *RAB32* and *RAB39B* have been identified to cause familial PD. In order to elucidate the interplay between Rab proteins and dysfunctional mitophagy in PD, we exploited PRKN-mutated and control human skin fibroblasts to evaluate levels and sub-cellular localization of a Rab protein subset. First of all, to make fibroblasts more sensitive to mitochondrial damages and metabolically more similar to neurons, we induced a metabolic reprogramming toward oxidative phosphorylation. The changes in CS and COX5B protein levels suggested that the protocol succeeded in the metabolic reprogramming of both control and *PRKN*-mutated fibroblasts. Moreover, we exploited mitochondrial toxins related to PD, Rotenone and 1-methyl-4-phenylpyridinium (MPP^+), to induce mitophagy. Both treatments induced mitochondrial depolarisation and alterations in mitochondrial marker levels, but MPP^+ was the selected toxin since it induced the higher mitochondrial depolarisation. Exploiting our final model, reprogrammed skin fibroblasts treated with a mitochondrial toxin, we evaluated the mitochondrial network morphology, the mitochondrial mass, and the Rab protein levels in PRKN-mutated fibroblasts. We observed increased RAB9 levels in *PRKN*-mutated fibroblasts especially after MPP^+ treatment. RAB9 is usually associated to alternative PINK1/Parkin-mediated mitophagy, thus hinting a role of Rab proteins in mitochondrial dynamics related to PD. In conclusion, this thesis established a set-up (metabolic reprogramming and MPP^+ treatment) that enables the use of skin fibroblasts as personalized cellular models to study mitochondrial dynamics related to PD. Furthermore, the preliminary study on Rab proteins involved in mitophagy revealed altered levels of these vesicular trafficking regulators in *PRKN*-mutated fibroblasts, particularly following mitophagy induction.

1. Introduction

1.1 Parkinson's disease

The second most common neurodegenerative disease worldwide is Parkinson's disease (PD). It is an age-related disorder characterised by aberrant proteostasis and mitochondrial dysfunction. The neuropathological hallmarks of PD are the abnormal accumulation and aggregation of α-synuclein (α-syn) in the form of Lewy bodies (LB) and the progressive loss of nigrostriatal dopaminergic neurons in the *pars compacta* of the *substantia nigra* in the midbrain (Poewe et al. 2017). PD is as a movement disorder, characterised by tremor, rigidity (stiffness), and slowness of movement. However, also non-motor symptoms are present, such as memory and thinking problems, sleep disorder, anxiety, and depression. The exact mechanisms underlying the pathological process are still to be clarified, however, PD cases can be broadly divided in genetic forms and sporadic forms.

For sporadic PD forms, also termed idiopathic, aging and environmental factors are the most common risk factors. In addition, genome-wide association studies (GWAS) identified independent gene risk variants, thus proposing a model where risk factors and genetic susceptibility interact together in the occurrence of PD (Singh and Muqit 2020)(A. H. Schapira 2004) (Fig. 1.1). Regarding the genetic forms, which represent the 5-10% of the total cases, 23 PD genes and loci have been identified and they can be classified into dominant genes, namely *SNCA* (α-synuclein), *LRRK2* (Leucine-rich repeat kinase 2, LRRK2) and *VPS35* (vacuolar protein–sorting-associated protein 35, VPS35), X-linked gene mutations in *RAB39B* (Rab39B) and autosomal recessive genes, including *PRKN* (Parkin), *PINK1* (PINK1), and *PARK7* (DJ-1) (Singh and Muqit 2020; Clark et al. 2021). A common feature of both sporadic and genetic forms is mitochondrial dysfunction. From the first studies describing parkinsonism-like symptoms consequent to the assumption of the toxin 1-methyl-4-phenyl-1,2,3,6-tetrahydropyridine (MPTP), a selective inhibitor of mitochondrial complex I, the link between PD and mitochondria was evident (J. W. Langston et al. 1983; Burns et al. 1985).

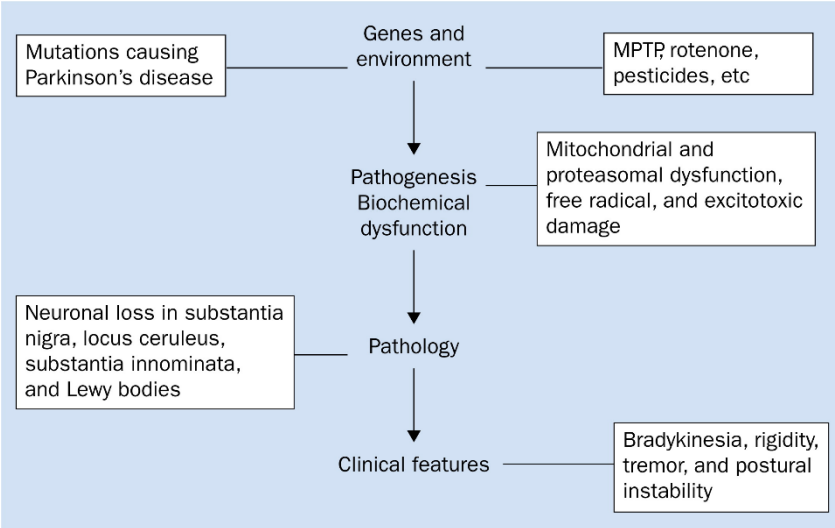

Figure 1.1. Aetiology and pathogenesis of PD (A. H. Schapira 2004).

Another mitochondrial complex I inhibitor used as a pesticide, Rotenone, has been linked to the pathology of PD (Heikkila, Hess, and Duvoisin 1984; Betarbet et al. 2000) and it is also commonly used to generate *in vivo* PD models.
For the genetic forms, *PRKN* and *PINK1* were the first genes found to be causative of recessive form of PD through linkage analysis (Matsumine et al. 1997; Hattori et al. 1998; Kitada et al. 1998; Bentivoglio et al. 2001; E. M. Valente et al. 2002). These two proteins are known to be involved in mitochondrial homeostasis through regulation of mitophagy, thus further supporting the pivotal role of mitochondria defects in PD pathology (Clark et al. 2021).
Other genes, not directly related to mitochondria, have been identified as causative of PD. RAB39B is a neuron enriched GTPase that was originally identified as a mutation locus for X-linked intellectual disability, but then also linked to early-onset PD (Wilson et al. 2014; Koss et al. 2021). The subcellular localization of RAB39B is predominantly within the Golgi apparatus, hinting a role in intracellular trafficking. In fact, Giannandrea and colleagues showed effects on vesicle trafficking and reduction in synapse formation in neuronal cell cultures knockdown for *RAB39B* (Giannandrea et al. 2010). Vesicular trafficking and mitophagy are two interconnected pathways. The first evidence describing a specific role for RAB proteins in mitophagy was the study in which RAB7 and its GTPase-activating protein (RAB7-GAP) TBC1D15 were implicated in the biogenesis of mito-autophagosomes (Yamano et al. 2014). Thus, PD pathology does not seem to be uniquely related to mitochondria, rather a combination of defective mitochondrial bioenergetics involving complex I activity, impaired mitophagy and dysregulation of vesicular trafficking.

1.2 Mitochondria

1.2.1 Structure

Mitochondria are small cytoplasmic organelles, 0.5–2 μm in size, that can be found as isolated entities or grouped in highly dynamic networks. The link with energy production and the "powerhouse of the cell" concept is limiting, since mitochondria have been proven to regulate many other functions such as autophagy, cell death, metabolism, inflammation, and cell differentiation. They are characterised by an outer mitochondrial membrane (OMM) and an inner mitochondrial membrane (IMM), the latter delimiting the mitochondrial matrix. The compartment in between of the IMM and the OMM is referred to as intermembrane space (IMS) (Fig. 1.2).

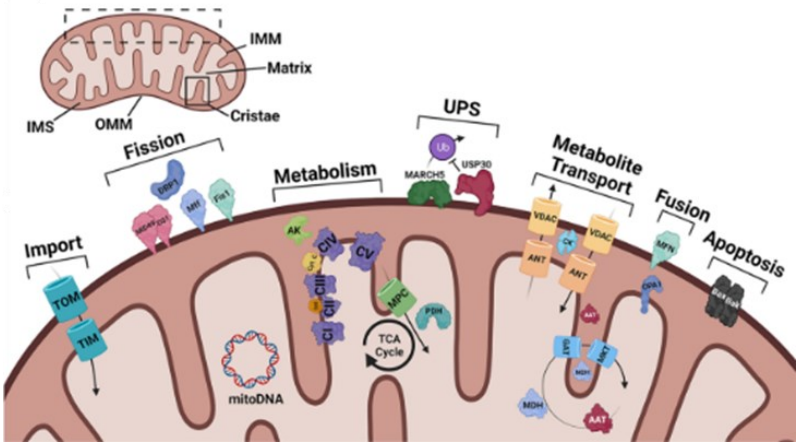

Figure 1.2. Schematic overview of mitochondrial structure and submitochondrial localization of major mitochondrial pathways. (Karbowski, Oshima, and Verhoeven 2022)

The two membranes differ in their biochemical composition and functions. The OMM allows mitochondria to communicate with the cellular environment. Due to its permeability, small molecules and ions are able to freely cross the membrane, while the flux of metabolic molecules like ATP/ADP and other respiratory substrates is regulated by the voltage-dependent anion channels (VDACs), gated porins that shift from an open, anion selective state to a closed conformation (Varughese, Buchanan, and Pitt 2021). Concerning proteins import, mitochondria rely on the translocator of the OMM (TOMM) complex, which represents the main entry gate for most mitochondrial proteins and sorts them to the correct compartment. Another complex located in the OMM is the sorting and assembly (SAM) complex, that is necessary for β-barrel membrane proteins insertion into the OMM and it is thus crucial for the assembly of the TOMM complex itself (Araiso, Imai, and Endo 2022).
The IMS is a highly reducing environment in which MIA40 is located, a complex involved in the import and folding of the cysteine-rich proteins. Once proteins are translocated in the IMS in their reduced form, MIA40 traps the substrate proteins to induce their oxidation promoting the subsequent folding. To complete the cycle, another component of the machinery, the sulfhydryl oxidase Erv1, allows MIA40 to return to the oxidized state (Hell 2008).
As for the IMM, one of the constitutive phospholipids is cardiolipin, which is synthetised within mitochondria. Its presence is confined in precise locations where its ability to form curved membrane regions is needed (Keenan, Watt, and Montgomery 2020). In fact, the IMM serves as anchor for the complexes of the electron transport chain (ETC) and to host as many complexes as possible it invaginates towards the matrix creating tubular structures called cristae (Fig. 1.3).
Mitochondrial cristae are dynamic compartments that are fundamental for mitochondria homeostasis hosting the complexes involved in the oxidative phosphorylation (OXPHOS) process. The positioning of ETC subunits is not accidental. For example, ATP synthase is usually restricted at the edge of cristae, while the other complexes are located along both sides. This pattern is helpful in the creation of proton gradient, whose flux is used to produce energy in the form of ATP. Electrons flow from the source complexes to the final acceptor, which is the molecular oxygen. Mitochondrial cristae are also involved in apoptosis. In fact, the release of cytochrome c, which is accumulated in the IMS, is allowed by the proapoptotic members of

the BCL-2 family which induce cristae junctions widening and cristae curvature remodelling (Cogliati, Enriquez, and Scorrano 2016a).

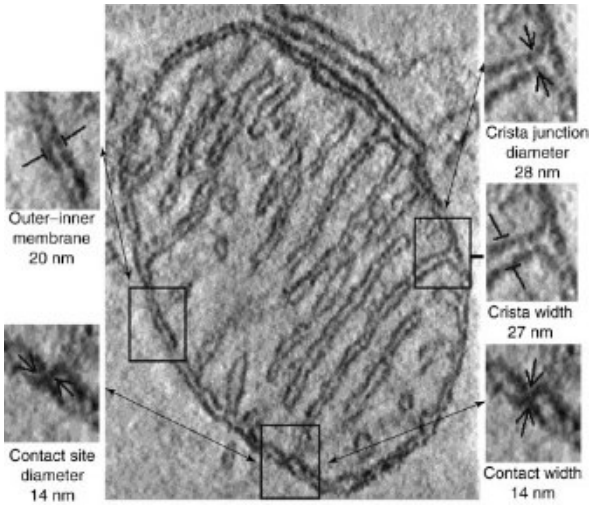

Figure 1.3. A single section through the 3D tomogram of the mitochondrion. (Frey and Mannella 2000)

1.2.2 Fusion and fission processes

Both OMM and IMM are also involved in other important processes which regulate mitochondrial dynamics, namely mitochondrial fusion and fission. These processes are central for the exchange of components among mitochondria and for the removal of dysfunctional parts from the network.

The key players that regulate fusion are Mitofusin 1 and 2 (MFN1 and 2) which reside on the outer membrane, and optic atrophy 1 (OPA1) that resides on the IMM. They are all GTPases; in fact, fusion of outer and subsequent inner membranes is driven by GTP hydrolysis which induce conformational changes that favour membrane tethering. For OMM fusion, an homotypic interaction between MFNs coming from the two fusing organelles is necessary, while for IMM fusion the interaction requires OPA1 coming from on organelle which then partners with cardiolipin on the opposing IMM (Liu and Chan 2017).

Regarding fission process, the OMM hosts fission 1 protein (Fis1), mitochondrial fission factor (Mff), mitochondrial dynamics protein of 49kDa (MiD49), and mitochondrial dynamics protein of 51kDa (MiD51), which recruit Drp1 allowing its oligomerization at the OMM constriction sites (Tokuyama and Yanagi 2023) (Samangouei et al. 2018). In PD pathology, beside impairment in mitophagy, dysfunctions in fusion and fission processes are also reported. Impairments in the balance between the two processes are generally the consequence, rather than the cause, of the pathological mechanism.

In primary skin fibroblasts from PD patients, fragmented mitochondrial network, decreased number of cristae, and reduced mitochondrial potential are observed (Exner et al. 2007). In neuroblastoma SH-SY5Y cells expressing PD-associated mutations of *PRKN* gene, it was described how impairments in Parkin-mediated ubiquitination negatively influence MFN1 degradation, cause hyperfusion and consequently hamper isolation of damaged mitochondria (Glauser et al. 2011). In *vivo* PD models using methyl-4-phenyl-1,2,3,6-tetrahydropyridine (MPTP) treatment to recapitulate complex I defect, showed an overall reduction in OPA1 protein levels, further confirmed by *in vitro* experiments in SH-SY5Y neuroblastoma cells,

where MPP^+-induced toxicity turns mitochondria into swollen organelles with poor cristae integrity (Ramonet et al. 2012). Alterations in PINK1 and Parkin are not the only causes for dysfunctional mitochondrial dynamics. Recent evidence suggests that mitochondria per se are not sufficient to initiate fusion or fission mechanism, rather they need the close proximity of endoplasmic reticulum (ER) to regulate both processes.

1.2.3 Mitochondria associated membranes (MAMs)

Besides being part of the mitochondrial network, mitochondria are also in physical and functional contact with other organelles inside the cell. Mitochondria-associated membranes (MAMs) are defined as the membranes which create physical contacts between mitochondria and the other organelles, namely ER, lysosome and endosome.
Mitochondria interaction sites with ER are also called mitochondria-ER contact sites (MERCS). These interactions have a key role in the regulation of many mitochondrial functions like fusion and fission processes, calcium buffering, mitochondrial biogenesis and mitophagy. In fact, MFN2 is present also on the ER membrane and it has been linked to regulation of mitochondrial Ca^{2+} uptake by the mitochondrial calcium uniporter (MCU), regulation of mitochondria-ER distance, besides being involved in mitochondrial fusion (de Brito and Scorrano 2008). The correct position between mitochondria and ER influences mitochondrial dynamics but also the correct disposal of damaged mitochondria.

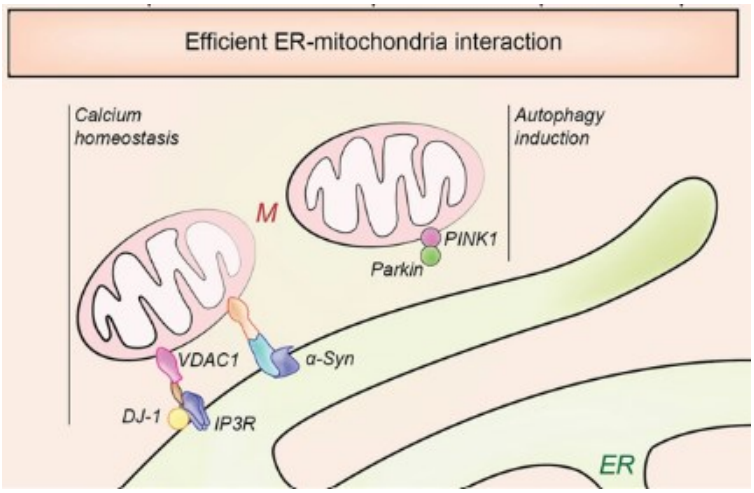

Figure 1.4. Modulators of ER–mitochondria associations. (Adapted from Gómez-Suaga et al. 2018)

The mitochondria-ER MAMs represent a crucial hub for pro-autophagic proteins and initiation site for autophagosome formation (Gómez-Suaga et al. 2018) (Fig. 1.4). Contact sites between ER and defective mitochondria mark also the region of Parkin-mediated mitophagy initiation (Gómez-Suaga et al. 2018), as this is confirmed also by an *in vitro* study where CCCP-treated cells displayed preferential ubiquitination where ER and impaired mitochondria overlapped (Yang and Yang 2013). In fact, in primary skin fibroblasts from PD patients with *PRKN* mutations, the proximity between ER-mitochondria is exacerbated with a consequent increased Ca^{2+} transfer from ER to mitochondria leading to cytotoxicity (Gautier et al. 2016).

Another crucial interaction is the mitochondria-lysosome contact sites, where both organelles benefit from a bidirectional regulation based on the modulation of their function, dynamics and metabolite transfer. Mitochondria linked to lysosomes are not targeted to mitophagy, since they are negative for autophagosome engulfment signals. Moreover, absence of autophagic receptors do not prevent the formation of these contact sites (Cisneros et al. 2022). Indeed, the main regulator of mitochondria-lysosome contact sites is RAB7, a small GTPase protein, whose switching between GTP-bound and GDP-bound state promotes contact formation and membrane untethering, respectively (Wong, Ysselstein, and Krainc 2018).

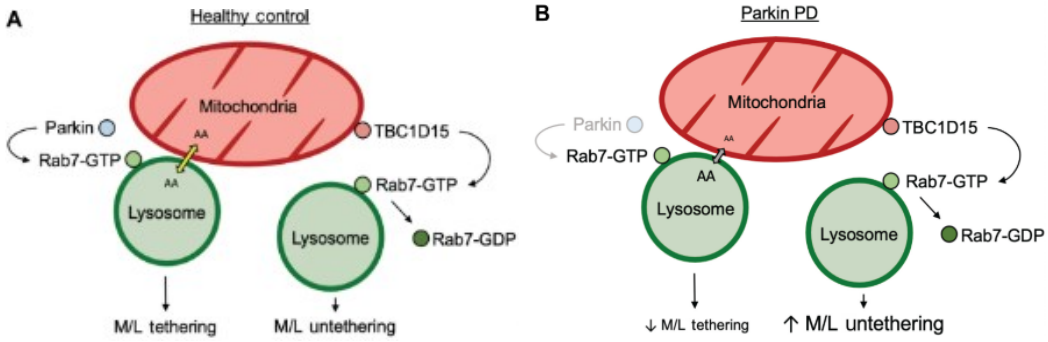

Figure 1.5. Parkin promotes mitochondria-lysosome tethering. (Peng et al. 2023)

Mitochondria-lysosome contact sites also influence Drp1 GTPase activity, thus regulating mitochondrial fission. Interestingly, in PD pathology the interaction between mitochondria and lysosome is compromised: in human iPSCs derived from a PD patient, the loss of Parkin has been demonstrated to disrupt mitochondria-lysosome contact sites due to the hampered ubiquitin-mediated RAB7 lysosomal targeting (Peng et al. 2023) (Fig. 1.5).

1.2.4 Bioenergetics

Cellular respiration is used for the generation of ATP and metabolites for survival and growth. Metabolic pathways related to energy production are: glycolysis, the Krebs cycle, and oxidative phosphorylation (OXPHOS). Glycolysis occurs in the cytosol and starting from glucose the final products are pyruvate, ATP and NADH. The Krebs cycle (also called tricarboxylic acid (TCA) cycle) takes place in the mitochondrial matrix and it generates additional ATP and NADH molecules. In the IMM, ETC complexes act as a series of electron donors and acceptors. NADH and $FADH_2$ are oxidised, and electrons move from electron donors to acceptors at higher redox potential. This process of electrons transport continues until electrons are transferred to oxygen, the final acceptor, which is reduced to water. The energy produced in each reaction is used to generate a proton gradient across the IMM by "pumping" protons into the IMS. This difference electrochemical gradient, through proton motive force, moves the protons back to the mitochondrial matrix, releasing energy that is used by ATP synthase to synthetise ATP.

In terms of energy production, glycolysis can be divided in two phases: an investment phase, that includes the first five enzymes of the pathway, and a payoff phase, that describes the last five reactions. From one molecule of glucose, it is produced two molecules of pyruvate and four of ATP. The following reactions related to OXPHOS occur in the mitochondria.

In order to begin, pyruvate has to be transported to the mitochondria where the pyruvate dehydrogenase complex (PDC) drives the conversion of pyruvate to acetyl-CoA and CO_2. The first reaction regards the formation of citrate from oxaloacetate and acetyl-CoA, which is then converted to isocitrate by aconitase. The production of the first NADH occurs in the next step, where isocitrate is oxidised by isocitrate dehydrogenase to alpha-ketoglutarate, the second NADH is generated during the conversion of alpha-ketoglutarate to succinyl-CoA. The enzyme succinate thiokinase catalyses the interconversion of succinyl-CoA to succinate with the concomitant production of ATP. The following enzyme, succinate dehydrogenase, is also part of the ETC and drive the oxidation of succinate to fumarate generating $FADH_2$. Fumarate hydratase catalyses the hydration to malate which is finally oxidised to oxaloacetate by malate dehydrogenase with the production of NADH.
The ETC resides on the IMM, and it is composed of four transmembrane complexes (CI, CII, CIII, CIV) which are located in the flat area of cristae, and they can also assembly into higher-order structures called supercomplexes. The fifth component, ATP synthase (CV) organise itself in dimers which are responsible for the curved shape of cristae edges (Fig. 1.6).

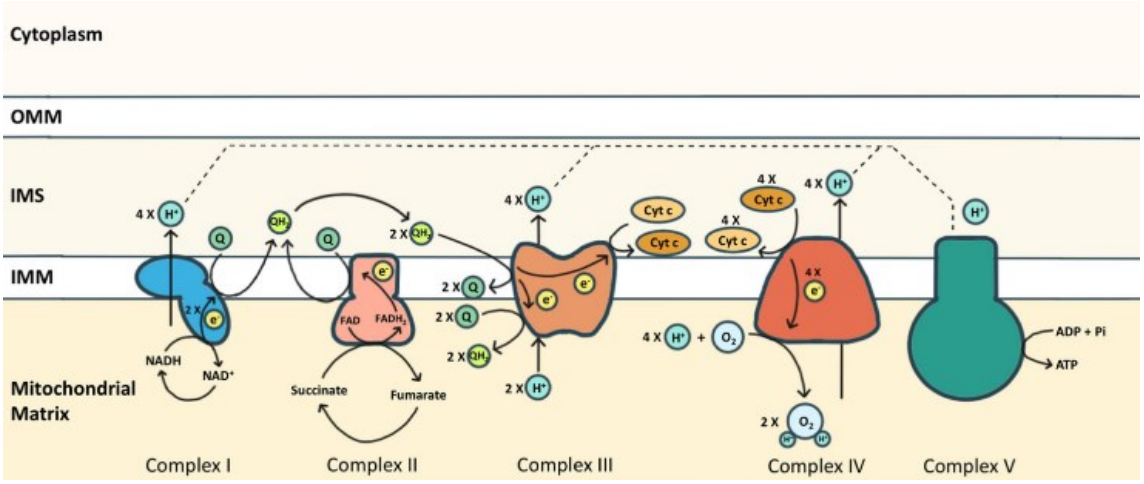

Fig. 1.6. The electron transport chain (ETC). (J.-L. Li et al. 2021)

Complex I (CI), or NADH-ubiquinone oxidoreductase, is the largest ETC complex, transferring electrons from NADH to ubiquinone. CI comprises three modules: the N- and Q-modules in the matrix handle NADH oxidation and electron transfer, while the P-module in the membrane pumps protons. CI has 14 core and 31 supernumerary subunits, with mitochondrial DNA encoding 7 matrix domain subunits. Complex II (CII), succinate dehydrogenase, links the TCA cycle to the ETC by oxidizing succinate to fumarate and transferring electrons to ubiquinone via FAD and Fe-S clusters. Complex III (CIII), cytochrome c reductase, oxidizes ubiquinol, reducing cytochrome c via the Q cycle, translocating protons to create a gradient. Complex IV (CIV), cytochrome c oxidase, oxidizes cytochrome c and reduces O_2 to H_2O, with 13 subunits and four redox centers contributing to proton translocation. Finally, Complex V, ATP synthase, consists of the F_0 domain in the IMM and the F_1 domain in the matrix. Proton flux through F_0 drives ADP phosphorylation by F_1, and ATP synthase oligomers help stabilize the IMM to enhance ATP production efficiency.

1.2.5 Mitochondrial Toxins related to PD

Alterations in the fine tuning of mitochondrial bioenergetics and mitochondrial dynamics negatively impact on cells functioning, especially on neurons which are characterised by a high energetic demand. In fact, dysfunctional mitochondrial dynamics have been widely associated to neurodegenerative diseases, like Parkinson's disease (PD). The first association between mitochondrial dysfunction and PD pathology goes back to the '80s, when a drug-user was diagnosed with schizophrenia but also showed parkinsonism (J. William Langston et al. 1983). The substance of abuse was 1-methyl-4-phenyl-1,2,3,6-tetrahydropyridine (MPTP) which is a lipophilic molecule able to cross the membranes, thus also the blood brain barrier (BBB). At the cellular level, monoamine oxidase B (MAO-B) catalyses the oxidation of MPTP to 1-methyl-4-phenylpyridinium (MPP^+) known to be a blocker of complex I (Chiba et al. 1985; Przedborski et al. 2004; J. William Langston 2017).

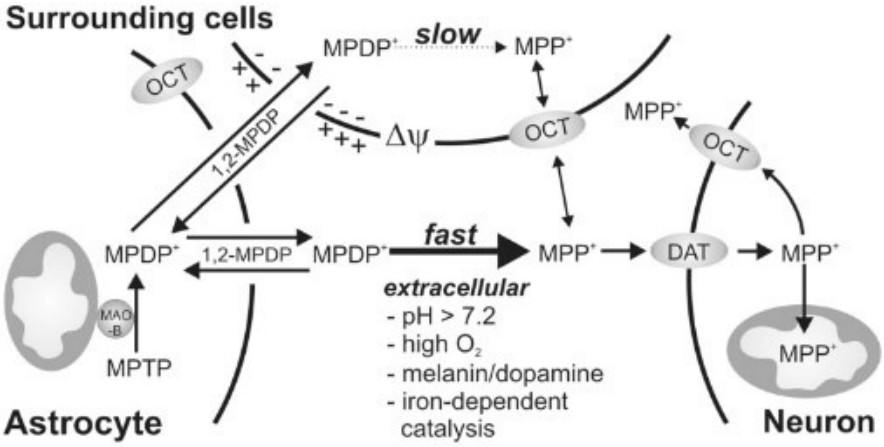

Figure 1.7. $MPDP^+$/1,2-MPDP is the main exported form of MPTP metabolites. (Schildknecht et al. 2015)

MPP^+ was discovered to be processed mostly in astrocytes, released in the extracellular space, and then uptaken with a higher affinity by dopamine transporter (DAT) causing the specific loss of nigrostriatal neurons (Heikkila, Hess, and Duvoisin 1984; Bezard et al. 1999; Watanabe, Himeda, and Araki 2005). More precisely, $MPDP^+$ is a membrane-crossing intermediate generated from MPTP by MAO-B in astrocytes. Once in the extracellular space, it is oxidised into MPP^+ that enters dopaminergic neurons via DAT-dependent uptake at high concentration (Schildknecht et al. 2015) (Fig. 1.7). Another transporter involved in the uptake of MPP^+ is the organic cation transporter 3 (OCT3) that is a bidirectional transporter highly expressed in the nigrostriatal dopaminergic pathway (Rappold et al. 2011). MPP^+ is a known substrate also for norepinephrine transporter (NET), and serotonin transporter (SERT) (Karpowicz et al. 2013).
The proposed mechanism of action implies the blockade of the electron transfer by binding to the complex I in the proximity of its quinone binding site, eventually lowering the ATP production (Ramsay et al. 1986; Banerjee et al. 2009).
Another molecule that exerts a similar effect is Rotenone. Rotenone is a natural compound widely used as a pesticide. It is a lipophilic molecule, which easily diffuses through cell membranes also crossing the BBB. The principal mechanism of action is the blockade of the oxidation of NADH to NAD (Rossetti, Stoker, and Ramos 2020). The implication of Rotenone with PD pathology was first described by Heikkila and colleagues (Heikkila et al. 1985) who

after stereotaxic administration of Rotenone observed damages to the dopaminergic nigrostriatal pathway in rats brain. Betarbet and colleagues (Betarbet et al. 2000) were then the first to exploit this toxin in order to provide an animal model of idiopathic PD.
Another mitochondrial toxin used to induce mitochondrial dysfunction is carbonyl cyanide m-chlorophenyl hydrazone (CCCP) (Zilocchi et al. 2018) (Hirata and Nagatsu 2005). CCCP is a lipophilic protonophore widely used to challenge mitochondrial function since it dissipates the proton motive force (Heytler and Prichard 1962) (Childress et al. 2018). The use of CCCP triggers PINK1/Parkin-mediated mitophagy thus providing a useful tool to assess several molecular aspects of PD pathology (Wang et al. 2023) (Ashrafi and Schwarz 2013).

1.2.6 Mitochondrial adaptation response to stressors

Mitochondrial nuclear communication is at the basis of the correct cellular function and feedback responses can be bidirectional. Being mitochondria the fine regulators of key cellular processes like redox homeostasis, energy production, calcium buffering and cell death through apoptosis, a prompt exchange of information is necessary both in a physiological situation and to develop a stress adaption response. Mitochondria and the ETC represent the major source of ROS in the cell. The main complexes responsible for ROS production are CI and CIII and the main byproduct produced is anion superoxide, whose level, if not maintained under control, can contribute to mito-inflammation (Hernansanz-Agustín and Enríquez 2021). In fact, mitochondria can be targeted by the same oxidative stress creating a reinforcement mechanism: mtDNA located in the matrix can easily undergo mutations, and IMM phospholipids peroxidation, with a consequent alteration in membrane fluidity and permeability, can in turn exacerbate ROS production.
The first line of action, the one against superoxide, is composed of superoxide dismutase (SOD) enzymes, which can convert superoxide to hydrogen peroxide (H_2O_2). H_2O_2 is less reactive but equally dangerous. Antioxidant enzymes like catalase (CAT), glutathione peroxidase (GPx) and antioxidant molecules, namely glutathione and ubiquinone are the principal component of this second line of defence (Napolitano, Fasciolo, and Venditti 2021) (Kowalczyk et al. 2021).
Besides ETC-derived oxidative stress, mitochondria can be challenged by other stressful conditions. There are several kinds of stressors, both endogenous and exogenous, that can impact cellular physiology thus triggering mitochondria to accomplish protective mechanisms. The most common challenges are represented by thermal stress, nutrient starvation and metabolic stress induced by a switch in the carbon source.
Hyperthermia and hypothermia can alter cellular homeostasis and they have also been linked to mitochondrial dysfunction. In case of prolonged stress, in which the adaption response is not able to restore physiological conditions, pathways like mitophagy and autophagy can occur. Bonello and colleagues developed a new model for studying Parkin-dependent mitophagy in human fibroblasts (Bonello et al. 2019) that exploit hypothermia to induce mitophagy without using the most common toxins like the protonophore CCCP.
Nutrients starvation is another stressful condition that mitochondria can face. Imbalance in the energy production, serum starvation and switch in the carbon source from which generate ATP represent the most common conditions mitochondria must challenge. When the production of energy is hampered, there is a raise in cellular cAMP level, which activates protein kinase A

(PKA). As an adaptive response, phosphorylation of DRP1 by PKA inhibit mitochondrial fission, thus preserving mitochondria from autophagic degradation (Rambold et al. 2011; Gomes, Di Benedetto, and Scorrano 2011). Serum starvation also deeply impacts on mitochondrial enzymes activity. As an example, this condition has been linked to up-regulation of succinate dehydrogenase activity thus contributing to an increased ROS production till the consequent cytochrome c release and caspase-9 activation, which lead to apoptotic cell death (Moon 2008).

AMP-activated protein kinase (AMPK) is another key player enzyme in metabolic adaptation during glucose shortage. In case of early starvation, glutamine is the preferable alternative carbon source, and AMPK is activated in order to phosphorylate glutaminase 1 (GLS1), a rate-limiting enzyme of glutaminolysis. Moreover, it has been seen that phosphorylation of PDZD8 is needed to increase mitochondria-ER contact sites required to regulate glutaminolysis (M. Li et al. 2024). Mitochondrial biogenesis can be another response to metabolic stress. Being AMPK a direct activator of proliferator-activated receptor-gamma coactivator-1α (PGC-1α), the downstream effects are the activation of mitochondrial biogenesis and the increased production of antioxidant proteins (Marcinko and Steinberg 2014; Rakshe et al. 2024). Alongside, the PGC-1α-mediated activation of transcription factors increases the expression of the nuclear-encoded mitochondrial transcription factor A (TFAM) which promotes an increase in replication and expression of mtDNA (Picca and Lezza 2015).

Mitochondrial response to metabolic switch can be also exploited to challenge mitochondria and study mitochondrial dysfunction related to pathological conditions. It is well known that cells like neurons in order to fulfil their energy demands rely on OXPHOS and thus, mitochondrial defects are at the basis of many neurodegenerative diseases like PD (Flønes et al. 2024; Subrahmanian and LaVoie 2021a; Marella et al. 2009; González-Rodríguez et al. 2021). By contrast, other cell types, such as fibroblasts, are not so strictly dependent on OXPHOS for energy production, being in turn less sensitive to mitochondrial insults.

One way to challenge cells and force them to rely on OXPHOS metabolism is to change the carbon source.

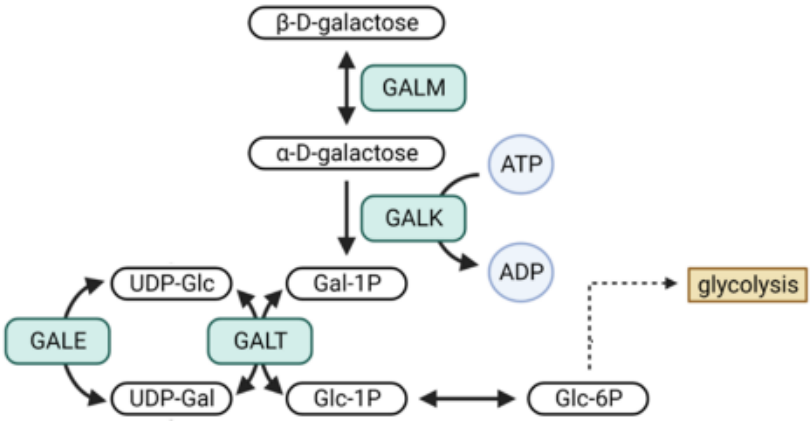

Figure 1.8. Leloir pathway. (Homolak et al. 2024).

Galactose is a monosaccharide sugar with both D- and L- forms, and only D-galactose can be metabolized by the human body. During glycolysis, the first step is the conversion of glucose to glucose-6-phosphate (G6P) by hexokinase using one molecule of ATP, whereas starting from

galactose, the conversion to G6P requires more steps. The Leloir pathway consists of a sequence of four enzymatic steps: i) galactose mutarotase (GalM) promotes the conversion of β-d-galactose to α-d-galactose, ii) galactokinase (GalK) phosphorylates α-d-galactose in galactose-1P, iii) the galactose-1-phosphate uridyltransferase (GalT) converts galactose-1P to glucose-1P, and iv) UDP-galactose 4′-epimerase (GalE), whose direction is influenced by substrate levels and biochemical demands of a tissue, mediates the interconversion of UDP-galactose and UDP-glucose (Conte et al. 2021) (Fig. 1.8). Since the conversion from galactose to G6P requires time and energy, the OXPHOS metabolism is preferred compared with the glycolytic one (Fos-Codoner et al. 2023; Reitzer, Wice, and Kennell 1979).
Many *in vitro* studies have reported that, after the administration of galactose, the adaptive response to cope with the new energy source was to increment the OXPHOS activity. This was correlated to an increase in the activity and the number of the ETC complexes, by an increase in the oxygen consumption rate (OCR) that reflects the active status of the ETC, and by an increased level of AMPK phosphorylation (Aguer et al. 2011; Homolak et al. 2024; Fos-Codoner et al. 2023; Rossignol et al. 2004). Exploiting this forced metabolic switch, cell lines maintained in galactose medium have been used in order to enhance mitochondrial liabilities (Aguer et al. 2011; Dott et al. 2014; Orlicka-Płocka et al. 2020) representing a good tool to study mitochondria-related pathologies like PD (Amo et al. 2011; González-Casacuberta et al. 2019; Payne et al. 2024; Deus et al. 2020a).
Despite all the adaptive responses put in place by mitochondria, when the damages or alterations are beyond a certain threshold, dysfunctional mitochondria must be removed through mitophagy.

1.2.7 Mitophagy

Dysfunctional mitochondria which must be disposed undergo mitophagy, a specific macroautophagy pathway, which selectively conveys mitochondria to lysosomes for degradation. Mitophagy is thus fundamental for the correct maintenance of the mitochondrial network. Mitophagy regulatory pathways are classified into two main mechanisms, according to how dysfunctional mitochondria are targeted and removed: i) ubiquitin-dependent mitophagy, and ii) receptor-mediated mitophagy. The canonical ubiquitin-dependent mitophagy involves the Serine/threonine PTEN-induced putative kinase 1 (PINK1) and the E3 ubiquitin ligase Parkin proteins. PINK1 and Parkin are responsible for the recruitment of the autophagosome molecular machinery and the consequent fusion with lysosomes (K. Ma et al. 2020; Wang et al. 2023).
Under physiological conditions, PINK1 is imported in the mitochondria owing to its N-terminal mitochondrial targeting sequence (MTS). In functional mitochondria, PINK1 is then sequentially processed and cleaved by the mitochondrial processing peptidase (MPP) and the presenilin-associated rhomboid-like (PARL) protease. The truncated form of PINK1 is then retro-translocated to the cytosol and rapidly degraded by the ubiquitin–proteasome system (Palikaras, Lionaki, and Tavernarakis 2018).

When mitochondria are depolarised, PINK1 translocation inside mitochondria is inhibited by the adenine nucleotide translocator (ANT) complex. In this way, PARL-dependent cleavage is prevented and PINK1 accumulates on the OMM. The TOMM complex helps PINK1 to stabilize itself so that it can auto-phosphorylate specific residues that regulate kinase activity against Parkin (Okatsu et al. 2012; Raimi et al. 2024). (Fig. 1.9)

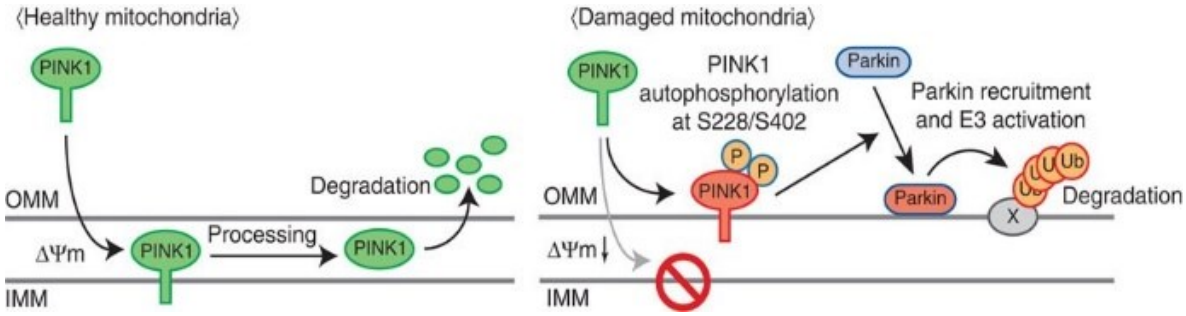

Figure 1.9. A model for Parkin recruitment to the damaged mitochondria. (Okatsu et al. 2012)

In fact, once PINK1 is activated, phosphorylation of Ser 65 in both the Parkin ubiquitin-like domain and in ubiquitin itself removes Parkin autoinhibition. Subsequently, Parkin forms an ubiquitin–thioester bond at Cys431 thus promoting OMM protein targets ubiquitination on dysfunctional mitochondria (Koyano and Matsuda 2015) (Fig. 1.10). This feed-forward mechanism mediated by Parkin ubiquitination accumulates poly-Ub chains on specific lysine residues of VDACs, MFN1, MFN2 and others OMM proteins, which are further phosphorylated by PINK1 thus amplifying the "eat me" signals (Seirafi, Kozlov, and Gehring 2015).

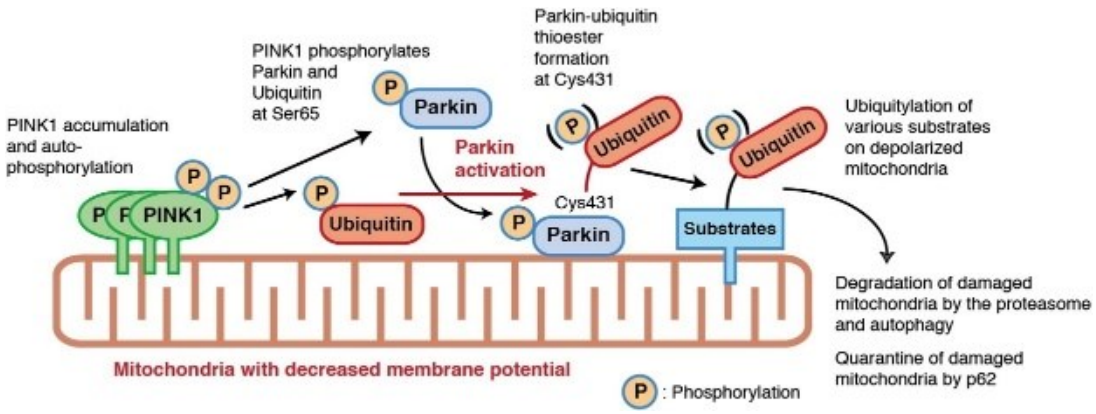

Figure 1.10. Model for the function of PINK1/Parkin/ubiquitin during mitochondrial quality control. (Koyano and Matsuda 2015)

After the amplification of the ubiquitination step, cargo adaptors are recruited onto the OMM, namely sequestosome 1 (P62/SQSTM1), nuclear dot protein 52 (NDP52/CALCOCO2), neighbour of BRCA1 gene 1 (NBR1), and optineurin (OPTN). These autophagic adapters are in charge of the engulfment of damaged mitochondria within autophagosomes, since they act as linker between the ubiquitinated cargoes and the autophagosomal membranes, owing an

LC3 interacting region (LIR) that interacts with ATG8 family proteins (Palikaras, Lionaki, and Tavernarakis 2018; Shafique et al. 2023) (Fig. 1.11)

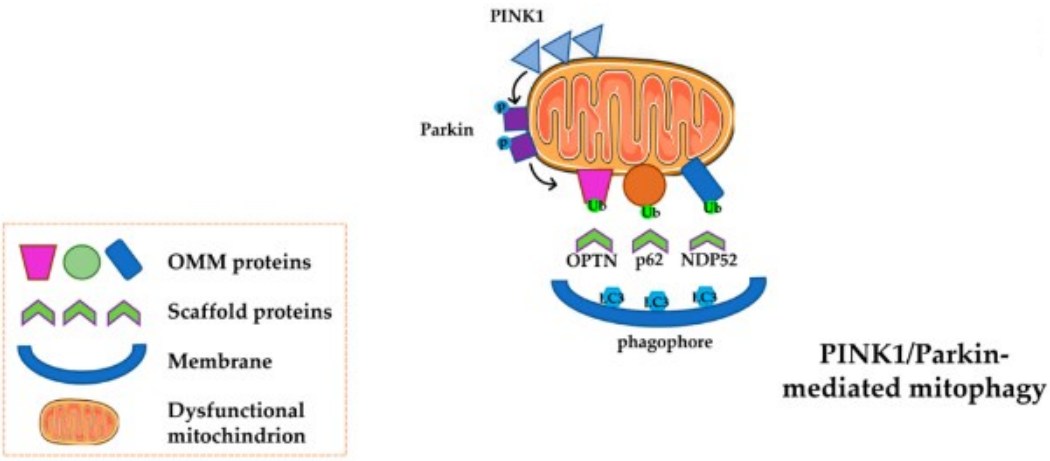

Figure 1.11. Mitochondrial dynamics defects in neurodegenerative diseases. Adapted from (Shafique et al. 2023)

After dysfunctional mitochondria recognition, the autophagic cascade proceed as it follows: ULK1 kinase regulates autophagy induction and promotes membranes formation on cargoes, class III phosphatidylinositol 3-kinase (PI3K) complexes orchestrate autophagosome nucleation, and finally phosphorylation of sequential autophagy-related (ATG) proteins is responsible for the expansion and maturation of the autophagosome and final lysosomal targeting.

Defects in the PINK1/Parkin mitophagic pathway have been associated to PD pathology. Starting from the late 1990s, several studies have linked mutations in the *PRKN* (Parkin) and *PINK1* genes to PD pathogenesis (Kitada et al. 1998; Matsumine et al. 1997; Shimura et al. 2000; Hattori et al. 1998; E. M. Valente et al. 2002; Bentivoglio et al. 2001; E. M. Valente et al. 2002). Fibroblasts derived from early-onset PD patients carrying mutations in *PRKN* gene have shown depolarized mitochondria without PINK1 accumulation resulting in a hampered mitophagy induction (Zilocchi et al. 2020). SH-SY5Y neuroblastoma cells, widely used to obtain a cellular model of altered dopamine homeostasis that recapitulates early stages of PD pathology(Xicoy, Wieringa, and Martens 2017a), display an hyperfused mitochondrial network and no recruitment of PINK1 at depolarized mitochondria, thus impairing their removal (Bondi et al. 2016).

1.3 RAB GTPases

1.3.1 RAB proteins and mitochondrial dynamics

Intracellular vesicle trafficking is mainly regulated by Rab (Ras analog in brain) proteins. Rab GTPases represent the largest family of small GTPases and they exert their activity by switching from an inactive GDP-bound form to an active GTP-bound form (Stenmark 2009). In the inactive GDP-bound form, Rab proteins are in the cytosol and they are recognized by a Rab escort protein (REP). REP facilitates the geranylgeranyl transferase (GGT) to geranylgeranylate the Rab on the carboxy-terminal Cys residues, which enables Rab proteins to be inserted into membranes. The Rab GDP dissociation inhibitor (GDI) covers their prenylated C terminus. When needed, the GDI displacement factor (GDF) allows them to be activated by guanine nucleotide exchange factors (GEFs), which also influences Rab proteins localisation. Nearby the target membrane, Rab proteins are bound by the cytosolic GTP and can recruit the other molecular effectors. Finally, conversion from the GTP- to the GDP-bound form occurs through GTP hydrolysis catalysed by GTPase-activating proteins (GAPs) (Stenmark 2009; Homma, Hiragi, and Fukuda 2020) (Fig. 1.12).

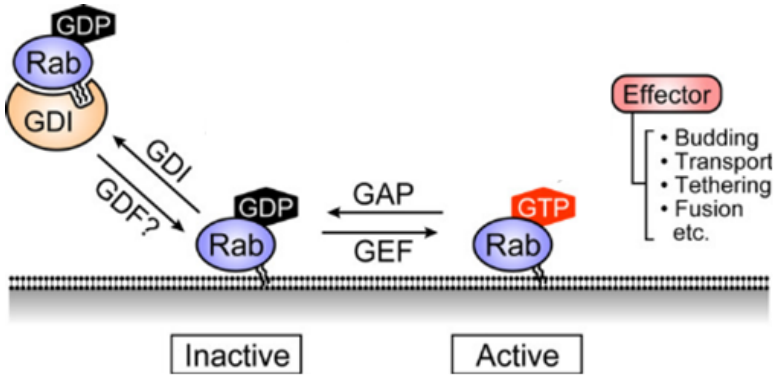

Figure 1.12. The Rab GTPase cycle. (Homma, Hiragi, and Fukuda 2020)

Rab proteins exert many functions and their direct or indirect connection to pathological conditions have been demonstrated for many diseases, including PD. The first evidence ascribing Rab proteins as a primary cause of PD was the discovery of X-linked mutations in *RAB39B* associated with early-onset PD (Wilson et al. 2014). Previously, *in vitro* studies using neuronal cultures knockdown for *RAB39B* revealed effects on vesicle trafficking and hampered synapse formation (Giannandrea et al. 2010). Moreover, *RAB39B* knockout mice were characterised by impaired learning and memory and dysfunctional basal autophagic flux (Niu et al. 2020). Another Rab protein denoted as a susceptibility factor for sporadic PD is RAB29. In physiological condition, RAB29 regulates LRRK2 kinase activity, while in case of pathogenic LRRK2 mutants this activity is up regulated, influencing the downstream effectors of LRRK2, among which we find other Rab proteins like RAB5, RAB8A, RAB10, RAB12 and RAB29 (Purlyte et al. 2018). Other Rab proteins related to the endo-lysosomal compartment, namely RAB5, RAB7, RAB9 and RAB11, have been associated to PD pathology. RAB5 is a marker for early endosomes and its role involves the regulation of vesicle fusion and receptor sorting in the early endosomes, and their biogenesis. Some studies have highlighted a role for RAB5 in the α-syn aggregation-induced PD neurodegeneration, since it promotes the internalisation of α-syn in neuronal cells (Sung et al. 2001; Dalfó et al. 2004). On

the contrary, RAB7 and RAB11 were associated to α-syn aggregates clearance, thereby showing a protective role (Singh and Muqit 2020).

Vesicular trafficking machinery plays a crucial role in the progression of mitophagy. Rab proteins are required for multiple steps in autophagy including the delivery of membranes to the site of phagophore formation and autophagosome-lysosome fusion (Søreng et al. 2018).

Yamano and colleagues were the first to describe the role of both RAB5 and RAB7 in the PINK1/Parkin-mediated mitophagy. RAB7 GTPase-activating protein (RAB7-GAP) TBC1D15 and TBC1D17 suppression has been associated to LC3 accumulation during mitophagy, excessive PINK1 retention on mitochondria and hampered clearance of damaged mitochondria that was mitigated by RAB7 knockdown, highlighting the critical role of RAB7 in the regulation of mito-autophagosome formation (Yamano et al. 2014).

Being RAB7 a marker for late endosome, the subsequent discovery of the role of RAB5 was crucial to figure out the molecular cascade. In fact, Yamano and colleagues demonstrated that after recruitment of PINK1 and Parkin, the RAB5-GEF RabGEF1 localises on mitochondria in ubiquitin- dependent manner via Parkin. This allows RabGEF1 to direct the recruitment of RAB5 to mitochondria, a prior step to Rab7 recruitment and activation via the MON1/CCZ1 complex, effectors of RAB5 (Yamano et al. 2018). Moreover, RAB7 enables the expansion of phagophore by inducing fusion of ATG9A vesicles with the phagophore, which is inhibited upon RAB7 knockdown (Yamano et al. 2018) (Fig. 1.13).

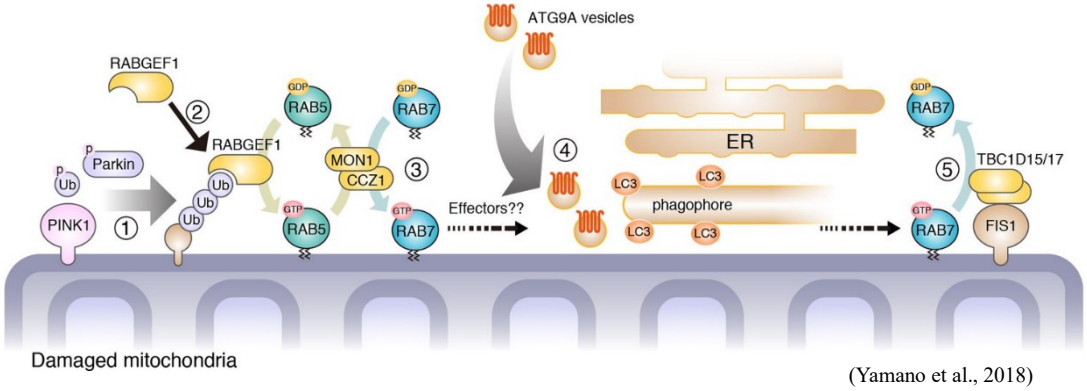

(Yamano et al., 2018)

Figure 1.13 Model of mitophagy regulated by endosomal Rab cycles. (Yamano et al. 2018)

Another evidence supporting the link between PINK1/Parkin mitophagy and Rab proteins was pointed out by shotgun proteomics and systems biology analyses, in which *PRKN*-mutated fibroblasts showed Rab proteins' involvement in mitochondrial proteome alterations and Rab7 recruitment to dysfunctional mitochondria without PINK1 accumulation (Zilocchi et al. 2020).

Many studies have also deepened the knowledge about RAB5 and its involvement in different pathways of mitochondrial quality control. RAB5 is the downstream effector of BNIP3 receptor-mediated mitophagy, in which Parkin is not involved, and promotes sequestration of mitochondria into RAB5-positive endosomes (Hammerling et al. 2020). It also promotes early endosome-mediated elimination of defective mitochondria preventing NLRP3 inflammasome activation in macrophages (Wu et al. 2021). However, in response to acute oxidative stress, RAB5 recruitment to mitochondria is not associated to mitophagy but it exerts a protective role by blocking cytochrome c release (Hsu et al. 2018).

Alternatively to PINK1/Parkin mediated mitophagy, damaged or dysfunctional part of mitochondria can be disposed by mitochondria-derived vesicles (MDVs) first described by Neuspiel and colleagues (Neuspiel et al. 2008). Biogenesis of MDVs can be divided into three phases: initiation, tubulation and scission. MDVs formation does not require the autophagic machinery. Moreover, the content of these vesicles is rather specific and they can be divided into single-membraned MDVs, exclusively formed by the OMM, and double-membraned MDVs, containing both outer and inner mitochondrial membrane contents (König and McBride 2024). RAB9, a late endosomal/Golgi GTPase, has been associate to MDVs shedding (Matheoud et al. 2016; Zhao et al. 2023). In the vast majority, MDVs serve as quality control mechanism in response to early oxidative stress. This mechanism differs from mitophagy since it does not require mitochondrial depolarisation or ATG5 and LC3 for the delivery to the lysosomes, but rather a complementary mechanism to mitophagy (Soubannier et al. 2012).
However, RAB9 involvement in a Parkin-independent mitophagy has been described. In the Ulk1/RAB9-mediated mitophagy, RAB9-associated trans-Golgi membranes are recruited after phosphorylation of RAB9 by Ulk1 and facilitate autophagosome formation (Saito et al. 2019) (Fig. 1.14).

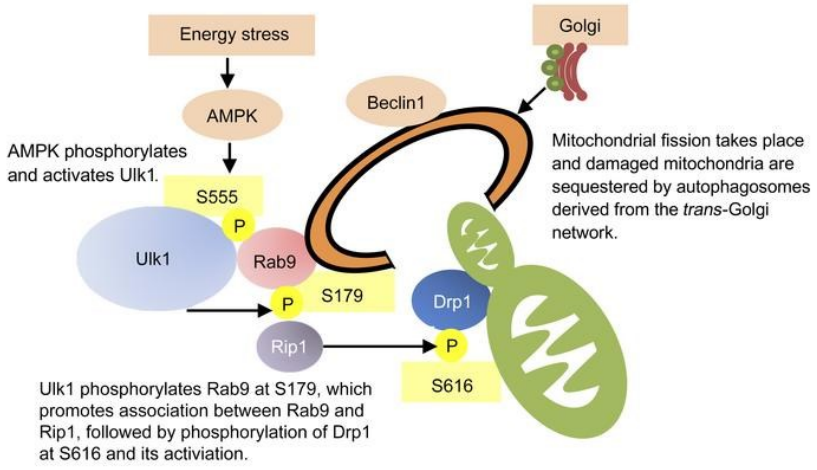

Figure 1.14 Alternative mitophagy pathway mediated by Rab9. (Saito et al. 2019)

1.4 Human skin fibroblasts as cellular model of Parkinson's disease

1.4.1 Fibroblasts cell culture: a valuable tool for studying mitochondrial impairment in neurological disorders

The main cellular population affected by PD pathology are neuronal cells, especially the dopaminergic neurons. In *vitro* models using primary neuronal cells have many advantages, but they also display some drawbacks: limited life span (days to weeks), difficult isolation and culture can be time-consuming, and expensive. Immortalised cell lines are also a useful tool to model PD. SH-SY5Y is a human neuroblastoma cell line characterised by neuron-like properties including neurite-like processes by differentiation. This cell line is widely used since it is characterised by ease of maintenance and catecholaminergic (though not strictly dopaminergic) properties (Xicoy, Wieringa, and Martens 2017b). Moreover, since their ability

to take up dopamine via the dopamine transporter is greater than their capability to store it into vesicles, SH-SY5Y are able to mimic altered dopamine homeostasis, which recapitulates early steps of PD pathogenesis (Alberio, Lopiano, and Fasano 2012; Bondi et al. 2016). Although promising, this cellular model owns cancer-like properties that influence their growth, metabolism, and genomic stability (Hoffmann et al. 2022). The isolation and culturing of primary dopaminergic neurons derived from animal models or iPSCs is time-consuming and expensive, too. Moreover, the only way to study the interested regions directly from patients is post-mortem tissues analysis, which is far from depicting the initial phases of a pathological condition. In the context of PD, it has been widely described the relevance of understanding the role of mitochondrial dysfunction to depict a clear picture of the mechanisms underlying the disease. The use of primary skin fibroblasts derived from PD patients, and generally from neurodegenerative disorders (NDs) patients, is becoming an alternative to neuronal cell cultures (Olesen, Villavicencio-Tejo, and Quintanilla 2022). Skin fibroblasts are peripheral cells that can be obtained almost non-invasively from patients. Moreover, they recapitulate the metabolic changes linked to mitochondrial dysfunction described in neurons: oxidative stress, bioenergetics defects, and mitochondrial dynamics abnormalities (Zilocchi et al. 2020; Deus et al. 2020b; Olesen, Villavicencio-Tejo, and Quintanilla 2022). If from one side there are many advantages, such as being patient-derived cells recapitulating the genetic background and the age-related damages of the subjects, skin fibroblasts are peripheral cells scarcely sensitive to stressors and characterized by metabolic features which make them very different from neuronal cells. In order to attenuate this differences, many studies have induced a metabolic reprogramming to force skin fibroblasts to rely on OXPHOS metabolism exposing metabolic and mitochondrial defects characteristic of fibroblasts from PD patients (Deus et al. 2020b). The most common tool is the replacement of the standard high-glucose culture medium with a galactose containing medium, thus obtaining skin fibroblasts that are more sensitive to mitochondrial toxins, display an altered metabolic activity with increased oxygen consumption rate and ATP levels and mitochondrial morphology alterations (Aguer et al. 2011; Amo et al. 2011; Hertig et al. 2019; Pinho et al. 2022; Deus et al. 2020b). Hence, the use of this model where skin fibroblasts are metabolically reprogrammed toward an OXPHOS metabolism represents a useful tool to better understand the molecular mechanisms leading to mitochondrial dysfunction during the development of PD pathology.

2 Aim of the project

PD is a multifactorial disease in which aging, genetic and environmental factors all contribute to the disease progression. Although the exact pathophysiological mechanism is not completely understood, aberrant mitochondrial dynamics, mitophagy alterations, and defects in complex I activity are all described as hallmarks in both sporadic and genetic forms of PD. Recent evidence has also highlighted the involvement of the endo-lysosomal pathway, specifically a subset of Rab proteins, in mitophagy. In this context, further studies unravelling the cross-talk between these molecular mechanisms are necessary to understand the pathobiology of the disease.

To this purpose, human skin fibroblasts of *PRKN*-mutated patients compared with healthy controls were used as cellular model to investigate the molecular mechanisms at the basis of PD. Fibroblasts derived from *PRKN*-mutated patients offer the key advantage of retaining the same genetic background, where loss-of-function mutations in Parkin gene disrupt the canonical mitophagic pathway dependent on the PINK1/Parkin axis, as already investigated in previous studies (Zanellati et al. 2015; Zilocchi et al. 2020). However, fibroblasts differ from neuron in terms of metabolism, relying on glycolysis rather than oxidative phosphorylation (OXPHOS).

The first aim (Aim 1) of this study was to generate personalized cellular models to investigate mitochondrial dynamics related to PD, by optimizing a protocol to induce mitochondrial dysfunction in human skin fibroblasts reprogrammed toward OXPHOS metabolism. To make fibroblasts more sensitive to mitochondrial damage and metabolically more similar to neurons, a metabolic reprogramming was induced by changing the carbon source from glucose to galactose in the culture medium. Cells were then either challenged with physical insults or chemical insults, known to trigger mitophagy. For physical insults, hypothermic stress was used, while for chemical insults, mitochondrial toxins targeting complex I activity, i.e., MPP^+ and Rotenone, were tested. Since these toxins are known to specifically affect dopaminergic neurons, a preliminary characterization of the dopaminergic system of both control and PRKN-mutated fibroblasts was necessary.

The second aim (Aim 2) of this study was to exploit this cellular model (Aim 1) to investigate mitochondrial network dynamics and RAB5, RAB7, and RAB9 total levels.

3 Materials and Methods

3.1 Materials

3.1.1 Reagents

The chemicals and reagents used in this study along with their suppliers are listed in Table 3.1.

Table 3.1. List of chemicals/reagents and their suppliers.

Product	**Supplier**
1X Phosphate Buffered Saline	Euroclone
2-Mercapthoethanol	Sigma-Aldrich
2-Propanol	EMPLURA® (Merck)
4',6-diamidino-2-phenylindole (DAPI)	Life Technologies
Absolute ethanol	Fluka
Ammonium Persulfate (APS)	Serva
Bovine serum albumin (BSA)	AppliChem
Bromophenol blue	GE Healthcare
CCCP	Sigma-Aldrich
Dimethyl sulfoxide (DMSO)	Sigma-Aldrich
Dithiothreitol (DTT)	AppliChem
Dulbecco's Modified Eagle's Medium (DMEM)	Euroclone
Dulbecco's Modified Eagle's Medium (DMEM) no glucose	Gibco
Fetal Bovine Serum	Euroclone
Galactose powder	Sigma Aldrich
Glycine	Sigma-Aldrich
L-Glutamine	Euroclone
Methanol	Sigma-Aldrich
Mowiol	AppliChem
MPP^+ powder	Sigma-Aldrich
Neutral Red powder	Sigma-Aldrich
Paraformaldehyde (PFA)	Thermo Fisher
Prestained Protein SHARPMASS™ VI	Euroclone
Penicillin	Euroclone
Penicillin/Streptomycin (P/S)	Gibco
Phosphatase Inhibitor Cocktail	Sigma
ProLong Gold Antifade Mounting medium	Invitrogen
Protease Inhibitor Cocktail	Sigma-Aldrich
Rotenone powder	Sigma-Aldrich
Sodium Pyruvate	Gibco

Sodium dodecyl sulfate (SDS)	Sigma-Aldrich
Skim Milk Powder	Sigma-Aldrich
Sodium chloride (NaCl)	Sigma-Aldrich
Sodium deoxycholate	Sigma-Aldrich
Streptomycin	Euroclone
Tetramethylethylenediamine (TEMED)	Euroclone
Tris Base	Sigma-Aldrich
Triton X-100	Sigma-Aldrich
Trypsin EDTA	Euroclone
Tween-20	Sigma-Aldrich

3.1.2 Kits

The commercial kits used in this study with their suppliers are listed in Table 3.2.

Table 3.2. List of kits and their suppliers.

Product	**Supplier**
GoTaq® 2-Step RT-qPCR System	Promega
Pierce™ ECL Western Blotting Substrate	Thermo Scientific
TGX Stain-Free™ FastCast™ Acrylamide Kit	Bio-Rad

3.1.3 Buffers and solutions

All buffers and solutions used in this study are listed below in Table 3.3. Unless otherwise stated, all buffers and solutions were prepared in ddH_2O. Buffers were also diluted in ddH_2O.

Table 3.3. List of buffers/solutions and their respective compositions.

Buffer/Solution	**Composition**
Blocking buffer	5% (w/v) Skim milk or BSA in TBS-T
Freezing medium	5% (v/v) DMSO, 30% (v/v) FBS in DMEM
Laemmli Buffer 5X	50 mM Tris-HCl pH 6.8, 2% SDS, 0.1% bromophenol blue, 10% glycerol
Neutral Red Solution	diluting 1:80 the stock (0,4 % v/v in distillated water) in DMEM
RIPA buffer	0.1% SDS, 25 mM Tris-HCl pH 7.4, 150 mM NaCl, 1% sodium deoxycholate, 1% Triton X-100
Running buffer 10X	250 mM Tris, 2 M glycine, 1% SDS w/v
Transfer buffer 10X	25 mM Tris, 1.5M glycine

TBS-T 10X	0.1 M Tris-HCl pH 8.8, 1.42 M NaCl, 0.5% v/v Tween-20
TBS 10X	0.1 M Tris-HCl pH 8.8, 1.42 M NaCl

3.1.4 Antibodies

Several primary (Table 3.4) and secondary antibodies (Table 3.5) were used for immunoblotting (IB) and immunofluorescence (IIF) in this study. These antibodies are listed below.

Table 3.4. List of primary antibodies.

Antibody	**Species**	**Clonality**	**Supplier**	**Catalog Number**	**1º Dilution**	**2º Dilution**
β-actin	Mouse	Monoclonal	GeneTex	GTX629630	1:8000	1:8000
ATP Synthase	Mouse	Monoclonal	Sigma-Aldrich	HPA034517	1:1500	1:1500
Citrate Synthase	Mouse	Monoclonal	Sigma-Aldrich	AMAb91006	1:1000	1:1500
COX5B	Rabbit	Polyclonal	Sigma-Aldrich	C4498	1:1000	1:2500
OPA1	Rabbit	Polyclonal	Sigma-Aldrich	HPA036927	1:250	1:2500
PINK1	Rabbit	Monoclonal	Cell Signaling	#6946	1:1000	1:2000
RAB5	Mouse	Monoclonal	Cell Signaling	#46449	1:1000	1:2000
RAB7	Rabbit	Monoclonal	Cell Signaling	#9367	1:1000	1:2000
RAB9	Rabbit	Monoclonal	Cell Signaling	#5118	1:1000	1:2000
TOMM20	Rabbit	Monoclonal	Cell Signaling	#42406	1:1000	1:2000

Table 3.5. List of secondary antibodies.

Antibody	**Supplier**	**Catalog Number**
HRP-conjugated anti-mouse IgG	Cell Signaling Technology	#7076
HRP-conjugated anti-rabbit IgG	Cell Signaling Technology	7074p2
Anti-mouse IgG (H+L), F(ab')2 Fragment (Alexa Fluor(R) 555 Conjugate)	Cell Signaling technology	BK4409S

3.1.5 Primers

The following primer pairs (Table 3.6) were used in this study.

Table 3.6. List of primers.

Gene	Species	Primer sequence	Application
ACTB	Human	F – 5'-CTGCCGTTTCCGTCTGTAGAG-3'	qRT-PCR
		R – 5'-TGTTATTGCGAGCAGGAACAAA-3'	
DRD1	Human	F – 5'- ATGGACGGGACTGGGCTGGT -3'	qRT-PCR
		R – 5'- GGAGCGTGGACAGGATGAGCA -3'	
DRD2	Human	F – 5'- AGCCTCCACTCTCCGCCTG -3'	qRT-PCR
		R – 5'- CCACTAAAGGGCAACTGTACTCACC -3'	
DRD3	Human	F – 5'- GGCACTCCCCGAGGTTGCAG -3'	qRT-PCR
		R – 5'- CGGAATTCCCTGAGTCCCACC -3'	
DRD4	Human	F – 5'- GCCGACCTCCTCCTCGCTCT -3'	qRT-PCR
		R – 5'- CGAACCTGTCCACGCTGATGG -3'	
DRD5	Human	F – 5'- TCTACCGCATCGCCCAGGTG -3'	qRT-PCR
		R – 5'- GCAGCCAGCAACACACGAAGA -3'	
VMAT1	Human	F – 5'- GCTTTCTTCAACAGCCACGGTG -3'	qRT-PCR
		R – 5'- CTGTGGTGGTGCCAATTGTGC -3'	
VMAT2	Human	F – 5'- CCATTGCGGATGTGGCATTT -3'	qRT-PCR
		R – 5'- TCTTCTTTGGCAGGTGGACTTCG -3'	
DAT1	Human	F – 5'- AGCCTGCCTGGGTCCTTTCG -3'	qRT-PCR
		R – 5'- AGTGGCGGAGCGTGAACTGG -3'	
TH	Human	F – 5'- CGACCCTGACCTGGACTTGGA -3'	qRT-PCR
		R – 5'- GGCAATCTCCTCGGCGGTGT -3'	

3.1.6 Equipment

All the equipment used in this study is listed below in Table 3.7.

Table 3.7. List of equipment and their manufacturers.

Equipment	Manufacturer
Centrifuge 5804 R	Eppendorf
CFX Connect Real-Time System	Bio-Rad
G:BOXChemi XT4	Syngene
iMark™ Microplate Reader	Bio-Rad
cooled CCD camera on an Olympus IX 81microscope	Olympus
Semi-Dry Transfer Unit	Hoefer

3.1.7 Software

The software used to acquire and analyse data are listed below in Table 3.8.

Table 3.8. List of software and their manufacturers.

Software	Manufacturer
GraphPad Prism 8	GraphPad Software Inc.
ImageJ	NIH

Microsoft Office	Microsoft Corporation
BioRad	CFX Manager™

3.2 Methods

3.2.1 Cell culture

In this study, five control fibroblasts cell lines and six *PRKN*-mutated fibroblasts cell lines were used to investigate cellular response to metabolic reprogramming, mitophagy induction, the combination of both challenges and the changes in RAB protein levels. The human neuroblastoma SH-SY5Y cell line was used as an internal control for some experimental set-up.

3.2.2 Primary skin fibroblast cell lines

Human primary skin fibroblasts cell lines from six *PRKN* patients and five control subjects were obtained from the "Cell line and DNA Bank of genetic Movement Disorder and Mitochondrial Diseases" of the Telethon Network of Genetic Biobanks (TNGB) and the Department of Molecular Medicine from University of Pavia. Personal and clinical data and genetic characterisation were collected from patients after specific informed consent. Control subjects gave their consent for research purposes.

Subject	**Gender**	**Age at onset**	**Age at skin biopsy**	***PRKN* mutation**
# 5	M		44	c.198C>T, p.Arg33* + Del etero esoni 3-4-5 (compound hetero)
# 10	M		49	c.101-102delAG (202-203delAG) p.Gln34Argfs*5 exon 2 (compound hetero)
# 3599	F	20		Del ex3/ del ex3
# 6153	F	32		Del ex2-4-5
# 3590	M	32		Del ex-4-5
# 3877	F	39		Del ex 5-6/c.101_102 Del AG (ex2)
# 2	M		30	CTRL
# 4	F		27	CTRL
# 7	F		51	CTRL
# 8	M		54	CTRL
# 11	F		25	CTRL

3.2.3 Cell culture conditions

Fibroblasts were cultured in two different media, high glucose Dulbecco's modified Eagle's medium (DMEM) (Euroclone) supplemented with 15% (v/v), fetal bovine serum (FBS) (Euroclone), 100 U/ml penicillin, 100 ug/ml streptomycin (Euroclone) and 2 mM L-glutamine (Euroclone) and galactose medium prepared using DMEM without glucose (Gibco), supplemented with 15% (v/v), fetal bovine serum (FBS) (Euroclone), 100 U/ml penicillin, 100 ug/ml streptomycin (Euroclone), 1 mM Sodium Pyruvate (Gibco) and galactose (1.8016 g/L)

10mM (Sigma Aldrich). Cells were maintained in 5% CO_2 humified atmosphere at 37 °C. Subculturing of cells were performed when they reached 80–90% confluence using Accutase (Euroclone) to detach cells and by centrifugating cells at 500 x *g* for 5 min at room temperature (RT) to remove the supernatant. The cell pellet was then resuspended in fresh complete DMEM and seeded in new flasks.

3.2.4 Metabolic reprogramming protocol

In order to induce a metabolic reprogramming via changing the culture medium, it was followed the protocol by Pinho and colleagues (Pinho et al. 2022). Starting from cells maintained in high glucose, after cells subculturing, a portion of the cells maintained in high glucose medium were gradually adapted to galactose medium during one cell passage. Following the confluence percentage, the cells were plated at a in a new flask with a mixture of medium (in a ratio of 75:25, high glucose and galactose respectively). At 50% confluence medium was replaced by a 50:50 ratio of high glucose and galactose medium. Another change of medium was performed at 70-75% confluence, with a 25:75 ratio of high glucose and galactose medium. Finally, when about 90% of confluence was reached, cells were passaged by Accutase to 100% galactose medium. Before experiments, cells were kept in galactose medium for at least two cell passages.

3.2.5 Western Blot analysis

Cell pellets from both control and *PRKN*-mutated fibroblasts were lysed in RIPA buffer supplemented with phosphatase and protease inhibitors cocktails and placed on ice for 30 minutes. Cellular lysates were then sonicated (0.5 cycles, 80% amplitude, 10 pulses) followed by centrifugation at 15,000 × *g* for 15 min at 4°C. Supernatants (containing the proteins) were collected in new microtubes and quantified through the BCA assay (Thermo Fisher Scientific). Proteins (30 μg) diluted in Laemmli loading buffer were loaded onto 10% or 12% fast-cast gels (prepared with TGX Stain-Free™ FastCast™ Acrylamide Kit, APS and TEMED) and transferred to polyvinylidene difluoride (PVDF) or nitrocellulose membranes (Millipore) at 1.0 mA/cm2 (TE77pwr, Hoefer). Membranes were then blocked in 5% skim milk powder prepared in tris-buffered saline with 0.05% TWEEN (TBS-T) for 2 h at RT and then probed overnight at 4°C against primary antibodies listed in Table 3.4. Next day, membranes underwent three washes in TBS-T and incubation with proper peroxidase-conjugated secondary antibody in 5% milk in TBS-T (Table 3.5). Protein bands were visualised by chemiluminescence using enhanced chemiluminescence substrate (Millipore Corporation). Images (16-bit grayscale) were acquired using the G:BOXChemi XT4 system and quantified using the ImageJ software.

3.2.6 Neutral red uptake assay

Neutral red uptake (NRU) is used to estimate of the number of viable cells in a culture. Neutral red dye, a weak cation dye, can be incorporated by living cells inside lysosome. Neutral red stock solution (0,4% w/V) was prepared by dissolving neutral red dye in ddH_2O. The neutral red dye working solution was preprepared by diluting 1:80 the stock (0,4 % v/v in ddH2O) in

DMEM. The working solution was pre-warmed for 10 minutes at 37°, followed by centrifugation at 1200 x g for 5 minutes and sterilization though filtration. Cell viability was assessed in control fibroblasts seeded onto 24 mw plate (3×10^4 cells/well) treated with different concentration of MPP^+. After 24h treatment, cells in each well were washed with DMEM without FBS and incubated for 2h at 37 °C with 500 µL of neutral red dye working solution. To remove the neutral red dye working solution, cells were washed with 500 µL washing solution (0,1% w/V $CaCl_2$ in ddH2O). Subsequentially, cellular lysis was induced by incubating the cells with the extraction solution (1% acetic acid and 49,5 % ethanol in ddH2O), for 20 min at RT on a shaker. Quantification was obtained using a UV-visible spectrophotometer by measuring the absorbance at 260 nm (UV-Vis Cary 50 Bio).

3.2.7 MPP^+ treatment of human skin fibroblasts

Mitochondrial toxin MPP^+ was used to induce mitophagy via blockade of complex I in our cell model. MPP^+ powder (Sigma Aldrich) was dissolved directly in DMEM medium, yielding a 5 mM stock solution. The stock solution was subsequently diluted directly in the medium to obtain a range of lower concentrations used to perform cell viability test and proteins levels evaluation. For the assessment of cell viability using the neutral red assay, control fibroblasts were seeded in 24-well plates at a density of 3×10^4 cells/well and treated in triplicate with seven different concentrations of MPP^+ (5 mM, 2.5 mM, 1 mM, 500 µM, 250 µm, 100 µM, 2.5 µM) for 24h. For proteins levels assessment, all five control and six patient-derived fibroblasts cell lines were seeded in T75 flask at a density of $2\text{-}3 \times 10^5$. After 24h, cells reached a 70–80% confluency and were treated with either 500µM of DMEM-dissolved MPP^+ (MPP^+) or DMEM alone (CTRL) for 24h. Treatments were performed once in every cell lines. Cells were then detached with trypsin-EDTA and centrifuged at 500 × *g* for 5 minutes All cellular pellets were flash-frozen in liquid nitrogen and maintained at −80°C for subsequent analyses.

3.2.8 Rotenone treatment of human skin fibroblasts

Mitochondrial toxin Rotenone was used to induce mitophagy via blockade of complex I in our cell model. Rotenone (Rot) powder (Sigma Aldrich) was dissolved in DMSO medium, yielding a 100 mM stock solution. The stock solution was subsequently diluted directly in the medium to obtain a range of lower concentrations used to perform cell viability test and proteins evaluation. For the assessment of cell viability using the neutral red assay, control fibroblasts were seeded in 24-well plates at a density of 3×10^4 cells/well and treated in triplicate with three different concentrations of Rotenone (500µM, 250µM and 50µM) for 24h. For proteins levels assessment, control fibroblasts cell lines were seeded in T75 flask at a density of $2\text{-}3 \times 10^5$. After 24h, cells reached a 70–80% confluency and were treated with either 50µM of DMEM-dissolved Rotenone (Rot) or DMSO alone (DMSO) for 24h. Treatments were performed once in every cell lines. Cells were then detached with trypsin-EDTA and centrifuged at 500 × g for 5 minutes All cellular pellets were flash-frozen in liquid nitrogen and maintained at −80°C for subsequent analyses.

3.2.9 CCCP treatment of human skin fibroblasts

Carbonyl cyanide 3-chlorophenylhydrazone (CCCP) (Sigma-Aldrich) is an uncoupler which dissipates the mitochondrial proton gradient and it was used as a positive control of mitophagy induction. During the preliminary analyses of the effect of MPP^+, CCCP treatment was carried out in parallel as reference. For proteins levels assessment, control fibroblasts were seeded in T75 flask at a density of 2-3 × 10^5. After 24h, cells reached a 70–80% confluency and were treated with either 60 μM DMSO-dissolved CCCP (CCCP) or DMSO alone (CTRL) in DMEM for 24h. Subsequently, cells were detached with trypsin-EDTA and centrifuged at 500 × *g* for 5 minutes. Treatments were performed in one control fibroblasts cell line in parallel with MPP^+ and Rotenone treatments during the cytotoxic effect evaluation of both toxins. All cellular pellets were flash-frozen in liquid nitrogen and maintained at −80°C for subsequent analyses.

3.2.10 Measurement of Mitochondrial Membrane Potential

In order to evaluate any changes in mitochondrial potential (ΔΨm) in our different experimental settings, we exploit the mitochondria-selective fluorescent probe Mitotracker® Orange CMTMRos (Life Technologies). Fibroblast cells were seeded in 96-well plates at 3.5 × 10^3 cells/well and mitotracker analysis were performed after treatments. Culture medium was removed and replaced with fresh DMEM supplemented with 100 nM Mitotracker Orange CMTMRos (Life Technologies). After 30min of incubation at 37°C, cells were washed with PBS and fixed with 4% paraformaldehyde (PFA) for 15min. Cells were washed with PBS to remove PFA excess and then permeabilize with 0.2% Triton X-100 in PBS for 10 min. After a washing step in PBS, nuclei counter-staining was carried out with 10 μM DAPI in PBS for 1 minute at RT. Images were acquired through a cooled CCD camera on an Olympus IX 81microscope (20×) for an acquisition time of 2 sec. For each well, three fields of view (fov) were acquired for both Mitotracker Orange CMTMRos and DAPI signal. For each whole fov, Mitotracker signal intensities were calculated measuring integrated density values (the total intensity of fluorescence in the defined area) minus the mean of background fluorescence values. The corrected intensity was normalized with respect to the number of cells, as defined by nuclear staining with DAPI. At least five fovs obtained from three technical replicates were evaluated for each condition.

3.2.11 Indirect Immunofluorescence

Fibroblast cells were seeded at a density of 15 × 10^3 per well onto 18 mm glass coverslips in 12-well plates and cultured for 24 h at 37°C in the presence of DMEM-dissolved MPP^+ (MPP^+) or DMEM alone (CTRL) for 24h. After 24h treatments, cells were washed with PBS and fixed with 4% paraformaldehyde for 15 min, permeabilized with Triton X-100 (0.2% Triton X-100 in PBS) for 5 min, and blocked with 5% FBS in PBS for 2 h at RT. Coverslips were incubated overnight at 4°C with the primary antibody in 5% FBS diluted in PBS. Fibroblast cells were then incubated with secondary antibodies in 5% FBS in PBS. Nuclei were counterstained with DAPI and coverslips were mounted on microscope slides.

3.2.12 Mitochondrial network analysis

Images were acquired through a cooled CCD camera on an Olympus IX 81microscope (60×) for an acquisition time of 0.250 sec.
Mitochondrial network morphology was analysed and quantified using the Mitochondrial Network Analysis tool (MiNA) using ImageJ (A. J. Valente et al. 2017). Three different morphological parameters were taken into account:

- branch length mean: the mean length of all the lines used to represent the mitochondrial structures.
- summed branch lengths mean: The mean of sum of all branch lengths divided by the number of independent skeletons.
- network branches mean: The mean number of attached lines used to represent each structure.

At least 30 cells per condition were randomly selected for the analysis related to hypothermic stress experiments, while 40-45 cells per condition for the analysis related to metabolic reprogramming combined with mitophagy induction.

3.2.13 Flow Cytometric Analysis

In order to evaluate any changes in mitochondrial potential ($\Delta\Psi m$) compared all three mitochondrial toxins used (CCCP, Rot and MPP^+), we exploit flow cytometric analysis after Mitotracker staining. Control fibroblasts were seeded in T25 flask at a density of 7×10^4. After 24h, cells reached a 70–80% confluency and were treated with mitochondrial toxins as already described. After 24h treatment, mitotracker staining protocol was performed (see above) without nuclear staining. Cells were then resuspended in 200/300 µL PBS and analysed using a FACScalibur Becton Dickinson flow cytometer equipped with an air-cooled argon ion laser (15mW, 488nm) using CellQuestPRO 5.1 software. The fluorescent emission of mitotracker was collected through a 575 nm band-pass filter. Mitotracker fluorescence in the treated samples was determined based on the shift of the peaks detected in monoparametric histograms acquired in log mode and compared to the fluorescence determined in control cells.

3.2.14 Quantitative RT-PCR

RNA from SH-SY5Y cells (at two different passage numbers), three control fibroblasts cell lines and two *PRKN*-mutated fibroblasts cell lines was extracted using ReliaPrep™ RNA Cell Miniprep System (Promega) following the manual. The extracted RNA samples were quantified using a UV-visible spectrophotometer by measuring the absorbance at 260 nm. cDNA synthesis and qPCR were performed using GoTaq® 2-Step RT-qPCR System (Promega). The qPCR reactions were run on the CFX Connect Real-Time System (Bio-Rad). Quality control of amplification and dissociation curves was performed. PCR amplification products were separated and visualized onto a 1.5% agarose gel.

3.2.15 Statistical Analyses

The results were analysed using Microsoft Excel and/or GraphPad Prism version 8. For Western blot analysis the mean of at least three independent biological replicates/subjects was considered. Statistical analyses for Western blot data were performed by either two-tailed, unpaired, Student's t test with Welch's correction or ANOVA (one or two-way depending on the number of variables considered). For mitochondrial network analysis, the non-parametric Wilcoxon test was used to verify if there were any significant differences in the parameters analysed. For all analyses, significance threshold was set at p-value < 0.05. The statistical approach used is always described in the "Results" section.

4 Results

The final aim of my three-year PhD project was to study the molecular mechanisms at the basis of PD pathology exploiting human skin fibroblasts of *PRKN*-mutated patients as a cellular model, in comparison with the same cells from healthy controls. As already stated before, being patient-derived cells, fibroblasts entail the main advantage of recapitulating the genetic background and the age-related damages of the subjects they are derived from. By contrast, they are peripheral cells scarcely sensitive to stressors, endowed with quite rudimental systems of biosignalling and trafficking, and characteristic metabolic features which make them very different from neuronal cells.

On this basis,I thoroughly investigated the behaviour of these cells in response to several stressors mainly acting at the mitochondrial level. First, I assessed them as possible players in the peripheral dopaminergic system. Then, I challenged fibroblasts with both physical and chemical insults to find the most suited protocol to induce mitophagy. Moreover, to obtain a cellular model more similar to neuronal cells and to exacerbate the sensitivity to mitochondrial damages, I optimized a protocol for metabolic reprogramming toward an OXPHOS metabolism, mimicking the neuronal one. Eventually, by combining metabolic reprogramming with mitochondrial insults, I analysed both mitochondrial dynamics and RABs dynamics, with the aim of elucidating some aspects of the interaction between two central factors, *i.e.*, mitochondrial dysfunction and vesicle trafficking alterations, in the context of PD pathology.

4.1 Characterization of the dopaminergic system in fibroblasts

Many PD models rely on the use of mitochondrial toxins that specifically target dopaminergic neurons. MPP^+ and Rotenone mechanisms of action and uptake have been widely characterised in neurons. Rotenone is a lipophilic molecule that can easily cross the blood brain barrier, and it is usually exploited to generate *in vivo* PD-models, while MPP^+ is more frequently used in cellular models (being MPTP used to generate PD toxic models). Regarding their use in non-neuronal cellular models little is known. In particular, MPP^+ cannot passively diffuse across cell membranes and exploits the dopamine transporter (DAT) expressed on dopaminergic neurons. Thus, the uptake mechanisms should be investigated in cells different from neurons, by assessing the presence of membrane transporters. Moreover, a preliminary characterization of the whole dopaminergic system (i.e., enzymes involved in DA synthesis, vesicular transporters, and receptors) in fibroblasts is mandatory to use them as a model to study PD mechanisms. Indeed, these cells may be part of the so-called peripheral dopaminergic system. Owing this, control and *PRKN*-mutated fibroblasts were used to assess the expression, at the transcript level, of the principal plasma membrane transporter (DAT1), the vesicular transporters (VMAT1, VMAT2), the receptors (DRD1, DRD2, DRD3, DRD4, DRD5), and the rate limiting enzyme in dopamine synthesis, tyrosine hydroxylase (TH). To this end, qRT-PCR reactions were performed on total RNAs from control fibroblasts (n=3), *PRKN*-mutated fibroblasts (n=2), and the human neuroblastoma SH-SY5Y cell line (n=2) as positive control, since the expression of all dopaminergic markers has been already verified in this cell line (Alberio et al. 2011). The amplification products were loaded and visualized on agarose gels (Fig. 4.1).

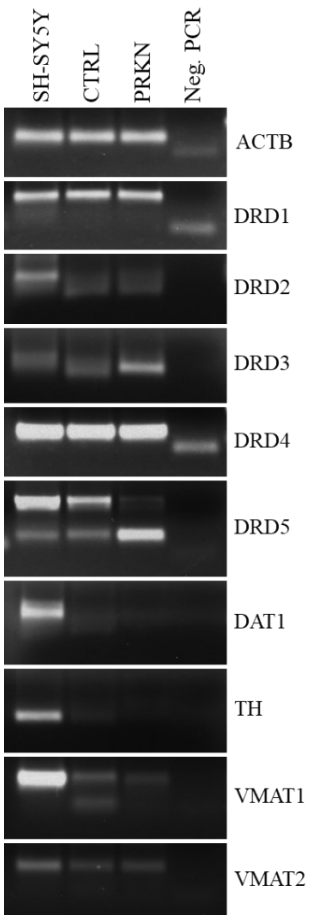

Fig. 4.1 Characterization of the dopaminergic system in fibroblasts by transcript levels analysis.
Representative PCR amplification products from SH-SY5Y cells, one control, and one *PRKN*-mutated patient. DRDn: dopamine receptor Dn. DAT1: dopamine transporter 1. TH: tyrosine hydroxylase. VMAT1: vesicular monoamine transporter 1. VMAT2: vesicular monoamine transporter 2.

As a result, fibroblast cells express DA receptors, even displaying different patterns of amplification products. By contrast, these cells do not express TH and DAT1, meaning that they cannot synthetize and internalize DA, respectively.

4.2 The effects of Hypothermic stress on mitochondrial homeostasis in primary skin fibroblasts

After the preliminary characterization of the dopaminergic system in fibroblasts, the following step was the setup of protocols to induce mitophagy in these cells. Among the possible physical stressors suitable to induce mitophagy, hypothermic stress was the first approach selected, since it has already been applied successfully in human fibroblasts (Bonello et al. 2019). Control fibroblasts only were used to this purpose.

4.2.1 Mitochondrial membrane potential analysis

In order to evaluate if thermal stress triggers mitophagy in human fibroblasts, we used Bonello and coworkers' protocol (Bonello et al. 2019). As described in the Materials and Methods section, control fibroblasts were exposed to hypothermic shock (24°C) for 45 min, followed by

45 min of recovery at 37°C. This condition was compared with control fibroblasts maintained at standard culture temperature of 37°C (CTRL). As positive control for mitophagy induction, control fibroblasts were treated with 60 µM CCCP (CCCP), also performing their respective treatment control (DMSO) (Zilocchi et al. 2020). To assess the effects of the hypothermic shock, the mitochondrial membrane potential was evaluated using the mitotracker probe. As expected, CCCP treatment induced a significant loss of mitochondrial membrane potential ($p = 0.0003$) compared to DMSO (Fig. 4.2A and 4.2B), while this was not observed upon the hypothermic shock (Fig. 4.2C and 4.2D).

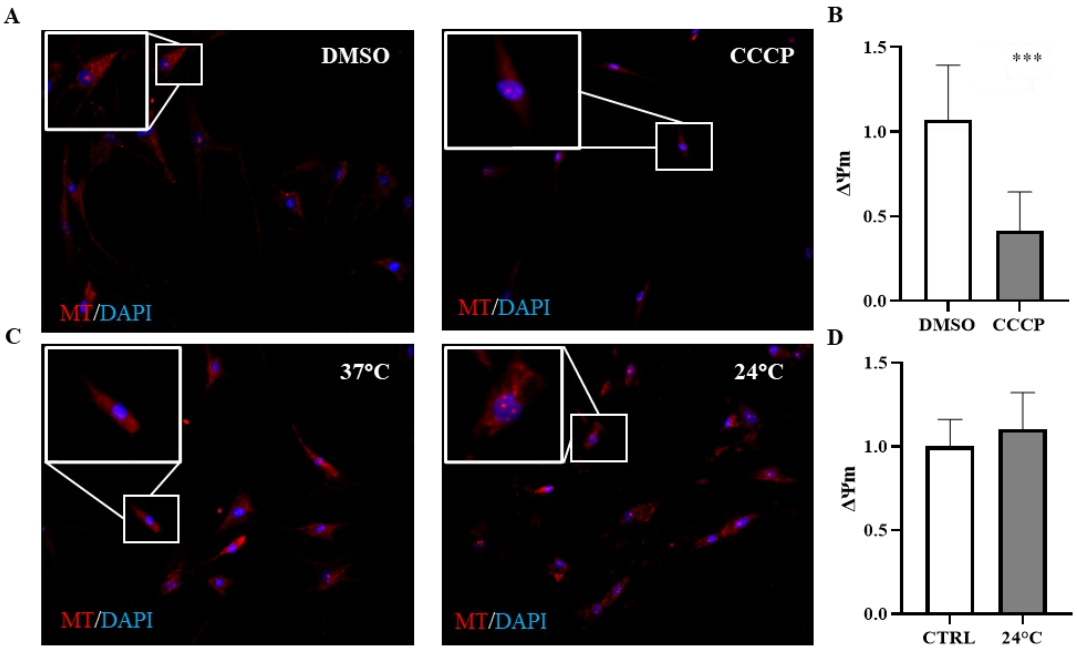

Fig. 4.2 Mitochondrial membrane potential of control fibroblasts is not altered after hypothermic shock.
(A) Representative images of fibroblast cells from one control subject stained with Mitotracker Orange CMTMRos after DMSO or CCCP treatment. (B) Quantification of Mitotracker Orange CMTMRos fluorescence normalized by the number of cells, n = 3 technical replicates. Data, expressed as mean ± SD, were analysed by two-tailed, unpaired Student's t-test with Welch's correction; ***$p < 0.001$. (C) Representative images of fibroblast cells from one control subjects stained with Mitotracker Orange CMTMRos after hypothermic shock. (D) Quantification of Mitotracker Orange CMTMRos fluorescence normalized by the number of cells, n = 3 technical replicates. Data, expressed as mean ± SD, were analysed by two-tailed, unpaired Student's t-test with Welch's correction.

4.2.2 Mitochondrial network morphology analysis

In addition to mitochondrial membrane potential, it was decided to evaluate further possible alterations at the level of mitochondrial network structure after hypothermic stress. As described in the Materials and Methods section, control fibroblasts were exposed to hypothermic shock (24°C) for 45 min, followed by 45 min of recovery at 37°C and to assess

the effects of the hypothermic shock on the mitochondrial network morphology, ATP Synthase was visualized by IIF (Fig. 4.3A).

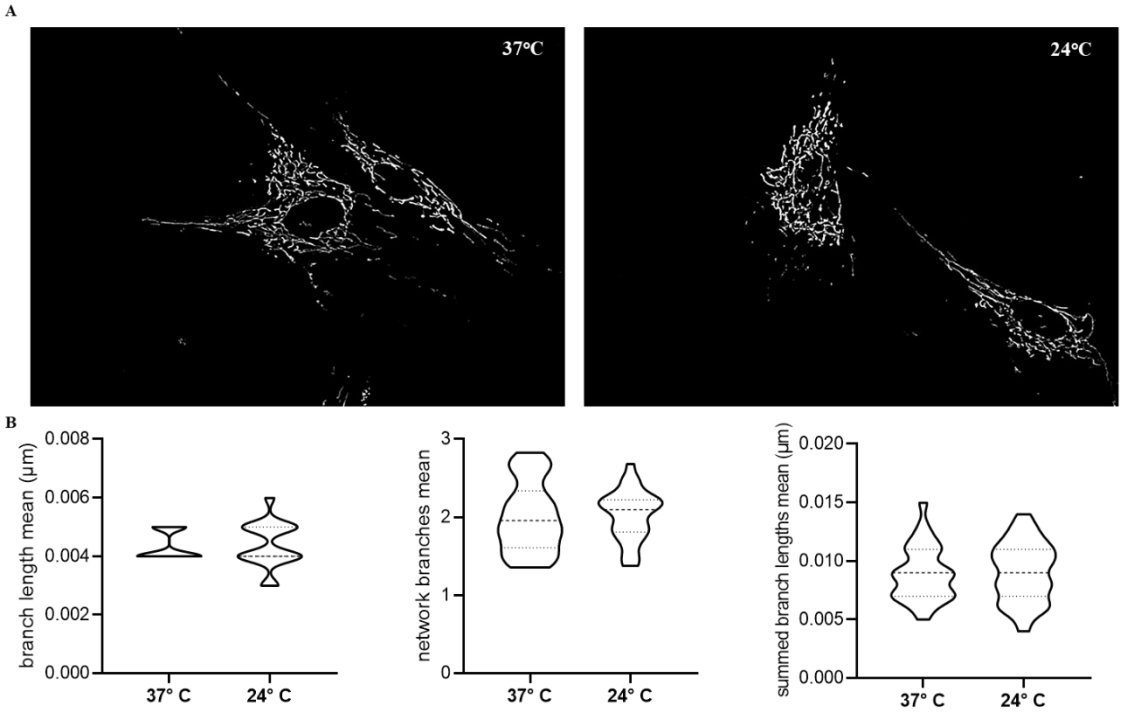

Fig. 4.3 Mitochondrial network morphology of control fibroblasts is not altered after hypothermic shock.
(A) Representative images of fibroblast cells from one control subject stained with ATP Synthase after hypothermic shock. (B) Quantification of branch length mean, summed branch lengths mean and network branches mean parameters were performed on at least 30 cells per condition. Data, expressed as mean ± SD, were analysed by the Mann Whitney test.

The signal was quantified by immunofluorescence and analysed using the Mitochondrial Network Analysis tool (MiNA) in order to evaluate branch length mean, summed branch lengths mean and network branches mean parameters. From the graphs in (Fig. 4.3B), after hypothermic stress there were no differences in the three parameters taken into consideration, suggesting no significant differences in mitochondrial network morphology after hypothermic stress.

4.2.3 Evaluation of the levels of mitophagy-related proteins

Control fibroblasts exposed to hypothermic stress were then used to evaluate any possible changes in protein levels of key mitophagy players. Levels of PINK1, OPA1 and COX5B were evaluated by Western blot analysis in control fibroblasts maintained at 37°C (CTRL) or exposed to hypothermic stress (24°C) (Fig. 4.4B). CCCP treatment was used as a positive control for mitophagy induction (Fig. 4.4A). CCCP treatment, as expected, caused the accumulation of PINK1, the disappearance of the long form of OPA1 (L-OPA1) with accumulation of the pro-fission short form of OPA1 (S-OPA1), and a decrease of the mitochondrial mass correlated to COX5B protein reduction (Fig. 4.4A).

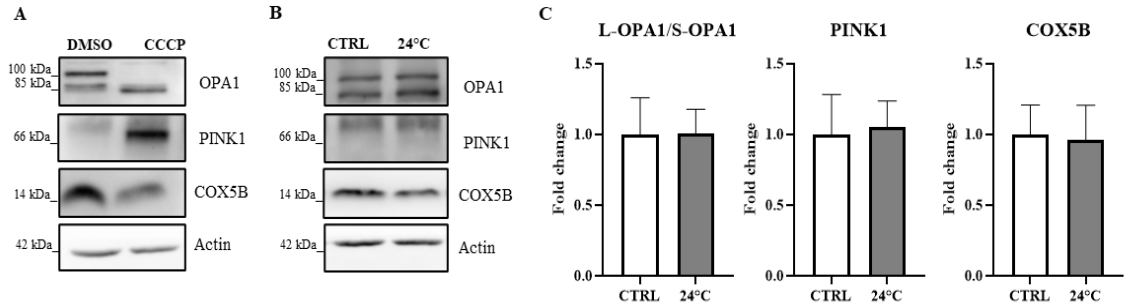

Fig. 4.4 Western blot analysis of mitochondrial markers related to mitophagy after hypothermic stress.
(A) Evaluation of mitochondrial markers related to mitophagy in fibroblast cells from one control subject after 24h treatment with 60 µM CCCP and relative DMO control condition. (B) Representative images of Western blot analysis for mitochondrial marker related to mitophagy in fibroblast cells from one control subject following 45 min exposure at 24°C. (C) Relative quantification expressed as mean ± SD, n = 3 biological replicates. Data were analysed by two-tailed, unpaired Student's t-test with Welch's correction; ns, not significant.

This was not paralleled in the hypothermic stress condition, since no changes in PINK1, OPA1 or COX5B were detected (Fig. 4.4C), concluding that a brief exposure to a lower temperature was not sufficient to trigger mitophagy in fibroblast cells.

4.2.4 Mitochondrial membrane potential analysis

The protocol by Bonello and coworkers was adapted by increasing the exposure time at 24h, in order to further challenge mitophagy induction in control fibroblasts. Accordingly, cells were exposed to hypothermic shock for 24h, followed by 45 min of recovery at 37°C. This condition was compared to control fibroblasts maintained at standard culture temperature of 37°C (Fig. 4.5A).

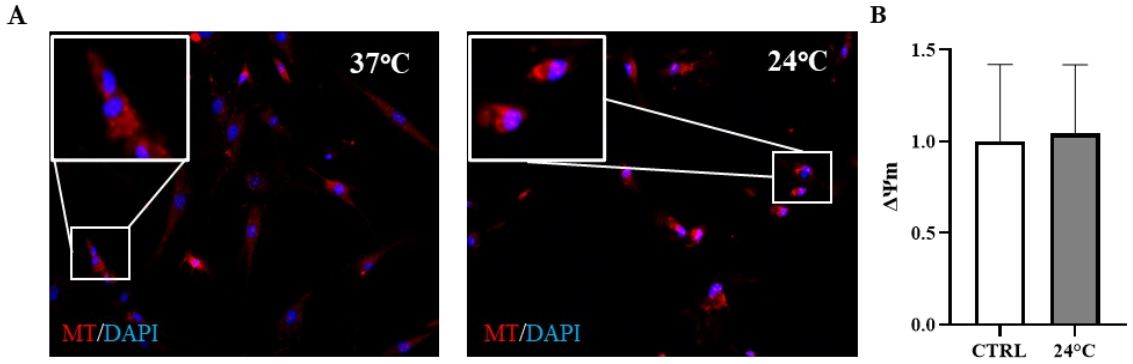

Fig. 4.5 Mitochondrial membrane potential of control fibroblasts is not altered after prolonged hypothermic shock.
(A) Representative images of fibroblast cells from one control subject stained with Mitotracker Orange CMTMRos after 24h exposure at 24°C. (B) Quantification of Mitotracker Orange CMTMRos fluorescence normalized by the number of cells, n = 3 technical replicates. Data, expressed as mean ± SD, were analysed by two-tailed, unpaired Student's t-test with Welch's correction.

As shown in (Fig. 4.5B), prolonged hypothermic stress did not significantly alter mitochondrial membrane potential. Thus, this physical stressor did not prove to be effective in mitophagy induction in our fibroblast cells.

4.2.5 Evaluation of the levels of mitophagy-related protein

The effect of prolonged exposure at 24°C for 24h in control fibroblasts were also analysed by assessing the protein levels of OPA1, PINK1 and COX5B. Being a preliminary investigation, a single cell line was used, and the experiment was performed once.

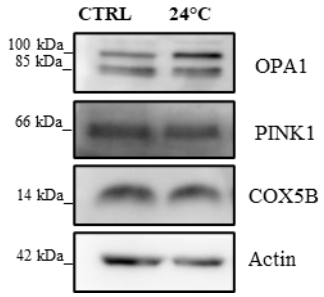

Fig. 4.6 Western blot analysis of mitochondrial markers related to mitophagy after prolonged hypothermic stress. Preliminary evaluation of mitochondrial markers related to mitophagy in fibroblast cells from one control subject after 24h exposure at 24°C.

Comparing control fibroblasts maintained at 37°C (CTRL) to the ones maintained at 24°C for 24h followed by 45 min of recovery at 37°C (24°C), there were no significant change in any of the mitochondrial marker evaluated, (Fig. 4.6), thus concluding that neither a prolonged exposure to 24°C was sufficient to trigger mitophagy.

4.3 The effects of mitochondrial toxins treatment on mitochondrial homeostasis in primary skin fibroblasts

After attempting to induce mitophagy using hypothermic stress as a physical insult, the next step involved using mitochondrial toxins. Little is known about the use of MPP^+ and Rotenone in fibroblasts compared to neurons. Therefore, it was first necessary to establish a range of concentrations to determine an effective final concentration based on mortality rate. This concentration was then tested to evaluate its effect on mitochondrial homeostasis.

4.3.1 Cell viability test after MPP^+ treatment at different concentrations

In order to assess the cytotoxic effect of MPP^+ and to determine the final concentration to be used in this study, we assessed both cell viability and the levels of mitochondrial marker proteins. Human skin fibroblasts from one control subject were treated with different concentration of MPP^+ for 24h followed by a neutral red viability test in technical triplicate (Fig. 4.7).

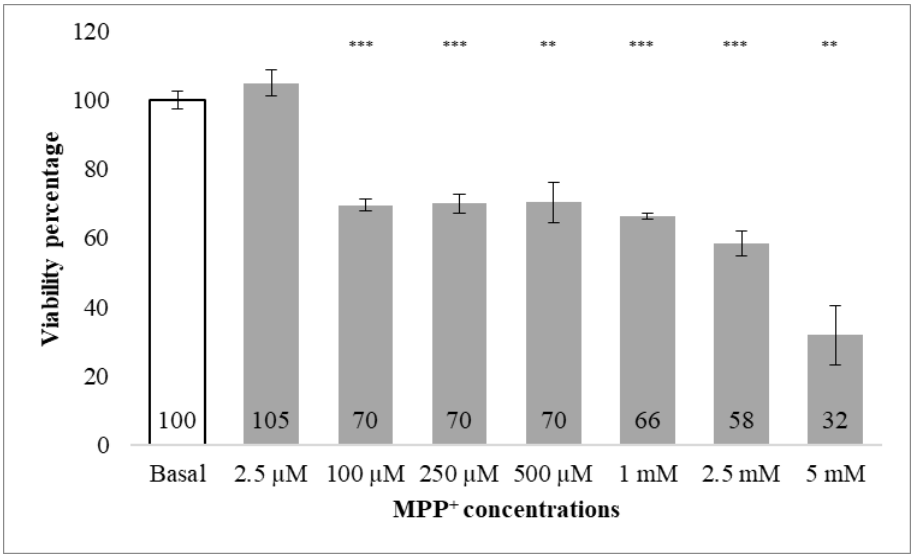

Fig. 4.7 Cell viability test after MPP^+ treatment.
Neutral red uptake (NRU) assay in control fibroblasts following the exposure to MPP^+ at different concentrations for 24 h. Data analysis was performed using one-way ANOVA. Values reported are mean ± SE of three technical replicates of the same experiment; ** $p<0.01$; *** $p<0.001$ vs basal.

From the total range of concentrations, we selected the ones causing a mortality rate of 30-40% to be used in the following experiments (500 µM, 1 mM and 2.5 mM).

4.3.2 Evaluation of mitochondrial markers protein levels after MPP^+ treatment at different concentrations

To determine the final concentration to be used, further mitochondrial marker proteins evaluation was performed with the narrowed range of concentrations. A single cell line of control fibroblasts was treated using three different concentrations of MPP^+ (500 µM, 1 mM and 2.5 mM). Control fibroblasts treated with 60 µM CCCP were used as a positive control of mitophagy induction. After 24h treatment, Western blot analysis was performed considering mitochondrial marker protein COX5B as an indicator of the total mitochondrial mass, while OPA1 was used as a marker of mitochondrial fusion (Fig. 4.8).

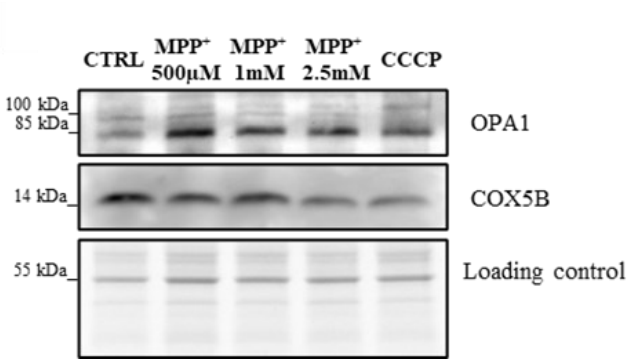

Fig. 4.8 Western blot analysis of mitochondrial markers proteins following MPP^+ treatment.
Preliminary evaluation of mitochondrial markers fibroblast cells from one control subject after 24h treatment with MPP^+ (500 µM, 1 mM and 2.5 mM) and 60 µM CCCP treatment as positive control.

From the qualitative evaluation of MPP^+ treatment effects, a reduction of COX5B level and accumulation of S-OPA1 isoform were visible at all three concentrations. Since it was possible to appreciate a qualitative reduction in mitochondrial mass and impairment of mitochondrial fusion, with the disappearance of L-OPA1, already from the lowest concentration, 500 µM was the selected concentration to perform the following experiments.

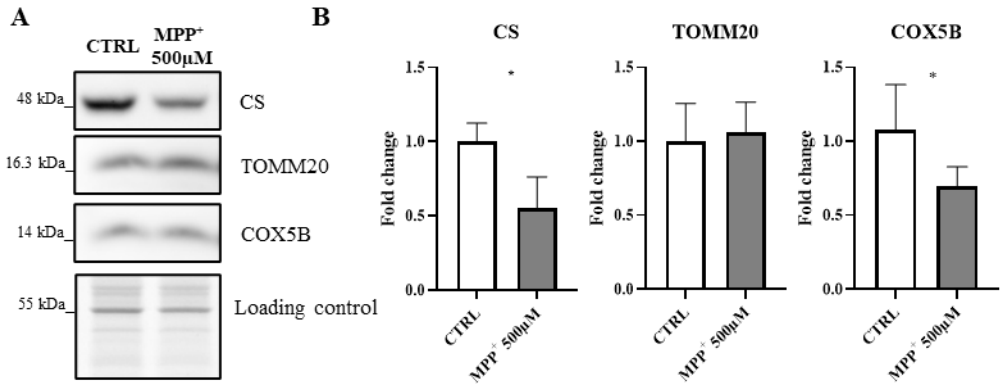

Fig. 4.9 Western blot analysis of mitochondrial markers after MPP^+ treatment.
(A) Representative Western blot images of mitochondrial marker proteins in fibroblast cells from one control subject following 500 µM MPP^+ treatment. (B) Relative quantification expressed as mean ± SD, n = 3 biological replicates. Data were analysed by two-tailed, unpaired Student's t-test with Welch's correction; * $p<0.05$.

Using the selected 500 µM concentration, other mitochondrial markers were evaluated by Western blot analysis: CS, TOMM20 and COX5B (Fig. 4.9A). The analysis showed a significant decrease of CS and COX5B level, while TOMM20 was unaltered (Fig. 4.9B).

4.3.3 Cell viability test after Rotenone treatment at different concentrations

In order to assess the cytotoxic effect of Rotenone and to determine the final concentration to be used in this study, we assessed both cell viability and the levels of mitochondrial marker proteins. Human skin fibroblasts from one control subject were treated with different concentration of DMSO-dissolved Rotenone for 24h followed by a neutral red viability test in technical triplicate (Fig. 4.10). We evaluate three different concentrations (50 µM, 250 µM and 500 µM) and their respective DMSO controls (0.05%, 0.25% and 0.5%).

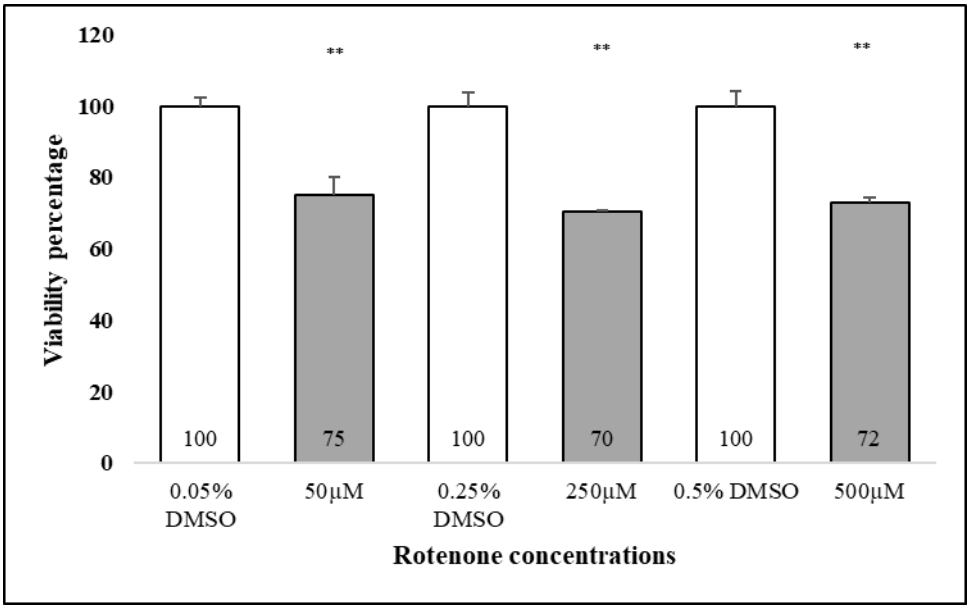

Fig. 4.10 Cell viability test after Rotenone treatment.
Neutral red uptake (NRU) assay in control fibroblasts following the exposure to Rotenone at different concentrations for 24 h. Data analysis was performed using one-way ANOVA. Values reported are mean ± SE of three technical replicates of the same experiment; ** $p<0.001$ vs DMSO.

All three concentrations caused a mortality rate of 30-40%, but the 500 µM concentration of Rotenone was discarder due to the higher percentage of DMSO.

4.3.4 Evaluation of mitochondrial markers protein levels after Rotenone treatment at different concentrations

In order to determine the final concentration to be used, further mitochondrial markers were evaluated in a narrowed range of concentrations. A single cell line of control fibroblasts was treated using two different concentrations of Rotenone (Rot) (50 µM and 250 µM). Control fibroblasts treated with 60 µM CCCP were used as a positive control of mitophagy induction. After 24h treatment, Western blot analysis was performed considering mitochondrial marker protein COX5B as an indicator of the total mitochondrial mass, while OPA1 was used as a marker of mitochondrial fusion (Fig. 4.11).

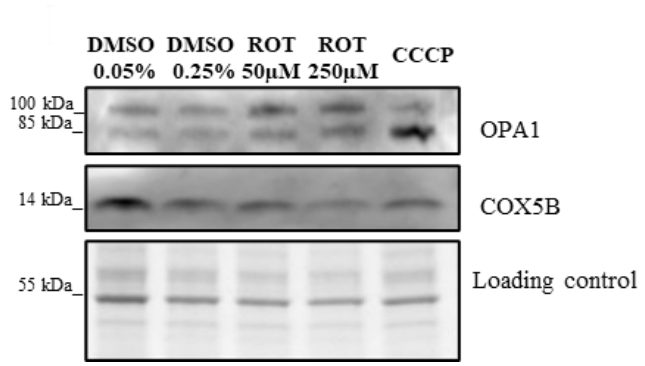

Fig. 4.11 Western blot analysis of mitochondrial markers proteins following Rotenone treatment.
Preliminary evaluation of mitochondrial markers in control fibroblasts after 24h treatment with Rotenone (50 µM and 500 µM) and relative DMSO concentrations as control condition.

From the qualitative evaluation of Rotenone treatment effects, no reduction of COX5B level was visible after Rotenone treatment neither alteration in the level of L-OPA1 and S-OPA1. Considering this, the final treatment condition selected to perform further analysis was 50 µM due to the lower DMSO concentration, preventing side effect from the vehicle toxicity.

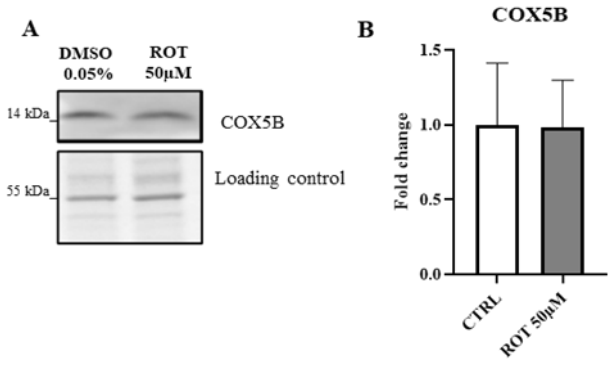

Fig. 4.12 Western blot analysis of mitochondrial mass marker after Rotenone treatment.
(A) Representative Western blot images of mitochondrial marker proteins in control fibroblasts following 24h treatment with 50µM Rotenone. (B) Relative quantification expressed as mean ± SD, n = 3 technical replicates. Data were analysed by two-tailed, unpaired Student's t-test with Welch's correction.

This single concentration was then used to treat a single cell line of control fibroblasts and assess any reduction in mitochondrial mass trough COX5B protein level evaluation (Fig. 4.12A). As it is shown in the graph, after 24h treatment with 50 µM Rotenone there was no significant change in COX5B level, suggesting no reduction in mitochondrial mass (Fig. 4.12B).

4.3.5 Mitochondrial depolarization analysis by flow cytometry

In addition to mitochondrial marker protein evaluation, it was assessed the extent of mitochondrial membrane depolarization after both toxins' treatment through mitotracker staining followed by cytofluorimetric analysis. Since the final aim was to exacerbate mitochondrial damage in already OXPHOS depending human skin fibroblasts using a single mitochondrial toxin, this further analysis was exploited to establish the more suitable mitochondrial toxin to be used. In order to standardise the procedure, MPP^+ powder was dissolved in 0.05% DMSO high glucose DMEM, using this condition as a common control between 50 µM Rotenone and 500 µM MPP^+ treatment. The treatment with 60 µM CCCP was carried out in parallel as positive control of mitochondrial membrane depolarisation.

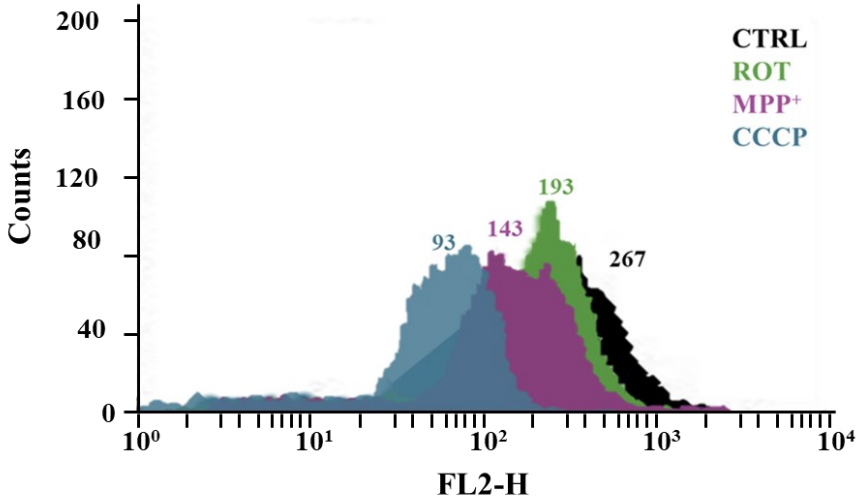

Fig. 4.13 Overlay of one-dimensional histograms representing the mean fluorescence intensity (MFI) of Mitotracker signal after 24h treatment with 60 µM CCCP, 500 µM MPP^+, 50 µM Rotenone and 0.05% DMSO as control condition in fibroblast cells from one control subject.

After 24h treatment, cells were stained with Mitotracker Orange CMTMRos and analysed at the flow cytometer. The data obtained represent the mean fluorescence intensity (MFI) of each treatment (Fig. 4.13). From the comparison of Mitotracker fluorescence peaks, CCCP showed the major shift from the control.

The second most depolarising toxin after CCCP was MPP^+, indicating a stronger effect compared to Rotenone. Owing this, treatment with 500 µM MPP^+ was selected as the standard protocol to induce mitophagy in my cellular model.

4.3.6 Metabolic reprogramming of fibroblasts towards OXPHOS

Human skin fibroblasts have been widely used to model and study neurodegenerative diseases. However, they show a highly glycolytic metabolism that make them different from neuronal cells, which are more sensitive to alterations in mitochondria. To highlight mitochondrial dysfunction and better understand the involvement of mitochondrial dynamics at the basis of neurodegenerative diseases, human skin fibroblasts were forced toward a mitochondrial metabolism. To this aim, the culture medium of both patient-derived and controls' fibroblasts was gradually changed from high glucose to galactose medium as proposed by Pinho and colleagues' protocol (Pinho et al. 2022). Evaluation of structural and molecular changes

induced by the metabolic reprogramming was then assessed via mitochondrial marker proteins, mitochondrial membrane potential and mitochondrial network analyses.

4.3.7 Protocol setup: evaluation of mitochondrial marker protein levels after metabolic reprogramming

The protocol by Pinho and colleagues was applied to one control fibroblasts cell lines and one patient-derived fibroblasts cell lines. After the gradual change of the medium and at least two cell passages (see Material and Methods), the protein level of CS, and COX5B was evaluated (Fig. 4.14).

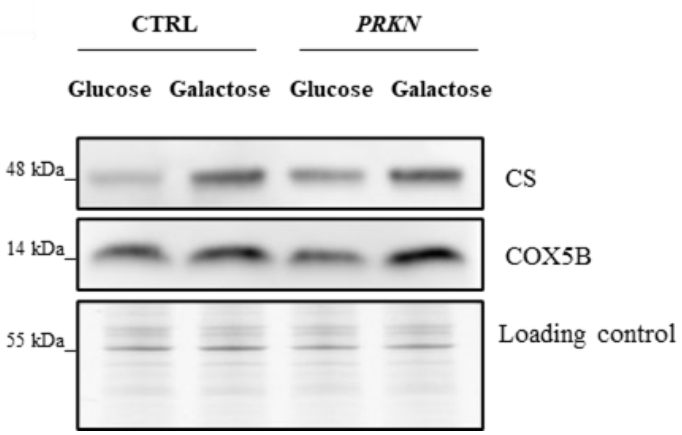

Fig. 4.14 Western blot analysis of mitochondrial marker after metabolic reprogramming.
Representative Western blot images of mitochondrial marker proteins one control and one patient-derived fibroblasts cell line maintained in 25 mM high glucose medium or 5 mM galactose medium after metabolic reprogramming protocol.

From these preliminary evaluations, it was observed an increase in CS and COX5B level, thus suggesting an effect related to the metabolic reprogramming. To determine whether the metabolic reprogramming had an impact on mitochondrial function, one control and one patient-derived fibroblasts cell line were stained with Mitotracker Orange CMTMRos.

4.4 Effects of the combination between metabolic reprogramming and toxins-induced mitochondrial stress: mitochondrial homeostasis and Rab proteins dynamics

After the protocol optimization for metabolic reprogramming toward an OXPHOS metabolism and the standardization of mitochondrial toxins mitophagy induction set up, control and *PRKN*-mutated fibroblasts were used to assess structural and molecular changes induced by the combination of both mitophagy induction and metabolic programming via mitochondrial marker proteins evaluation, and mitochondrial network analyses. Both control and *PRKN*-mutated fibroblasts were maintained in either high glucose medium or 5 mM galactose medium after metabolic reprogramming. Starting from these four conditions, cells were treated with either 500 μM MPP^+ or underwent cell culture medium replacement. In Fig. 4.15, light microscope images from control fibroblasts are reported, representing the four conditions to be compared after 24h treatment: glucose (GLC) control (CTRL), glucose (GLC) treated with 500

µM MPP^+, galactose (GAL) control (CTRL) and galactose (GAL) treated with 500 µM MPP^+. This was only a qualitative assessment to determine any possible macroscopic change in the morphology of the cells.

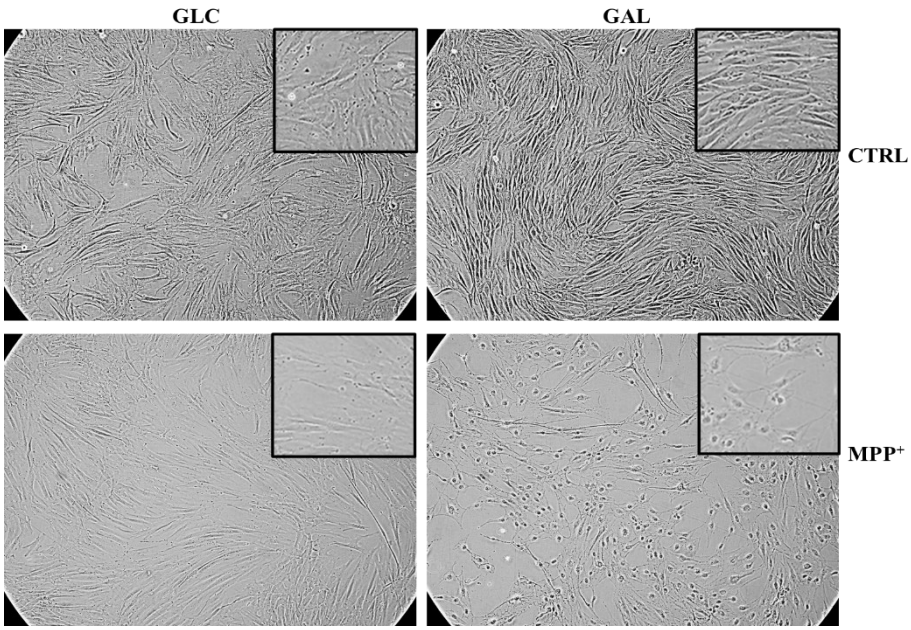

Fig. 4.15 Morphological changes in cultured control fibroblasts recorded by light microscopy.
Representative images of control fibroblasts in four different experimental conditions: glucose only, glucose combined with 500 µM MPP^+ treatment, galactose only and galactose combined with 500 µM MPP^+ treatment.

As it can be appreciated, cells maintained in galactose medium and treated with 500 µM MPP^+, showed a more senescent morphology. The same was done for patient-derived cells after 24h treatment, and cells maintained in galactose treated with 500 µM MPP^+ showed the same characteristic. This specific pattern was always observed in all the biological replicates performed.

4.4.1 Mitochondrial network morphology analysis

Mitochondrial dynamics play a crucial role in the mitochondrial quality control and are exploited by these organelles in response to various physiological cues. For this reason, it was decided to evaluate further possible alterations at the level of mitochondrial network structure in both control and *PRKN*-mutated fibroblasts after MPP^+-induce mitophagy in combination with metabolic reprogramming. As described in the Materials and Methods section, control fibroblasts stained with ATP Synthase were analysed in four conditions: glucose only, glucose combined with 500 µM MPP^+ treatment, galactose only and galactose combined with 500 µM MPP^+ treatment (Fig. 4.16). The same four conditions were compared also in *PRKN*-mutated fibroblasts (Fig. 4.17).

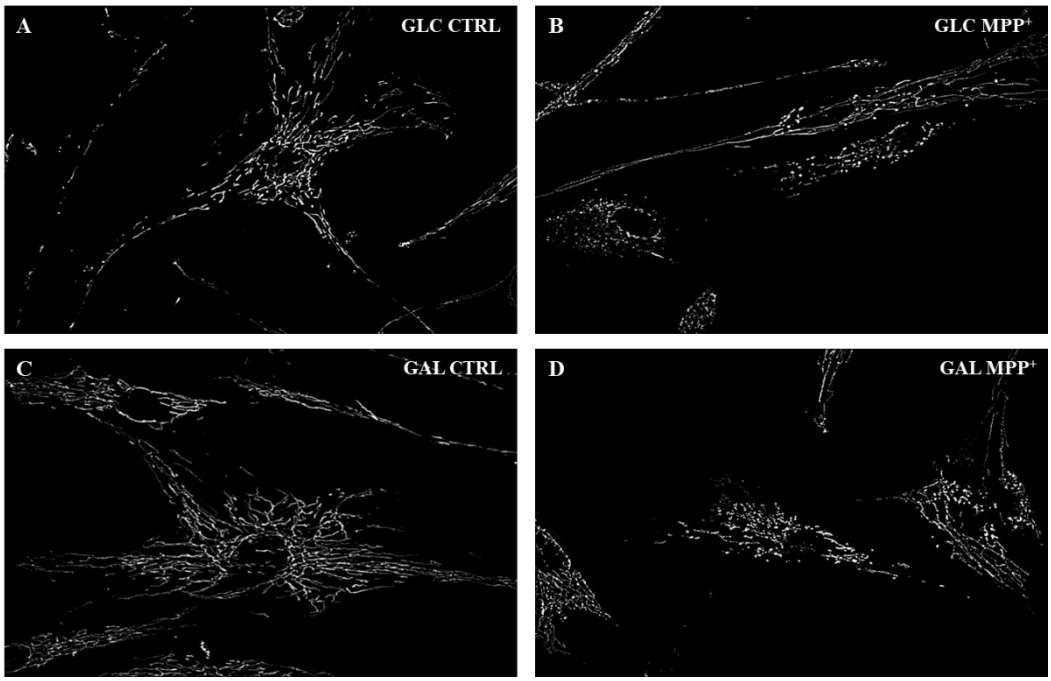

Fig. 4.16 Mitochondrial network morphology of control fibroblasts upon metabolic reprogramming combined with MPP^+ treatment.

Representative images of fibroblast cells from one control subject stained with ATP Synthase. (A) Standard culture medium, treatment control. (B) Standard culture medium, MPP^+ treatment. (C) Galactose medium, treatment control. (D) Galactose medium, MPP^+ treatment.

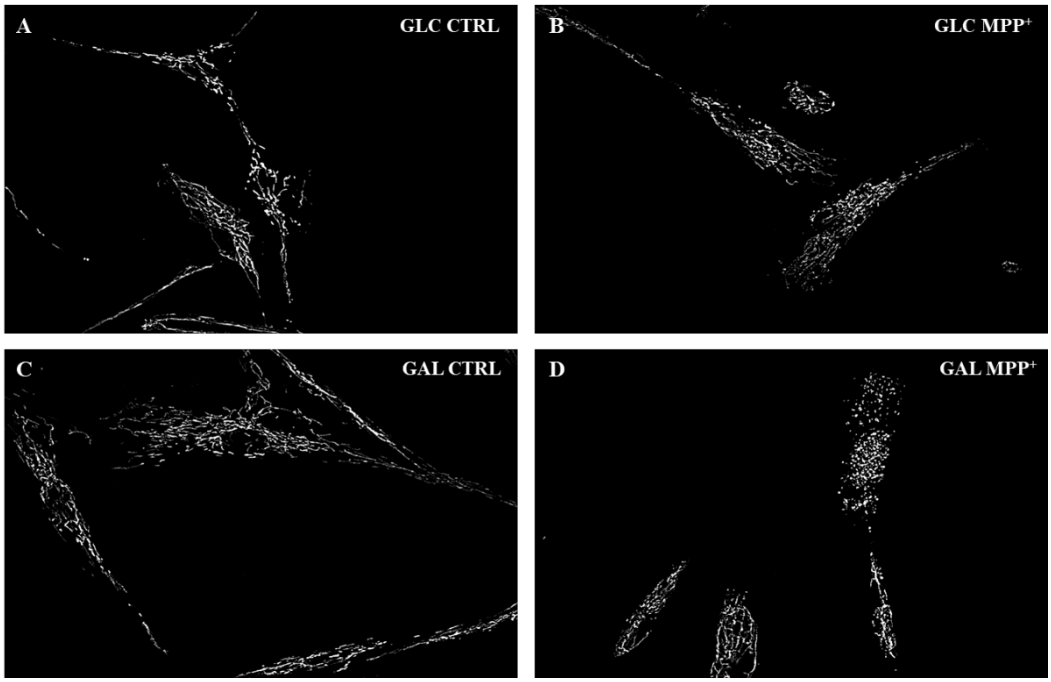

Fig. 4.17 Mitochondrial network morphology of patient-derived fibroblasts upon metabolic reprogramming combined with MPP^+ treatment.

Representative images of fibroblast cells from one patient stained with ATP Synthase. (A) Standard culture medium, treatment control. (B) Standard culture medium, MPP^+ treatment. (C) Galactose medium, treatment control. (D) Galactose medium, MPP^+ treatment.

The quantitative assessment of the visible differences in the morphology of the mitochondrial network was performed by the evaluation of some specific parameters that describe the length and connectivity of network branches, i.e., branch length, network branches, and summed branch length.

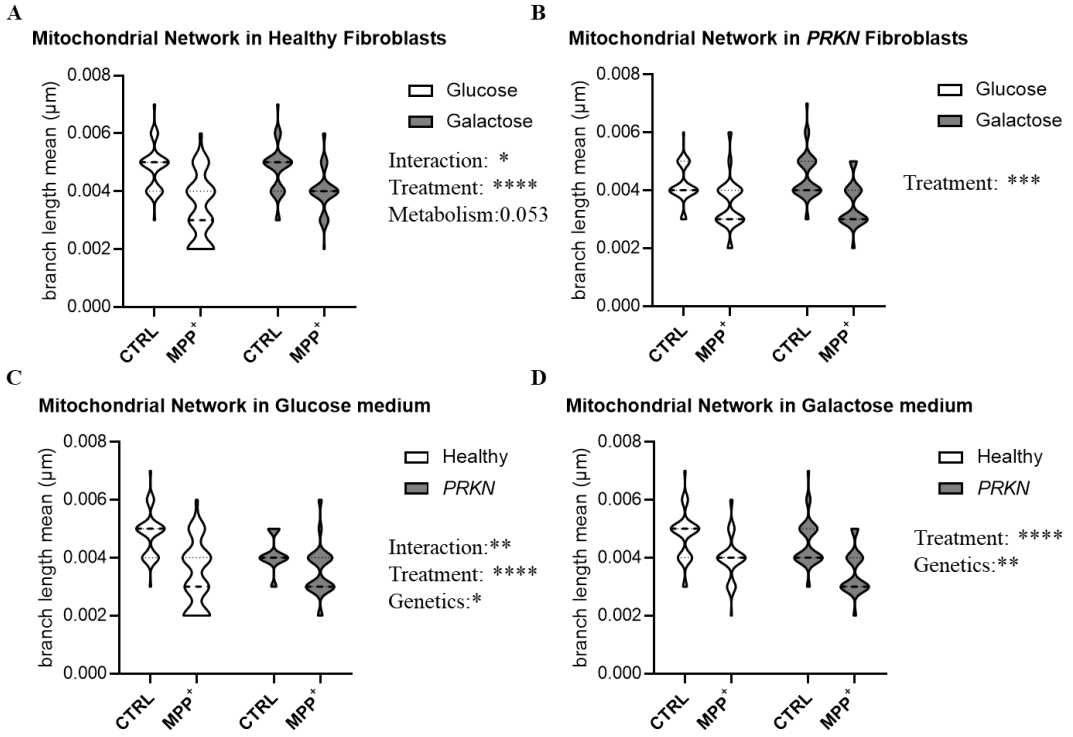

Fig. 4.18 Quantitative analysis of the mitochondrial network morphology upon metabolic reprogramming combined with MPP$^+$ treatment.

Fibroblasts from one healthy subject and one *PRKN*-mutated patient were analysed. A total number of 45 cells have been quantified per group. (A) Violin plots representing the measurement of branch length mean parameter in mitochondrial network analysis in healthy fibroblasts only, expressed as mean. Data were analysed by two-way ANOVA. "Interaction" (p = 0.0142; F = 6.132) and "Treatment" (p <0.0001; F = 67.23) resulted to be a significant source of variation. (B) Violin plots representing the measurement of branch length mean in *PRKN*-mutated fibroblasts only, expressed as mean. Data were analysed by two-way ANOVA. "Treatment" (p <0. 0001; F =51.24) resulted to be a significant source of variation. (C) Violin plots representing the measurement of branch length mean in standard culture conditions (glucose) expressed as mean. Data were analysed by two-way ANOVA. "Interaction" (p = 0.0016; F = 10.22), "Treatment" (p <0.0001; F = 61.48) and "Genetics" (p =0.0288; F = 4.859) resulted to be a significant source of variation. (D) Violin plots representing the measurement of branch length mean in galactose only and galactose treated with MPP$^+$ in both healthy and *PRKN*-mutated fibroblasts expressed as mean. Data were analysed by two-way ANOVA. "Treatment" (p<0.0001; F = 55.14) and "Genetics" (p =0.0020; F = 9.874) resulted to be a significant source of variation.

The evaluation of branch length mean parameter was assessed in one healthy fibroblasts cell line compared to one *PRKN*-mutated fibroblasts maintained in either glucose medium or galactose medium after 24h treatment with MPP$^+$. In control healthy fibroblasts the measurement of branch length mean was significantly affected by MPP$^+$ treatment ("Treatment", p <0.0001; F = 67.23). Moreover, the parameter was differently affected according to the culture medium, specifically, it was observed a shortening in the branch length mean in glucose medium that was enhanced in galactose medium ("Interaction", p = 0.0142; F = 6.132) (Fig. 4.18A). In addition, it was observed a tendency (p=0.0537) in the effect of the

metabolism factor. In *PRKN*-mutated fibroblasts, treatment with MPP^+ significantly decreased the branch length mean in both glucose and galactose medium ("Treatment", p <0. 0001; F =51.24) (Fig. 4.18B). In glucose condition, the branch length is significantly influenced by MPP^+ treatment with a different trend in healthy fibroblasts compared with the PRKN-mutated one ("Interaction", p = 0.0016; F = 10.22, "Treatment", p <0.0001; F = 61.48, and "Genetics", p =0.0288; F = 4.859) (Fig. 4.18C). After metabolic reprogramming, the branch length mean was significantly reduced after MPP^+ treatment ("Treatment", p<0.0001; F = 55.14) and it was observed a general shortening in PD patients compared to controls ("Genetics", p=0.0020; F = 9. 874) (Fig. 4.18D).

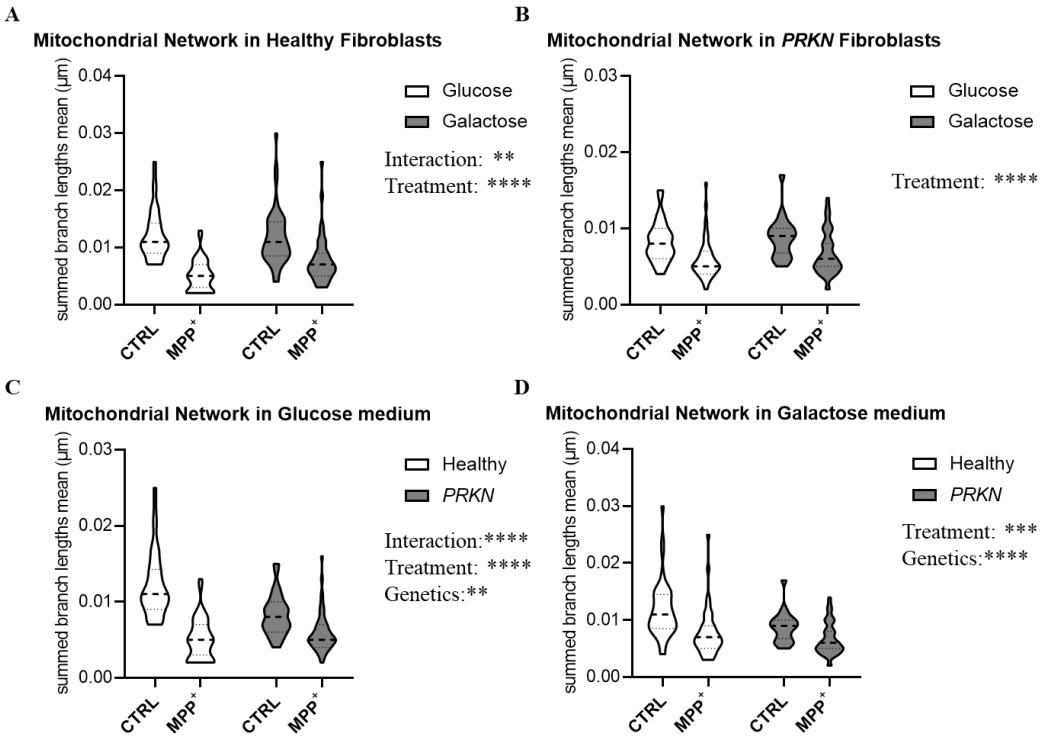

Fig. 4.19 Quantitative analysis of the mitochondrial network morphology upon metabolic reprogramming combined with MPP^+ treatment.

Fibroblasts from one healthy subject and one *PRKN*-mutated patient were analysed. A total number of 45 cells have been quantified per group. (A) Violin plots representing the measurement of the summed branch lengths mean parameter in mitochondrial network analysis in healthy fibroblasts only, expressed as mean. Data were analysed by two-way ANOVA. "Interaction" (p = 0.0100; F = 6.78) and "Treatment" (p <0.0001; F = 85.16) resulted to be a significant source of variation. (B) Violin plots representing the measurement of the summed branch lengths mean in *PRKN*-mutated fibroblasts only, expressed as mean. Data were analysed by two-way ANOVA. "Treatment" (p <0.0001; F =30.98) resulted to be a significant source of variation. (C) Violin plots representing the measurement of the summed branch lengths mean in standard culture conditions (glucose) expressed as mean. Data were analysed by two-way ANOVA. "Interaction" (p <0.0001; F = 27.84), "Treatment" (p <0.0001; F = 105.9) and "Genetics" (p =0.0010; F = 11.10) resulted to be a significant source of variation. (D) Violin plots representing the measurement of the summed branch lengths mean in galactose only and galactose treated with MPP^+ in both healthy and *PRKN*-mutated fibroblasts expressed as mean. Data were analysed by two-way ANOVA. "Treatment" (p<0.0001; F = 29.74) and "Genetics" (p =0.0004; F = 13.205) resulted to be a significant source of variation.

The evaluation of summed branch length mean parameter was assessed in one healthy fibroblasts cell line compared to one *PRKN*-mutated fibroblasts maintained in either glucose medium or galactose medium after 24h treatment with MPP^+. In control healthy fibroblasts the summed branch length mean was significantly affected by MPP^+ treatment ("Treatment", p

<0.0001; F = 85.16). Moreover, the parameter was differently affected according to the culture medium, specifically, it was observed a shortening in the branch length mean in galactose medium that was enhanced in glucose medium ("Interaction", p = 0.0100; F = 6.78) (Fig. 4.19A). In *PRKN*-mutated fibroblasts, treatment with MPP^+ significantly decreased in the summed branch length mean in both glucose and galactose medium ("Treatment", p <0.0001; F =30.98) (Fig. 4.19B). In glucose condition, the effect of MPP^+ treatment and the genetic background significantly decreased the summed branch length in both control healthy and *PRKN*-mutated fibroblasts ("Treatment", p <0.0001; F = 105.9, "Genetics" p =0.0010; F = 11.10) (Fig. 4.19C), moreover, the effect of MPP^+ treatment was different according to the genetic background (Interaction", p <0.0001; F = 27.84). After metabolic reprogramming, the summed branch length mean was significantly reduced after MPP^+ treatment ("Treatment", p<0.0001; F = 29.74) and it was observed a general shortening in PD patients compared to controls ("Genetics", p =0.0004; F = 13.205) (Fig. 4.19D).

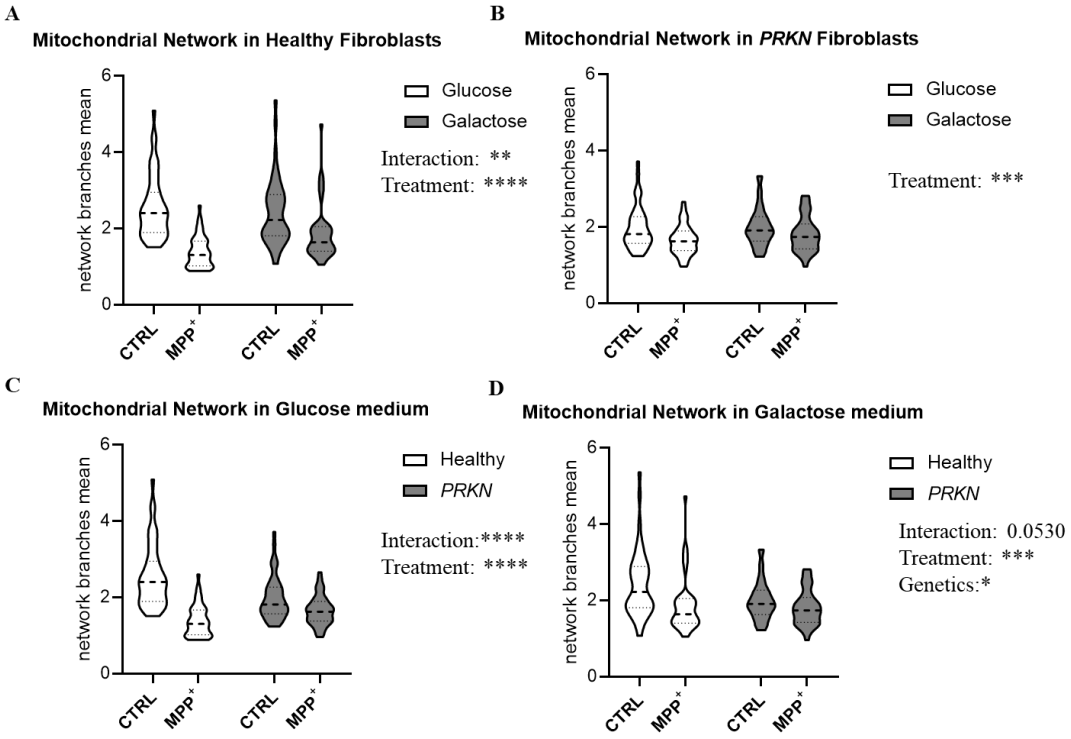

Fig. 4.20 Quantitative analysis of the mitochondrial network morphology upon metabolic reprogramming combined with MPP^+ treatment.

Fibroblasts from one healthy subject and one *PRKN*-mutated patient were analysed. A total number of 45 cells have been quantified per group. (A) Violin plots representing the measurement of network branches mean parameter in mitochondrial network analysis in healthy fibroblasts only, expressed as mean. Data were analysed by two-way ANOVA. "Interaction" (p = 0.0048; F = 8.170) and "Treatment" (p <0.0001; F = 65.41) resulted to be a significant source of variation. (B) Violin plots representing the measurement of network branches mean in PRKN-mutated fibroblasts only, expressed as mean. Data were analysed by two-way ANOVA. "Treatment" (p =0. 0005; F =12.68) resulted to be a significant source of variation. (C) Violin plots representing the measurement of network branches mean in standard culture conditions (glucose) expressed as mean. Data were analysed by two-way ANOVA. "Interaction" (p <0.0001; F = 25.37) and "Treatment" (p <0.0001; F = 80.27) resulted to be a significant source of variation. (D) Violin plots representing the measurement of branch length mean in galactose only and galactose treated with MPP^+ in both healthy and *PRKN*-mutated fibroblasts expressed as mean. Data were analysed by two-way ANOVA. "Treatment" (p=0.0002; F = 14.19) and "Genetics" (p =0.0135; F = 6.22) resulted to be a significant source of variation.

The evaluation of network branches mean parameter was assessed in one healthy fibroblasts cell line compared to one *PRKN*-mutated fibroblasts maintained in either glucose medium or galactose medium after 24h treatment with MPP^+. In control healthy fibroblasts the measurement of network branches mean was significantly affected by MPP^+ treatment ("Treatment", $p < 0.0001$; $F = 65.41$). Moreover, the parameter was differently affected according to the culture medium, specifically, it was observed a shortening in the network branches mean after metabolic reprogramming that was enhanced in glucose medium ("Interaction", $p = 0.0048$; $F = 8.170$) (Fig. 4.20A). In *PRKN*-mutated fibroblasts, treatment with MPP^+ significantly decreased in the branch length mean in both glucose and galactose medium ("Treatment", $p = 0.0005$; $F = 12.68$) (Fig. 4.20B). In glucose condition, the effect of MPP^+ significantly affected network branches mean in both control healthy and *PRKN*-mutated fibroblasts ("Treatment", $p < 0.0001$; $F = 80.27$) with a different extent in the different genetic background ("Interaction", ($p < 0.0001$; $F = 25.37$) (Fig. 4.20C). After metabolic reprogramming, the network branches mean was significantly reduced after MPP^+ treatment ("Treatment", $p = 0.0002$; $F = 14.19$) and it was also influenced by the genetic background ("Genetics", $p = 0.0135$; $F = 6.22$) (Fig. 4.20D).

4.4.2 Evaluation of mitochondrial markers protein levels after the combined treatment

After the assessment of the mitochondrial network morphology, which highlighted a significant reshaping in response to both metabolic switch and MPP^+ treatment, the quantification of the levels of two mitochondrial marker proteins (i.e., CS and COX5B) was performed by WB analysis (Fig. 4.21).

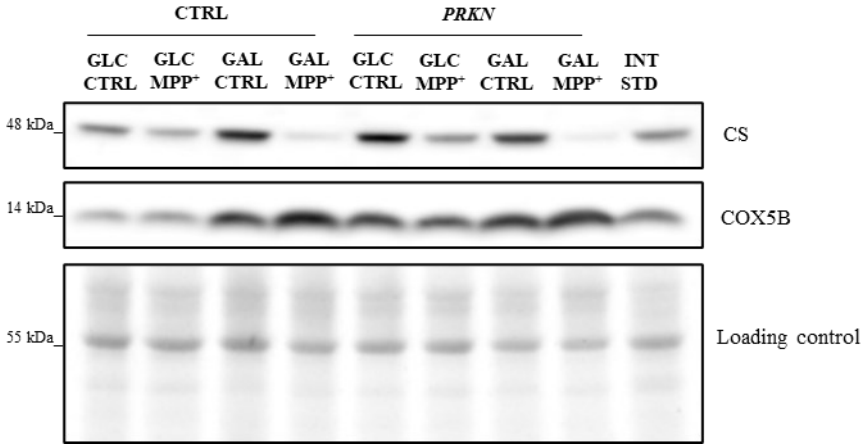

Fig. 4.21 Western blot analysis of mitochondrial markers after the combined treatment.
Representative Western blot images of CS and COX5B protein levels in one control and one patient-derived fibroblast cell lines, after metabolic reprogramming and MPP^+ treatment.

A striking effect of MPP^+ treatment was observed, especially in metabolically reprogrammed cells. Thus, at least three patient-derived fibroblast lines were compared with three controls and the effects of the three variables (i.e., genetic background, metabolic reprogramming, and MPP^+ treatment) and their possible interactions were analysed.

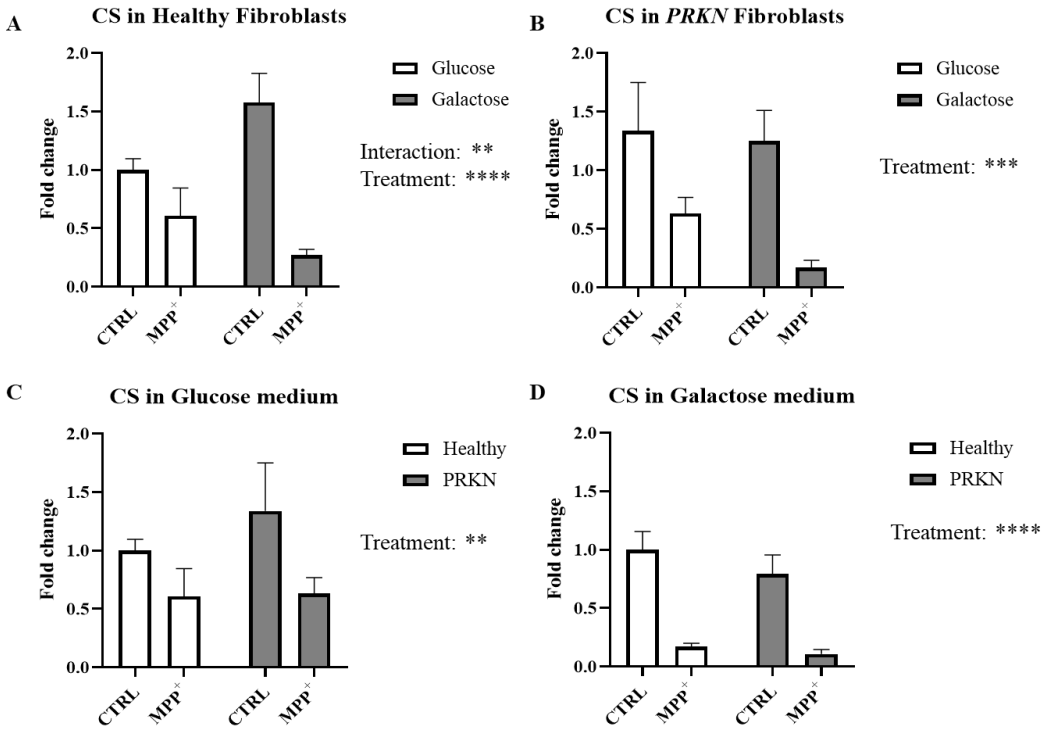

Fig. 4.22 Evaluation of CS levels upon metabolic reprogramming combined with MPP^+ treatment.
Fibroblasts from three healthy subjects and three *PRKN*-mutated patients were analysed. (A) Bars plot representing relative quantification of CS in healthy fibroblasts only, expressed as mean ± SD. Data were analysed by two-way ANOVA. "Interaction" (p = 0.0024; F = 19.14) and "Treatment" (p <0.0001; F = 66.30) resulted to be significant sources of variation. (B) Bars plot representing relative quantification of CS in *PRKN*-mutated fibroblasts only, expressed as mean ± SD relative to control conditions in healthy subjects. Data were analysed by two-way ANOVA. "Treatment" (p =0.0003; F =73.63) resulted to be a significant source of variation. (C) Bars plot representing relative quantification of CS in standard culture conditions (glucose) expressed as mean ± SD. Data were analysed by two-way ANOVA. "Treatment" (p = 0.0055; F = 14.18) resulted to be a significant source of variation. (D) Bars plot representing relative quantification of CS after metabolic reprogramming (galactose) expressed as mean ± SD. Data were analysed by two-way ANOVA. "Treatment" (p<0.0001; F = 129.1) resulted to be a significant source of variation.

The quantification of CS was assessed in three healthy fibroblasts cell lines compared to three *PRKN*-mutated fibroblasts maintained in either glucose medium or galactose medium after 24h treatment with MPP^+. In control healthy fibroblasts the level of CS was significantly deceased after MPP^+ treatment, both in glucose and galactose medium ("Treatment", p <0.0001; F = 66.30) (Fig. 4.22A). The reduction in CS level was greater in control healthy fibroblasts maintained in galactose medium ("Interaction", p = 0.0024; F = 19.14). In PRKN-mutated fibroblasts, treatment with MPP^+ significantly deceased the level of CS in both glucose and galactose medium ("Treatment", p =0.0003; F =73.63) (Fig. 4.22B). In glucose condition, the effect of MPP^+ significantly decrease CS in both control healthy and PRKN-mutated fibroblasts ("Treatment", p = 0.0055; F = 14.18) (Fig. 4.22C). The same statistically significant reduction was observed in galactose condition in both control healthy and PRKN-mutated fibroblasts ("Treatment", p<0.0001; F = 129.1) (Fig. 4.22D).

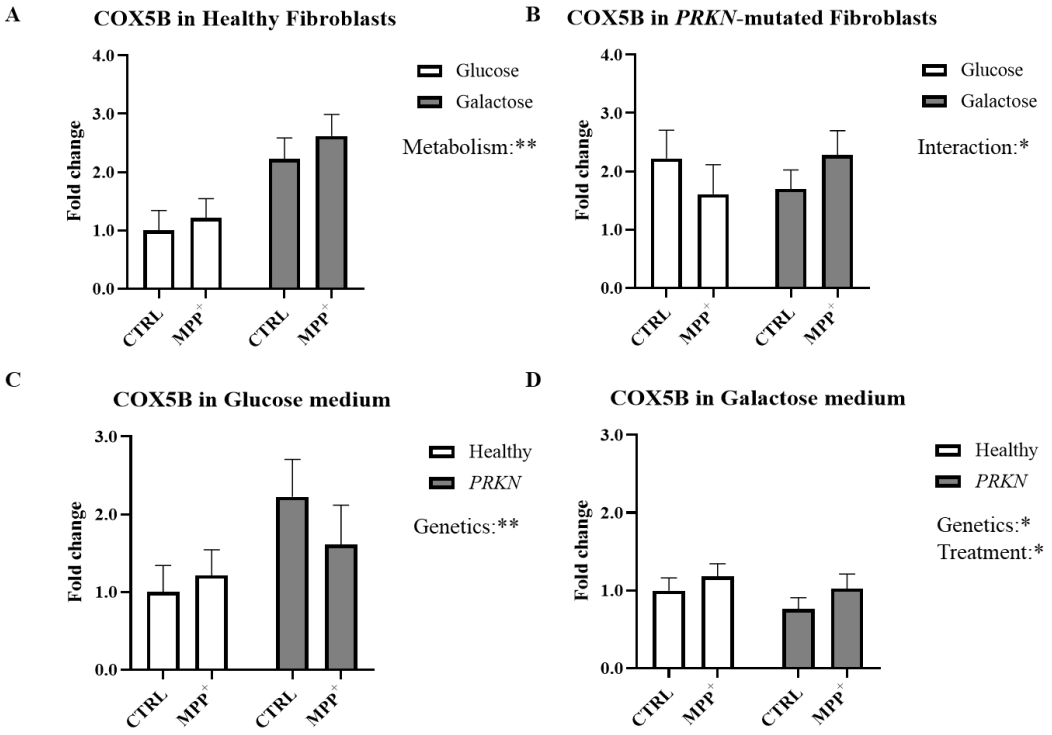

Fig. 4.23 Evaluation of COX5B levels upon metabolic reprogramming combined with MPP^+ treatment.
Fibroblasts from four healthy subjects and four *PRKN*-mutated patients were analysed. (A) Bars plot representing relative quantification of COX5B in healthy fibroblasts only, expressed as mean ± SD. Data were analysed by two-way ANOVA. "Metabolism" ($p< 0.0001$; $F = 56.68$) resulted to be a significant source of variation. (B) Bars plot representing relative quantification of COX5B in *PRKN*-mutated fibroblasts only, expressed as mean ± SD relative to control conditions in healthy subjects. Data were analysed by two-way ANOVA. "Interaction" ($p =0.0185$; $F =7.417$) resulted to be a significant source of variation. (C) Bars plot representing relative quantification of COX5B in standard culture conditions (glucose) expressed as mean ± SD. Data were analysed by two-way ANOVA. "Genetics" ($p = 0.0024$; $F = 14.67$) resulted to be a significant source of variation. (D) Bars plot representing relative quantification of COX5B after metabolic reprogramming (galactose) expressed as mean ± SD. Data were analysed by two-way ANOVA. "Treatment" ($p=0.0212$; $F = 7.022$) and "Genetics" ($p =0.0367$; $F = 5.525$) resulted to be significant sources of variation.

The quantification of COX5B was assessed in four healthy fibroblasts cell lines compared to four *PRKN*-mutated fibroblasts maintained in either glucose medium or galactose medium after 24h treatment with MPP^+. In healthy fibroblasts the level of COX5B was significantly increased after the change of medium into galactose ("Medium", p <0.0001; F = 56.68) (Fig. 4.23A). In *PRKN*-mutated fibroblasts the effect of MPP^+ on COX5B level was different according to the culture medium highlighting an interaction between factors (Fig. 4.23B). In glucose medium, the level of COX5B was reduced after MPP^+ treatment, while it was observed an accumulation after MPP^+ treatment in galactose medium ("Interaction", p =0.0185; F =7.417) (Fig. 4.23C). In glucose condition, it was not present a treatment effect, but the analysis underlined a genetics effect between healthy and *PRKN*-mutated fibroblasts ("Genetics", p = 0.0024; F = 14.67). In galactose condition, the level of COX5B was affected by both treatment and genetics effects ("Treatment", p=0.0212; F = 7.022; "Genetics", p =0.0367; F = 5.525) (Fig. 4.23D).

4.4.3 Investigation of Rab proteins dynamics after metabolic reprogramming and mitophagy induction in PRKN-mutated fibroblasts

After the analysis of the effects of the combined treatment on mitochondrial homeostasis, the levels of selected Rab proteins were analysed by WB analysis, namely RAB5, RAB7 and RAB9 (Fig. 4.24).

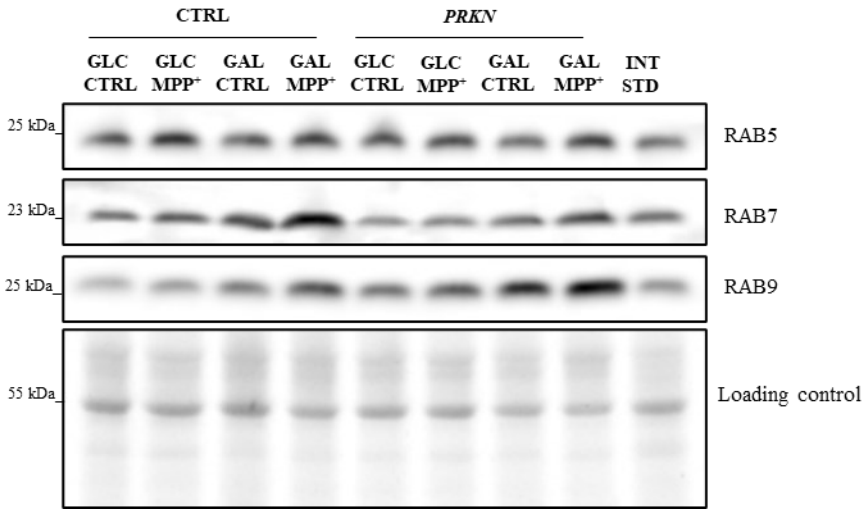

Fig. 4.24 Western blot analysis of Rab proteins after the combined treatment.
Representative Western blot images of RAB5, RAB7 and RAB9 protein levels in one control and one patient-derived fibroblast cell lines, after metabolic reprogramming and MPP^+ treatment.

Qualitatively, the levels of Rab proteins resulted to be influenced by both metabolic reprogramming and MPP^+ treatment. Thus, also here at least three patient-derived fibroblast lines were compared with three controls and the effects of the three variables (i.e., genetic background, metabolic reprogramming, and MPP^+ treatment) and their possible interactions were analysed.

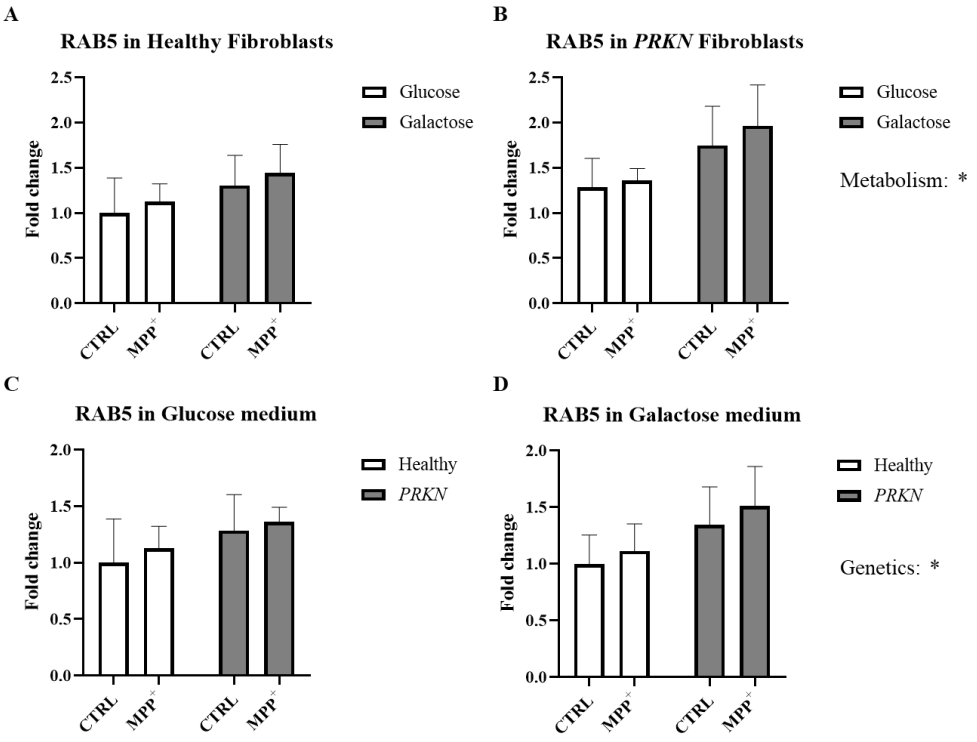

Fig. 4.25 Evaluation of RAB5 levels upon metabolic reprogramming combined with MPP^+ treatment.
Fibroblasts from four healthy subjects and three *PRKN*-mutated patients were analysed. (A) Bars plot representing relative quantification of RAB5 in healthy fibroblasts only, expressed as mean ± SD. Data were analysed by two-way ANOVA. (B) Bars plot representing relative quantification of RAB5 in *PRKN*-mutated fibroblasts only, expressed as mean ± SD relative to control conditions in healthy subjects. Data were analysed by two-way ANOVA. "Metabolism" (p =0.0116; F =8.856) resulted to be a significant source of variation. (C) Bars plot representing relative quantification of RAB5 in standard culture conditions (glucose) expressed as mean ± SD. Data were analysed by two-way ANOVA. (D) Bars plot representing relative quantification of RAB5 after metabolic reprogramming (galactose) expressed as mean ± SD. Data were analysed by two-way ANOVA. "Genetics" (p =0.0283; F = 6.215) resulted to be a significant source of variation for RAB5.

The quantification of RAB5 was assessed in four healthy fibroblasts cell lines compared to four *PRKN*-mutated fibroblasts maintained in either glucose medium or galactose medium after 24h treatment with MPP^+. In healthy fibroblasts the level of RAB5 was not significantly altered neither by MPP^+ treatment nor by the metabolic reprogramming (Fig. 4.25A). On the contrary, in *PRKN*-mutated fibroblasts the effect metabolism significantly increased the level of RAB5 ("Metabolism", p =0.0116; F =8.856) (Fig. 4.25B). In glucose medium, the level of RAB5 was not affected by the MPP^+ treatment and it was not observed any variation due to the genetic background (Fig. 4.25C). In galactose condition, it was observed a higher level of RAB5 in PD patients compared to controls ("Genetics", p =0.0283; F = 6.215) (Fig. 4.25D).

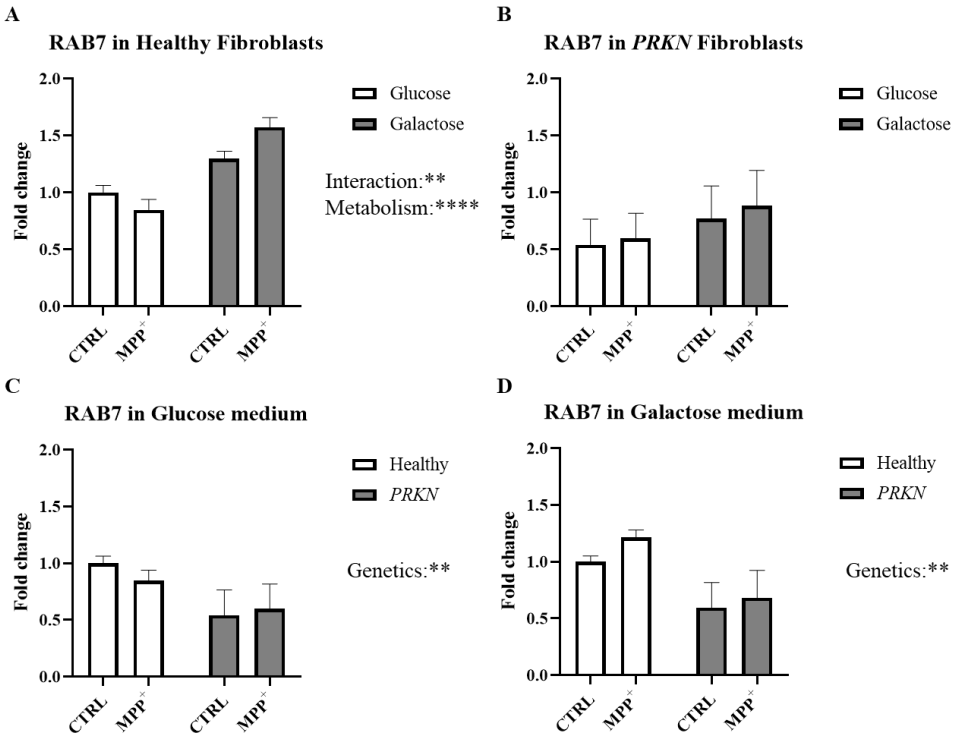

Fig. 4.26 Evaluation of RAB7 levels upon metabolic reprogramming combined with MPP$^+$ treatment.
Fibroblasts from three healthy subjects and three *PRKN*-mutated patients were analysed. (A) Bars plot representing relative quantification of RAB7 in healthy fibroblasts only, expressed as mean ± SD. Data were analysed by two-way ANOVA. "Metabolism" (p=0.0013; F = 23.41) and "Interaction" (p<0.0001; F = 132.6) resulted to be significant sources of variation. (B) Bars plot representing relative quantification of RAB7 in *PRKN*-mutated fibroblasts only, expressed as mean ± SD relative to control conditions in healthy subjects. Data were analysed by two-way ANOVA. (C) Bars plot representing relative quantification of RAB7 in standard culture conditions (glucose) expressed as mean ± SD. Data were analysed by two-way ANOVA. "Genetics" (p = 0.0063; F = 13.49) resulted to be a significant source of variation. (D) Bars plot representing relative quantification of RAB7 after metabolic reprogramming (galactose) expressed as mean ± SD. Data were analysed by two-way ANOVA. "Genetics" (p=0.0014; F = 22.89) resulted to be a significant source of variation for RAB7.

The quantification of RAB7 was assessed in three healthy fibroblasts cell lines compared to three *PRKN*-mutated fibroblasts maintained in either glucose medium or galactose medium after 24h treatment with MPP$^+$. In healthy fibroblasts, it was observed a general increase in RAB7 level after metabolic reprogramming ("Metabolism", p=0.0013; F = 23.41) (Fig. Xa). Moreover, the level of RAB7 was differently affected by MPP$^+$ treatment, in relation to the culture medium. RAB7 level showed a decrease in glucose medium, while after metabolic reprogramming there was an increase in its level, as described by the effect of interaction ("Interaction", p<0.0001; F = 132.6) (Fig. 4.26A). In *PRKN*-mutated fibroblasts the levels of RAB7 were not altered neither by the MPP$^+$ treatment nor by the metabolic reprogramming (Fig. 4.26B). In glucose medium, the level of RAB7 was lower in *PRKN*-mutated fibroblasts compared to healthy ones ("Genetics", p = 0.0063; F = 13.49) (Fig. 4.26C). In galactose condition, it was observed the difference between controls and PD patients, with lower level of RAB7 in PRKN-mutated fibroblasts ("Genetics", p =0.0014; F = 22.89) (Fig. 4.26D).

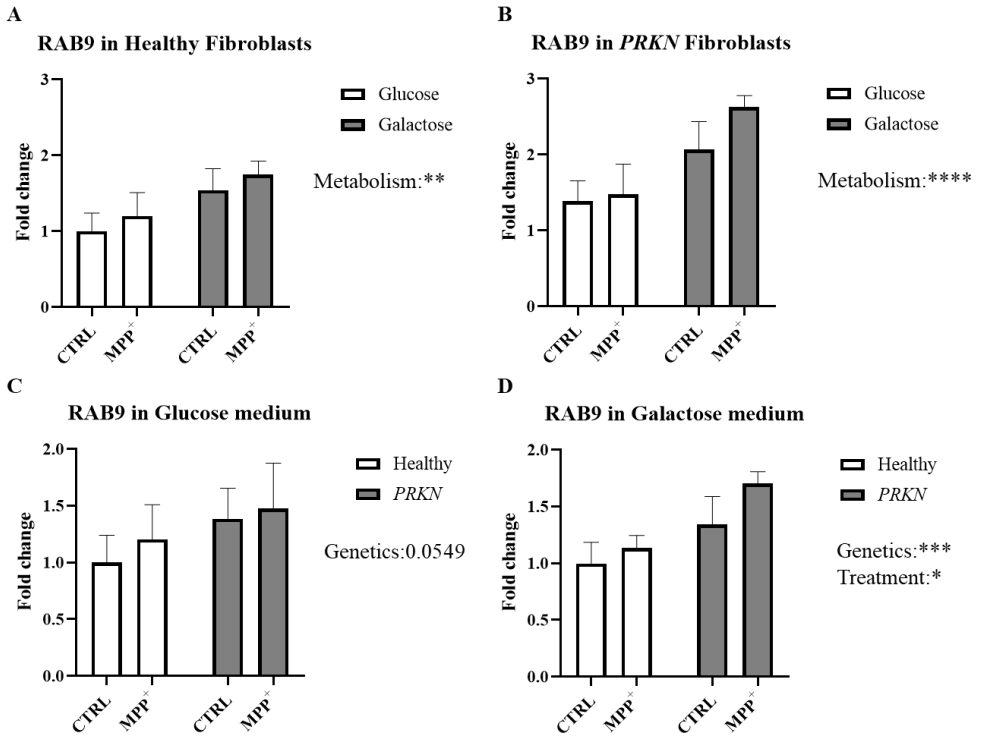

Fig. 4.27 Evaluation of RAB9 levels upon metabolic reprogramming combined with MPP$^+$ treatment.
Fibroblasts from three healthy subjects and three *PRKN*-mutated patients were analysed. (A) Bars plot representing relative quantification of RAB9 in healthy fibroblasts only, expressed as mean ± SD. Data were analysed by two-way ANOVA. "Metabolism" (p=0.0012; F = 17.82) resulted to be a significant source of variation. (B) Bars plot representing relative quantification of RAB9 in *PRKN*-mutated fibroblasts only, expressed as mean ± SD relative to control conditions in healthy subjects. Data were analysed by two-way ANOVA. "Metabolism" (p <0.0001; F =33.90) resulted to be a significant source of variation. (C) Bars plot representing relative quantification of RAB9 in standard culture conditions (glucose) expressed as mean ± SD. Data were analysed by two-way ANOVA. (D) Bars plot representing relative quantification of RAB9 after metabolic reprogramming (galactose) expressed as mean ± SD. Data were analysed by two-way ANOVA. "Genetics" (p=0.0137; F = 8.328) and "Treatment" (p =0.0002; F = 28.02) resulted to be significant sources of variation.

The quantification of RAB9 was assessed in four healthy fibroblasts cell lines compared to four *PRKN*-mutated fibroblasts maintained in either glucose medium or galactose medium after 24h treatment with MPP$^+$. In healthy fibroblasts the level of RAB9 was significantly increased after the change of medium into galactose ("Metabolism", p=0.0012; F = 17.82) (Fig. 4.27A). The same significant increase in RAB9 levels due to galactose medium was also observed in *PRKN*-mutated fibroblasts ("Metabolism", p <0.0001; F =33.90) (Fig. 4.27B). In glucose medium, the comparison between healthy and PRKN-mutated fibroblasts showed a tendency towards higher level of RAB9 in PD patients ("Genetics", p =0.0549) (Fig. 4.27C). In galactose condition, the level of RAB9 was affected by both treatment and genetics effects ("Treatment", p =0.0002; F = 28.02; "Genetics", p =0.0137; F = 8.328) (Fig. 4.27D). *PRKN*-mutated fibroblasts displayed a higher level of RAB9 after MPP$^+$ treatment after the metabolic reprogramming and this increase was higher compared to controls.

5 Discussion

In Parkinson's disease, genetic, aging and environmental exposure are described as synergistic factors in the development of the pathology. In addition to the progressive loss of dopaminergic neurons, both sporadic and familial forms share a common feature: mitochondrial dysfunction. From the initial studies correlating MPTP to parkinsonism (J. William Langston et al. 1983) and the first studies describing alterations in mitochondrial functions (A. H. V. Schapira et al. 1989), defects in the ETC complex I activity have been increasingly associated to PD pathology (Marella et al. 2009; Subrahmanian and LaVoie 2021b). Since mitochondria are involved in a wide spectrum of cellular functions such as metabolism, autophagy and intracellular signaling, mitochondrial homeostasis is at the basis of the wellbeing of cells, especially neuronal cells, whose metabolism is based on OXPHOS (Son and Han 2018). The prompt removal of damaged mitochondria via mitophagy is fundamental for the correct functioning of neurons and, in fact, many neurodegenerative diseases like PD show impairment in the mitophagic pathway (Clark et al. 2021). Mutations in the key regulators of mitophagy, PINK1 and Parkin, have been linked to genetic forms of PD (Youle and Narendra 2011). Many studies based on the use of mitochondrial toxins, such as MPP^+, and cellular models recapitulating mitophagic dysfunctions have helped in understanding the molecular mechanisms at the basis of PD pathology (Auburger et al. 2012; Zilocchi et al. 2018; 2020; Risiglione et al. 2020). The use of neuronal cell models displays many advantages among which representing the main cellular type affected, but other cells like fibroblasts represent a useful tool to model PD pathophysiology. Skin fibroblasts from PD patients present the same mutations and the cumulative cellular damage of neuronal populations (Auburger et al. 2012). Being primary cells, they represent a better model compared with immortalized cells, and they are affected by bioenergetics deficits that characterise early stages of PD (Auburger et al. 2012). Moreover, PINK1 and Parkin are highly expressed in fibroblasts, so that they can be exploited to study the mitophagic cascade (Auburger et al. 2012). Intensive investigations of mitophagic process have also highlighted the pivotal role of vesicular trafficking in the correct execution of mitochondrial disposal, pointing out the importance of key molecular players as Rab GTPases and the endo-lysosomal pathway (Singh and Muqit 2020).

In our laboratory, previous studies investigating mitochondrial and Rabs dynamics in control and *PRKN*-mutated fibroblasts have been already performed (Zilocchi et al. 2020). *PRKN*-mutated fibroblasts showed a reduced mitochondrial membrane potential, with no accumulation of PINK, even after CCCP treatment, and the analysis of the mitochondrial network morphology did not reveal any significant alterations. In this study was also highlighted the implications of Rab proteins in PD pathology. By using shotgun proteomics and systems biology analyses, Zilocchi and colleagues showed Rab proteins involvement in mitochondrial proteome alterations of *PRKN*-mutated fibroblasts compared to control. Interestingly, the study reported RAB7 recruitment to dysfunctional mitochondria without PINK1 accumulation.

Taken together these considerations, to further study mitochondrial alterations linked to PD, skin fibroblasts from control and *PRKN*-mutated patients were employed in this study. They have been used as a model to optimise a metabolic reprogramming protocol towards OXPHOS

in combination with mitochondrial toxin induced-mitochondrial stress, and ultimately exploited to characterise Rab proteins dynamics in PD pathology. To achieve this goal, a preliminary characterization of this cellular model was mandatory, also to investigate a possible role of this cellular population in the context of the peripheral dopaminergic system. Indeed, peripheral cells are earning attention in PD research not only as models to investigate the pathobiology of the disease but also for biomarker discovery and pharmacological studies. Thus, the presence and the levels of some markers of the cellular dopaminergic system were assessed in skin fibroblasts from both PD patients and healthy control subjects. The comparison was made including the human neuroblastoma SH-SY5Y cell line, which is known to be endowed with a complete dopaminergic system. The presence of specific transcripts was visualised after qRT-PCR, namely the five dopamine surface receptors, dopamine transporters, and the Tyrosine Hydroxylase (TH) enzyme involved in the synthesis of the neurotransmitter. As a result, all dopamine surface receptors resulted to be expressed in fibroblast cells, displaying a different pattern in *PRKN*-mutated fibroblasts with respect to control ones. This evidence suggests the possible expression of specific receptor isoforms linked to Parkin loss of function. By contrast, fibroblasts do not express DAT1, supporting the fact that these cells cannot uptake dopamine. However, the expression of the vesicular transporters VMAT1 and VMAT2 was observed, suggesting that fibroblasts can have a rudimental system for catecholamines storage. This aspect is important to correctly interpret the effects of the treatment with mitochondrial toxins that mimic the action of dopamine, such as MPP^+. Indeed, it has been demonstrated that VMAT2 is responsible for the transport and storage of MPP^+ inside vesicles, thus sequestering the drug and limiting the effectiveness of the treatment (Guillot and Miller 2009). Eventually, the expression of TH was not detectable in fibroblasts; this is not surprising since there is no evidence for dopamine synthesis in these cells. To obtain a definitive confirmation of these results, a quantitative assessment will be performed using fibroblasts from all healthy and *PRKN*-mutated subjects. This will give a clear picture of the relative levels and pattern of expression of the markers investigated. In addition, the analysis will be performed also at the protein level, to verify and quantify the presence of the protein products. Collectively, this preliminary characterization of the cellular model of choice provided new evidence for an active role of fibroblast cells in the peripheric dopaminergic system, together with other cells types that have been described to have this role, such as peripheral blood mononuclear cells (Alberio et al. 2011), adipocytes, and endothelial cells (Amenta et al. 2002). Of note, the expression of dopamine receptors on fibroblasts suggests a possible usage of these cells as a model for pharmacological studies. For instance, the toxicity and off-target effects of dopamine agonist drugs may be assessed using this cellular model.

After this characterization of dopamine-related features in fibroblast cells, the next step was the optimization of a protocol for mitochondrial stress and mitophagy induction, owing that their metabolism and sensitivity to mitochondrial insults are different from those of neuronal cells.

In this work both physical and chemical insults were taken into consideration to challenge mitochondrial homeostasis. Starting from physical insults, the first that was tested was the change of culture temperature to induce a hypothermic stress. The protocol described by Bonello and colleagues involved a mild hypothermic stress induced by placing fibroblasts at

24°C degrees for 45 minutes (Bonello et al. 2019). The same protocol was applied to control fibroblasts (from healthy donors) and the effect of this shift in temperature was assessed by mitochondrial membrane potential analysis, network morphology analysis, and mitochondrial marker proteins levels evaluation, using CCCP treatment as a positive control of mitophagy induction. Following mild hypothermic stress, it was not observed any alteration in mitochondrial membrane potential nor changes in mitochondrial network morphology. From the protein levels assessment, mitochondrial mass (COX5B) and mitochondrial dynamics (OPA1) were not altered. Moreover, PINK1 accumulation was not observed, suggesting that mild hypothermic stress was not sufficient to trigger mitophagy. The absence of al terations in mitochondrial dynamics could be ascribed to the short duration of the stress, therefore, the protocol was modified prolonging the exposure time from 45 min to 24h. The effect of this "chronic" hypothermic stress was assessed by mitochondrial membrane potential and mitochondrial marker protein levels evaluations. Also in this case, mitochondrial membrane potential was not altered and there were no changes in mitochondrial marker proteins levels (COX5B, OPA1 and PINK1). Being hypothermic stress a very nonspecific insult, a possible explanation for the unaltered mitochondrial homeostasis is that a generic cellular stress response is triggered instead of a specific mitochondrial one. Since mitophagy is the specific mechanism for dysfunctional mitochondria disposal, the adaptive response mounted by cells might involve autophagy instead of mitophagy, or simply be too mild, although in disagreement with the work of Bonello and colleagues on the same cells.

Discarding the possibility of using mild physical insults, the alternative strategy to provoke mitochondrial insults in the cellular model of choice was to use chemical insults, specifically targeting the ETC complex I activity. Rotenone and MPP^+ are well known complex I blockers, whose mechanism of action is widely characterised in neuronal cells. The advantages of using these two compounds are the direct link with PD pathology, since they are used to generate both *in vivo* and *in vitro* model of PD, and the specificity of their mechanism of action. Since their application in non-neuronal cells is poorly described, an initial step of optimization of treatment conditions was necessary. For both toxins several concentrations were selected gathering data from literature (Ambrosi et al. 2014; Carrion et al. 2018; Zilocchi et al. 2018). They were then used to treat control fibroblasts and eventually choose treatment conditions. The first aspect evaluated was cell viability, thus estimating the effects of both treatments and narrow the conditions range to be further tested. Mitochondrial markers were used to estimate any variations in mitochondrial mass (COX5B) and mitochondrial dynamics (OPA1). These evaluations were fundamental to select a single concentration. For MPP^+ the mechanism of entrance is poorly understood, although suggested to rely on specific OCT transporters. The evaluation of treatment effectiveness was assessed taking into consideration markers of all three mitochondrial compartments: TOMM20 for the OMM, COX5B for the IMM and CS for the mitochondrial matrix. From the data obtained, MPP^+-induced mitochondrial stress was effective, provoking a significant reduction of two markers (CS and COX5B) out of three. The unvaried levels of TOMM20 despite the decrease of the other marker of the total mitochondrial mass (i.e., COX5B) prompted us to verify the activity and specificity of the antibody against TOMM20 by indirect immunofluorescence (data not shown). The antibody resulted to be nonspecific in the recognition of mitochondrial structures and for this reason it was not used in

other experiments. In control fibroblasts treated with Rotenone, only COX5B levels were evaluated as indicator of the mitochondrial mass. No alterations in COX5B levels were observed upon Rotenone treatment at the selected concentration. In addition to WB analysis, a more functional evaluation was performed using flow cytometry analysis. Control fibroblasts treated with either Rotenone or MPP^+, and CCCP used as positive control, were stained with mitotracker probe and then analysed by flow cytometry. The main advantages of this technique were i) the evaluation of a greater number of cells compared to a standard fluorescence analysis, and ii) the simplified experimental workflow, so that it was possible to simultaneously perform a comparative analysis between the two complex I inhibitors. From the flow cytometry analysis, MPP^+ treatment resulted more effective in mitochondrial depolarization induction than Rotenone. Moreover, Rotenone should be dissolved in DMSO, which is known to have aspecific toxic effects, thus limiting the possibility to increase Rotenone (and related DMSO) concentration above a certain threshold. Owing this, MPP^+ was selected as the mitochondrial toxin to be used in both control and *PRKN*-mutated fibroblasts in combination with the metabolic reprogramming, which was set up in parallel.

Recent studies have highlighted how the use of different sources of carbohydrates from glucose like galactose can be exploited to enhance mitochondrial metabolism, thus representing a good model to study mitochondrial dysfunctions in neurodegenerative diseases like PD (Aguer et al. 2011; Pinho et al. 2022; Protasoni and Taanman 2023). In order to make both control and *PRKN*-mutated fibroblasts more sensitive to mitochondrial insults, the gradual change from glucose medium to galactose medium described by Pinho and colleagues (Pinho et al. 2022) was applied to one control fibroblasts cell line and one *PRKN*-mutated fibroblasts cell line as a preliminary trial. The concentration of galactose powder dissolved in the culture medium was selected according to the most common condition found in literature. Once glucose medium was completely replaced with galactose medium, fibroblasts were kept in this culture condition for at least 2-3 doubling times prior to analysis, as suggested by Protasoni and colleagues (Protasoni and Taanman 2023). To evaluate the effectiveness of the metabolic reprogramming, it was assessed the level of two mitochondrial marker proteins representing the IMM (COX5B) and the mitochondrial matrix (CS). Specifically, both control and *PRKN*-mutated fibroblasts showed a qualitative increase in COX5B and more strikingly in CS levels. From the above-mentioned studies, the data collected to address the effectiveness of metabolic reprogramming were mainly related to mitochondrial enzymes and ETC complexes activity and mitochondrial respiration assays. With our molecular markers aligning with previous functional assays, we chose to use COX5B and CS as indicators of successful reprogramming for further studies.

After the optimization of both experimental set-ups to be applied, control and *PRKN*-mutated fibroblasts were finally challenged with both mitochondrial stress induction and metabolic reprogramming. Collectively, the four conditions which were always investigated in control and *PRKN*-mutated fibroblasts were fibroblasts maintained in standard culture medium (glucose), fibroblasts cultured in galactose medium, fibroblasts treated with MPP^+ in standard culture medium and fibroblasts treated with MPP^+ after metabolic reprogramming (galactose medium). The first observation that was done, although qualitative, was the evaluation of morphological changes in both control and *PRKN*-mutated fibroblasts recorded by light microscopy. Upon MPP^+-treatment combined with metabolic reprogramming, healthy and PD

patients' fibroblasts showed a different diffraction pattern resulting more transparent and displaying morphological changes. Further imaging analysis were performed to better characterise the mitochondrial network morphology.
The quantitative assessment of the visible differences in the morphology of the mitochondrial network was performed by the evaluation of some specific parameters that describe the length and connectivity of network branches, i.e., branch length, network branches, and summed branch length. The branch length mean is the mean length of all the lines used to represent the mitochondrial structures. The summed branch lengths mean is the mean of sum of all branch lengths divided by the number of independent skeletons. The network branches mean is the mean number of attached lines used to represent each structure. To represent these data, violin plots were used to better highlight the presence of different cell populations in each experimental condition (subpopulations more sensitive or more resilient to MPP^+ treatment). Moreover, since the variables to be considered were many, namely mutations causing the disease (genetics), the metabolic reprogramming (metabolism), and the MPP^+ treatment (treatment), a statistical strategy was set-up to analyse data in all the combination studies. In particular, two two-way ANOVAs were used: the first to compare the effect of mitophagy induction in metabolically reprogrammed fibroblasts (separately in healthy controls' and PD patients' fibroblasts), the second to compare healthy controls' and PD patients' fibroblasts (separately in Glucose and Galactose medium).

The three network morphological parameters mentioned above are strictly related to one another. The data deriving from the branch length mean and the summed branch length mean parameters can be grouped together since, beside showing the same statical significances in all conditions, the summed branch mean derives from the branch length mean parameter. In control fibroblasts, treatment and interaction factors resulted statistically significant, meaning a different effect of the MPP^+ treatment after metabolic reprogramming. From the representative images, it is visible how after MPP^+-treatment the entire morphology shifts from a tubular one (standard culture medium) to a more dotted one. This fragmentation was more evident in glucose medium compared to galactose medium. The lower length of mitochondrial branches, also mirrored from the summed branch mean parameter, can be linked to fission process activated by the treatment. Before mitophagy occurs, mitochondrial network must isolate the dysfunctional part in order to be disposed. This effect is clear in standard culture conditions and other cellular models recapitulating PD after either CCCP or MPP^+ treatment described the same morphological changes (Bondi et al. 2016; H.-J. Ma et al. 2020). The less pronounced decrement in branch length mean and summed branch lengths mean after MPP^+ treatment in galactose cultured fibroblasts can be ascribed to the effect of metabolic reprogramming. In fact, although not statistically significant, the analysis reported a tendency ($p=0.0537$) toward longer measurements in the branch length mean. This tendency was not paralleled in the summed branch lengths mean ($p=0.0674$), probably because the positive effect in prolonging the branches after the metabolic reprogramming is diluted due to the way of calculating the parameter: all branch lengths divided by the number of mitochondrial structures.
In *PRKN*-mutated fibroblasts, statistical analysis showed a treatment effect in both glucose and galactose conditions. From the representative images, the mitochondrial network from treated *PRKN*-mutated fibroblasts resulted highly fragmented, even more compared to healthy control

fibroblasts. To sum up, the effect of treatment was detected in both culture media and in both genetic backgrounds. In line with this, images from transmission electron microscopy in PD fibroblasts after MPP^+-treatment highlighted fragmented mitochondria showing reduced and disorganized cristae (Carrion et al. 2018). Moreover, the absence of an interaction effect in the galactose-maintained cells can be ascribed to an increase in the branches length that compensates the treatment effect. Another parameter that was taken into consideration was the network branches mean. The MiNA tool recognises "networks" as the mitochondrial structures with at least a single node and three branches, thus representing an indicator of network ramification. In control fibroblasts, the effect of MPP^+ provoked a decreased in the network branches mean that was higher in glucose medium and less evident in galactose, as described by an interaction effect. In *PRKN*-mutated fibroblasts only a treatment effect was observed, with no differences related to the metabolism. The data were then analysed separating all the conditions according to the culture medium. In glucose-maintained fibroblasts, it was highlighted a treatment effect and an interaction effect (genetics effect was $p=0.06$), while in galactose-maintained fibroblasts it was observed a treatment and a genetics effect with a tendency for the interaction of both ($p=0.0530$). Taken together, these data showed how the network branches mean was significantly affected by the treatment in both genetic backgrounds and that in control fibroblasts this effect was also differently effective according to the culture medium. Moreover, clustering the conditions based on the culture medium, it was possible to highlight a treatment and interaction effect only in glucose-maintained fibroblasts, meaning that the effect of MPP^+ treatment in *PRKN*-mutated fibroblasts, although significant, was less evident than in control fibroblasts. This can be explained by the presence of an already less branched mitochondrial network. In fact, after metabolic reprogramming, the effect of MPP^+ treatment in *PRKN*-mutated fibroblasts, although significant, was not comparable to control fibroblast. In line with this, a tendency for the interaction between genetics and treatment factors ($p=0.053$) in the galactose-maintained fibroblasts was observed, suggesting a different response to the metabolic reprogramming according to the genetic background, that attenuate the MPP^+-induced alteration to the mitochondrial network ramification only in control fibroblasts.

Following these morphological analyses, the effect of the MPP^+ treatment combined with metabolic reprogramming was tested considering CS and COX5B levels. The level of CS was significantly decreased after MPP^+ treatment, this reduction was evident in control and *PRKN*-mutated fibroblasts either considering cells maintained in standard culture condition (glucose), and after the metabolic reprogramming. In control fibroblasts, it was also observed an interaction effect between treatment and metabolism, suggesting a stronger reduction in CS after the metabolic reprogramming. Future analysis with an increased number of samples may underline an effect of metabolism too, since the level of CS in galactose-maintained control fibroblasts seems higher than in glucose condition. In PD patients, although the analysis did not show any difference in CS level compared to controls at the baseline, the level of CS in glucose-maintained cells were similar to those of galactose-maintained cells, explaining the absence of variations in CS levels after the metabolic reprogramming and no effect of the interaction. The data were then analysed separating all the conditions according to the culture medium. From these comparisons it was observed how the level of CS was significantly

affected by the treatment before and after the metabolic reprogramming independently from the genetic background. CS was found to be higher in *PRKN*-mutated fibroblasts compared to control in standard culture conditions. This is in line with an already described increased enzymatic activity in correlation to *PRKN* mutations (Grünewald et al. 2010). Previous studies have already described a higher enzymatic CS activity in cells, among which fibroblasts, maintained in galactose medium (Aguer et al. 2011; Protasoni and Taanman 2023). Further experiments implementing the number of samples are necessary to better characterise CS level and activity after metabolic reprogramming.

Regarding the level of COX5B, in glucose condition it was highlighted a genetics effect according to which PD patients show a higher level of COX5B. The effect of the metabolic reprogramming in increasing its level was only detected in control fibroblasts. However, in *PRKN*-mutated fibroblasts the data underlined an interaction effect, since in control fibroblasts COX5B level decreases after MPP^+ treatment, but in PD derived cells this trend is reversed. In line with this, in galactose-maintained cells it was observed a genetics effect. Moreover, data showed how the combined effect of MPP^+ treatment and metabolism increased the level of COX5B in both genetic backgrounds. Little is known about the protein levels of COX5B in PD since the most studied aspect regards its activity. However, it has been demonstrated the link between mitochondrial network morphology and cristae remodelling with ETC complex IV (Cogliati, Enriquez, and Scorrano 2016b). Thus, the genetics effect observed in glucose-maintained fibroblasts could be related to the alterations in branch length described before. Moreover, being already increased, the level of COX5B was not altered by metabolic reprogramming in *PRKN*-mutated fibroblasts as in control ones. The already higher level of COX5B in *PRKN*-mutated fibroblasts could be explained by a compensatory effect. Complex I, III and IV, interact together to form a supercomplex called respirasome (Reyes-Galindo et al. 2019). Dysfunction in complex I activity are commonly associated to *PRKN* mutation (Pacelli et al. 2011). Thus, to compensate for alterations in complex I activity, mitochondria may exert an adaptive response by modulating other components of the ETC. On the contrary, the higher level of COX5B in control fibroblasts could be a response from healthy mitochondria to provide for OXPHOS boosting.

After the evaluation of mitochondrial markers, the alteration of RAB proteins upon metabolic reprogramming combined with MPP^+ treatment was investigated. RAB5 level was not affected by the treatment nor by metabolism in control fibroblasts, whereas in *PRKN*-mutated fibroblasts RAB5 level was significantly increased after metabolic reprogramming. RAB5 increment in *PRKN*-mutated fibroblasts after metabolic reprogramming can be related to an attempt to recruit early endosomes, since it has been demonstrated that RAB5 recruitment is involved in the early steps of mitophagy (Yamano et al. 2018). Clustering data according to the medium highlighted a genetics effect in galactose-maintained fibroblasts.

RAB7 level was not affected in PRKN-mutated fibroblasts neither by MPP^+ treatment nor by metabolism. On the contrary, in control fibroblasts it was observed a significant effect of the metabolic reprogramming. Moreover, it was underlined an interaction effect showing a decrease in RAB7 level after MPP^+ treatment in glucose medium and an increase in galactose-maintained fibroblasts. A clear genetics effect was visible before and after metabolic

reprogramming. In *PRKN*-mutated fibroblasts there is a lower level of RAB7 compared to controls. This reduction is observed in both glucose-maintained cells and in galactose-maintained cells. This is in line with the Parkin-mediated recruitment of both RAB5 and RAB7 (Yamano et al. 2018), that in these cells is hampered.

RAB9 was significantly more abundant after metabolic reprogramming in both control and *PRKN*-mutated fibroblasts. In galactose-maintained fibroblasts, there was a significant increment in RAB9 level due to genetics and MPP^+ treatment. Interestingly, RAB9 level is significantly higher in metabolically reprogrammed *PRKN*-mutated fibroblasts after MPP^+ treatment with respect to healthy control fibroblasts, thus suggesting the up-regulation of an alternative Parkin-independent mitophagy and an attempt to eliminate dysfunctional mitochondria (Saito et al. 2019). However, it was already observed that dysfunctional mitochondria accumulate in these cells rather than being disposed (Zilocchi et al. 2020).

Being aware that these interpretations are based on the assessment of total protein extracts, further analyses focusing on functional assays are necessary. This model of metabolic reprogrammed fibroblasts toward OXPHOS, thus metabolically more similar to neurons, can be further exploited in the study of PD pathology. Evaluations of mitochondrial marker proteins levels on mitochondrial extracts and immunofluorescence investigating the localisation of Rab proteins are needed to better understand the effect of these two experimental conditions combined. Moreover, in vision of better characterise the effects of metabolic reprogramming, enzymatic activity evaluation and mitochondrial respiration assessment must be further explored.

6 Conclusion

In conclusion, primary human skin fibroblasts proved to be a useful model for studying the crosstalk between mitochondrial dysfunction and vesicular trafficking alterations in PD pathology. From the preliminary characterization of the dopaminergic system in these cells, they showed dopamine-related features, further supporting the role of peripheral cells in both the pathobiology of the disease and the response to pharmacological treatments. To challenge mitochondria and mimic the selective dopaminergic neurons degeneration, among the investigated physical and chemical insults, MPP^+ treatment was selected as the tool to trigger mitophagy in this study. Moreover, since another crucial aim was to render fibroblasts more similar to neurons from a metabolic perspective, the main take-home messages of this project are focused on galactose-maintained *PRKN*-mutated fibroblasts compared to controls (summarized in Fig. 6.1):

- **MPP^+** treatment (500 μM, 24h) was effective in triggering mitochondria depolarization, mitochondrial network fragmentation, and a reduction of the mitochondrial mass.
- The **morphological analysis** of the mitochondrial network revealed an already more fragmented network in PD samples compared to controls.
- **COX5B** was significantly increased after MPP^+ treatment in both genetic backgrounds, probably for a rebound effect (an increase of Complex IV activity, due to the blockade of Complex I). Moreover, *PRKN*-mutated fibroblasts showed a lower level of COX5B compared to control ones at the basal level, possibly mirroring some metabolic rearrangements.
- **CS** is a reliable marker for mitochondrial mass in our system. After MPP^+ treatment it was observed a decrease in both genetic backgrounds. *PRKN*-mutated fibroblasts showed lower CS levels at the basal level and, even more strikingly, after mitophagy induction.
- **RAB5** was found to be more abundant in *PRKN*-mutated fibroblasts only after metabolic reprogramming, with no effect observed from MPP^+ treatment. This could be associated with early endosome recruitment as an initial step in mitophagy (prior to Parkin involvement) or could represent a transcriptional program aimed at mitochondrial disposal (which would ultimately fail due to the absence of Parkin).
- *PRKN*-mutated fibroblasts showed a lower level of **RAB7** compared to control fibroblasts. This data is in line with the presence of Parkin loss-of-function mutations that prevent RAB7 Parkin-mediated recruitment to initiate mitophagy.
- Finally, the data on **RAB9** were the most interesting. An increase in RAB9 levels was observed in PRKN-mutated fibroblasts both at the basal level and after MPP^+ treatment. In both conditions, this may indicate a possible activation of RAB9-mediated mitophagy as an alternative to the dysfunctional PINK1/Parkin-mediated pathway in PD patients. We already know, however, that this is not sufficient to eliminate dysfunctional mitochondria in PRKN-mutated fibroblasts.

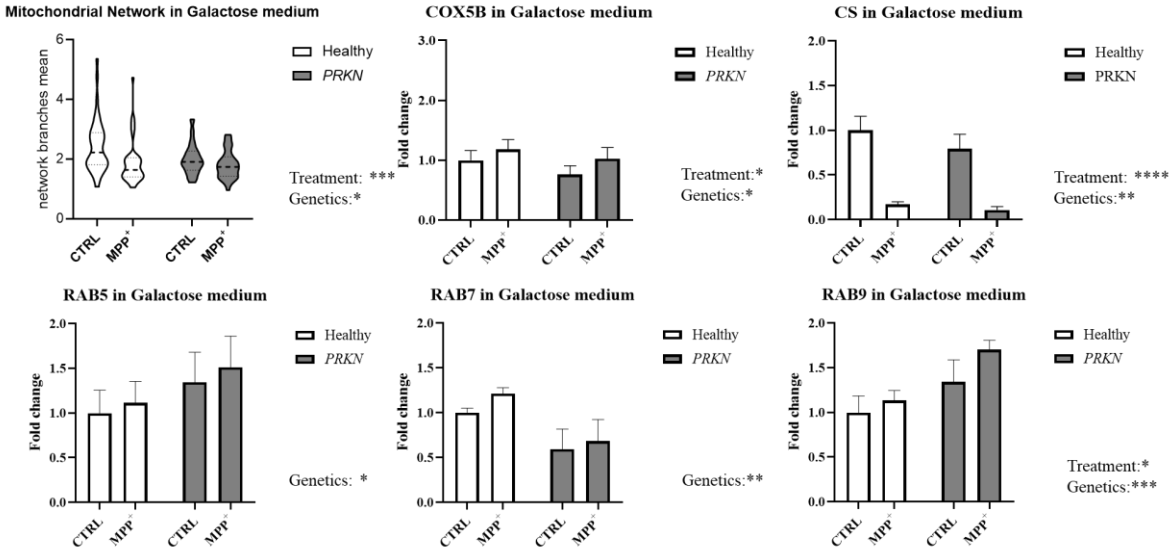

Fig. 6.1 Summary of all results related to metabolically reprogramed control and *PRKN*-mutated fibroblasts after MPP$^+$ treatment.

7 Bibliography

Aguer, Céline, Daniela Gambarotta, Ryan Mailloux, Cynthia Moffat, Robert Dent, Ruth Mcpherson, and Mary-Ellen Harper. 2011. 'Galactose Enhances Oxidative Metabolism and Reveals Mitochondrial Dysfunction in Human Primary Muscle Cells'. *PloS One* 6 (December):e28536. https://doi.org/10.1371/journal.pone.0028536.

Alberio, Tiziana, Claudia Anchieri, Luca Piacentini, Giovanna Gentile, Maurizio Simmaco, Mara Biasin, and Mauro Fasano. 2011. 'Proteomic Characterization of Jurkat T Leukemic Cells after Dopamine Stimulation: A Model of Circulating Dopamine-Sensitive Cells'. *Biochimie* 93 (5): 892–98. https://doi.org/10.1016/j.biochi.2011.01.015.

Alberio, Tiziana, Leonardo Lopiano, and Mauro Fasano. 2012. 'Cellular Models to Investigate Biochemical Pathways in Parkinson's Disease'. *The FEBS Journal* 279 (7): 1146–55. https://doi.org/10.1111/j.1742-4658.2012.08516.x.

Ambrosi, Giulia, Cristina Ghezzi, Sara Sepe, Chiara Milanese, Cesar Payan-Gomez, Cintia R. Bombardieri, Marie-Therese Armentero, et al. 2014. 'Bioenergetic and Proteolytic Defects in Fibroblasts from Patients with Sporadic Parkinson's Disease'. *Biochimica et Biophysica Acta (BBA) - Molecular Basis of Disease* 1842 (9): 1385–94. https://doi.org/10.1016/j.bbadis.2014.05.008.

Amenta, F., A. Ricci, S. K. Tayebati, and D. Zaccheo. 2002. 'The Peripheral Dopaminergic System: Morphological Analysis, Functional and Clinical Applications'. *Italian Journal of Anatomy and Embryology = Archivio Italiano Di Anatomia Ed Embriologia* 107 (3): 145–67.

Amo, Taku, Shigeto Sato, Shinji Saiki, Alexander M. Wolf, Masaaki Toyomizu, Clement A. Gautier, Jie Shen, Shigeo Ohta, and Nobutaka Hattori. 2011. 'Mitochondrial Membrane Potential Decrease Caused by Loss of PINK1 Is Not Due to Proton Leak, but to Respiratory Chain Defects'. *Neurobiology of Disease* 41 (1): 111–18. https://doi.org/10.1016/j.nbd.2010.08.027.

Araiso, Yuhei, Kenichiro Imai, and Toshiya Endo. 2022. 'Role of the TOM Complex in Protein Import into Mitochondria: Structural Views'. *Annual Review of Biochemistry* 91 (1): 679–703. https://doi.org/10.1146/annurev-biochem-032620-104527.

Ashrafi, G., and T. L. Schwarz. 2013. 'The Pathways of Mitophagy for Quality Control and Clearance of Mitochondria'. *Cell Death & Differentiation* 20 (1): 31–42. https://doi.org/10.1038/cdd.2012.81.

Auburger, Georg, Michael Klinkenberg, Jessica Drost, Katrin Marcus, Blas Morales-Gordo, Wolfram S. Kunz, Ulrich Brandt, et al. 2012. 'Primary Skin Fibroblasts as a Model of Parkinson's Disease'. *Molecular Neurobiology* 46 (1): 20–27. https://doi.org/10.1007/s12035-012-8245-1.

Banerjee, Rebecca, Anatoly A. Starkov, M. Flint Beal, and Bobby Thomas. 2009. 'Mitochondrial Dysfunction in the Limelight of Parkinson's Disease Pathogenesis'. *Biochimica et Biophysica Acta (BBA) - Molecular Basis of Disease*, Parkinson's Disease, 1792 (7): 651–63. https://doi.org/10.1016/j.bbadis.2008.11.007.

Bentivoglio, A. R., P. Cortelli, E. M. Valente, T. Ialongo, A. Ferraris, A. Elia, P. Montagna, and A. Albanese. 2001. 'Phenotypic Characterisation of Autosomal Recessive PARK6-Linked Parkinsonism in Three Unrelated Italian Families'. *Movement Disorders: Official Journal of the Movement Disorder Society* 16 (6): 999–1006. https://doi.org/10.1002/mds.10034.

Betarbet, Ranjita, Todd B. Sherer, Gillian MacKenzie, Monica Garcia-Osuna, Alexander V. Panov, and J. Timothy Greenamyre. 2000. 'Chronic Systemic Pesticide Exposure Reproduces Features of Parkinson's Disease'. *Nature Neuroscience* 3 (12): 1301–6. https://doi.org/10.1038/81834.

Bezard, Erwan, Christian E. Gross, Marie-Christine Fournier, Sandra Dovero, Bertrand Bloch, and Mohamed Jaber. 1999. 'Absence of MPTP-Induced Neuronal Death in Mice Lacking

the Dopamine Transporter'. *Experimental Neurology* 155 (2): 268–73. https://doi.org/10.1006/exnr.1998.6995.

Bondi, Heather, Mara Zilocchi, Maria Gabriella Mare, Gianluca D'Agostino, Stefano Giovannardi, Santiago Ambrosio, Mauro Fasano, and Tiziana Alberio. 2016. 'Dopamine Induces Mitochondrial Depolarization without Activating PINK1-Mediated Mitophagy'. *Journal of Neurochemistry* 136 (6): 1219–31. https://doi.org/10.1111/jnc.13506.

Bonello, Fiona, Sidi-Mohamed Hassoun, François Mouton-Liger, Yea Seul Shin, Adeline Muscat, Christelle Tesson, Suzanne Lesage, et al. 2019. 'LRRK2 Impairs PINK1/Parkin-Dependent Mitophagy via Its Kinase Activity: Pathologic Insights into Parkinson's Disease'. *Human Molecular Genetics* 28 (10): 1645–60. https://doi.org/10.1093/hmg/ddz004.

Brito, Olga Martins de, and Luca Scorrano. 2008. 'Mitofusin 2 Tethers Endoplasmic Reticulum to Mitochondria'. *Nature* 456 (7222): 605–10. https://doi.org/10.1038/nature07534.

Burns, R. S., P. A. LeWitt, M. H. Ebert, H. Pakkenberg, and I. J. Kopin. 1985. 'The Clinical Syndrome of Striatal Dopamine Deficiency. Parkinsonism Induced by 1-Methyl-4-Phenyl-1,2,3,6-Tetrahydropyridine (MPTP)'. *The New England Journal of Medicine* 312 (22): 1418–21. https://doi.org/10.1056/NEJM198505303122203.

Carrion, Maria Perez, Francesca Pischedda, Alice Biosa, Isabella Russo, Letizia Straniero, Laura Civiero, Marianna Guida, et al. 2018. 'The LRRK2 Variant E193K Prevents Mitochondrial Fission Upon MPP+ Treatment by Altering LRRK2 Binding to DRP1'. *Frontiers in Molecular Neuroscience* 11 (February):64. https://doi.org/10.3389/fnmol.2018.00064.

Chiba, K., L. A. Peterson, K. P. Castagnoli, A. J. Trevor, and N. Castagnoli. 1985. 'Studies on the Molecular Mechanism of Bioactivation of the Selective Nigrostriatal Toxin 1-Methyl-4-Phenyl-1,2,3,6-Tetrahydropyridine'. *Drug Metabolism and Disposition: The Biological Fate of Chemicals* 13 (3): 342–47.

Childress, Elizabeth S., Stephanie J. Alexopoulos, Kyle L. Hoehn, and Webster L. Santos. 2018. 'Small Molecule Mitochondrial Uncouplers and Their Therapeutic Potential'. *Journal of Medicinal Chemistry* 61 (11): 4641–55. https://doi.org/10.1021/acs.jmedchem.7b01182.

Cisneros, Jasmine, Tayler B. Belton, George C. Shum, Catherine G. Molakal, and Yvette C. Wong. 2022. 'Mitochondria-Lysosome Contact Site Dynamics and Misregulation in Neurodegenerative Diseases'. *Trends in Neurosciences* 45 (4): 312. https://doi.org/10.1016/j.tins.2022.01.005.

Clark, Emily H., Aurelio Vázquez de la Torre, Tamaki Hoshikawa, and Thomas Briston. 2021. 'Targeting Mitophagy in Parkinson's Disease'. *Journal of Biological Chemistry* 296 (January). https://doi.org/10.1074/jbc.REV120.014294.

Cogliati, Sara, Jose A. Enriquez, and Luca Scorrano. 2016a. 'Mitochondrial Cristae: Where Beauty Meets Functionality'. *Trends in Biochemical Sciences* 41 (3): 261–73. https://doi.org/10.1016/j.tibs.2016.01.001.

———. 2016b. 'Mitochondrial Cristae: Where Beauty Meets Functionality'. *Trends in Biochemical Sciences* 41 (3): 261–73. https://doi.org/10.1016/j.tibs.2016.01.001.

Conte, Federica, Nicole van Buuringen, Nicol C. Voermans, and Dirk J. Lefeber. 2021. 'Galactose in Human Metabolism, Glycosylation and Congenital Metabolic Diseases: Time for a Closer Look'. *Biochimica et Biophysica Acta (BBA) - General Subjects* 1865 (8): 129898. https://doi.org/10.1016/j.bbagen.2021.129898.

Dalfó, E., T. Gómez-Isla, J. L. Rosa, M. Nieto Bodelón, M. Cuadrado Tejedor, M. Barrachina, S. Ambrosio, and I. Ferrer. 2004. 'Abnormal Alpha-Synuclein Interactions with Rab Proteins in Alpha-Synuclein A30P Transgenic Mice'. *Journal of Neuropathology and Experimental Neurology* 63 (4): 302–13. https://doi.org/10.1093/jnen/63.4.302.

Deus, Cláudia M., Susana P. Pereira, Teresa Cunha-Oliveira, Francisco B. Pereira, Nuno Raimundo, and Paulo J. Oliveira. 2020a. 'Mitochondrial Remodeling in Human Skin Fibroblasts from Sporadic Male Parkinson's Disease Patients Uncovers Metabolic and

Mitochondrial Bioenergetic Defects'. *Biochimica et Biophysica Acta (BBA) - Molecular Basis of Disease* 1866 (3): 165615. https://doi.org/10.1016/j.bbadis.2019.165615.

———. 2020b. 'Mitochondrial Remodeling in Human Skin Fibroblasts from Sporadic Male Parkinson's Disease Patients Uncovers Metabolic and Mitochondrial Bioenergetic Defects'. *Biochimica et Biophysica Acta (BBA) - Molecular Basis of Disease* 1866 (3): 165615. https://doi.org/10.1016/j.bbadis.2019.165615.

Dott, William, Pratibha Mistry, Jayne Wright, Kelvin Cain, and Karl E Herbert. 2014. 'Modulation of Mitochondrial Bioenergetics in a Skeletal Muscle Cell Line Model of Mitochondrial Toxicity'. *Redox Biology* 2 (January):224–33. https://doi.org/10.1016/j.redox.2013.12.028.

Exner, Nicole, Bettina Treske, Dominik Paquet, Kira Holmström, Carola Schiesling, Suzana Gispert, Iria Carballo-Carbajal, et al. 2007. 'Loss-of-Function of Human PINK1 Results in Mitochondrial Pathology and Can Be Rescued by Parkin'. *The Journal of Neuroscience* 27 (45): 12413. https://doi.org/10.1523/JNEUROSCI.0719-07.2007.

Flønes, Irene H., Lilah Toker, Dagny Ann Sandnes, Martina Castelli, Sepideh Mostafavi, Njål Lura, Omnia Shadad, et al. 2024. 'Mitochondrial Complex I Deficiency Stratifies Idiopathic Parkinson's Disease'. *Nature Communications* 15 (1): 3631. https://doi.org/10.1038/s41467-024-47867-4.

Fos-Codoner, Ferran S., Lianne M. S. Bouwman, Jaap Keijer, and Evert M. van Schothorst. 2023. 'Dietary Galactose Increases the Expression of Mitochondrial OXPHOS Genes and Modulates the Carbohydrate Oxidation Pathways in Mouse Intestinal Mucosa'. *The Journal of Nutrition* 153 (12): 3448–57. https://doi.org/10.1016/j.tjnut.2023.10.011.

Frey, Terrence G., and Carmen A. Mannella. 2000. 'The Internal Structure of Mitochondria'. *Trends in Biochemical Sciences* 25 (7): 319–24. https://doi.org/10.1016/S0968-0004(00)01609-1.

Gautier, Clément A., Zoi Erpapazoglou, François Mouton-Liger, Marie Paule Muriel, Florence Cormier, Stéphanie Bigou, Sophie Duffaure, et al. 2016. 'The Endoplasmic Reticulum-Mitochondria Interface Is Perturbed in PARK2 Knockout Mice and Patients with PARK2 Mutations'. *Human Molecular Genetics* 25 (14): 2972–84. https://doi.org/10.1093/hmg/ddw148.

Giannandrea, Maila, Veronica Bianchi, Maria Lidia Mignogna, Alessandra Sirri, Salvatore Carrabino, Errico D'Elia, Matteo Vecellio, et al. 2010. 'Mutations in the Small GTPase Gene RAB39B Are Responsible for X-Linked Mental Retardation Associated with Autism, Epilepsy, and Macrocephaly'. *American Journal of Human Genetics* 86 (2): 185–95. https://doi.org/10.1016/j.ajhg.2010.01.011.

Glauser, Liliane, Sarah Sonnay, Klodjan Stafa, and Darren J. Moore. 2011. 'Parkin Promotes the Ubiquitination and Degradation of the Mitochondrial Fusion Factor Mitofusin 1'. *Journal of Neurochemistry* 118 (4): 636–45. https://doi.org/10.1111/j.1471-4159.2011.07318.x.

Gomes, Ligia C., Giulietta Di Benedetto, and Luca Scorrano. 2011. 'During Autophagy Mitochondria Elongate, Are Spared from Degradation and Sustain Cell Viability'. *Nature Cell Biology* 13 (5): 589–98. https://doi.org/10.1038/ncb2220.

Gómez-Suaga, Patricia, José M. Bravo-San Pedro, Rosa A. González-Polo, José M. Fuentes, and Mireia Niso-Santano. 2018. 'ER–Mitochondria Signaling in Parkinson's Disease'. *Cell Death & Disease* 9 (3): 1–12. https://doi.org/10.1038/s41419-017-0079-3.

González-Casacuberta, Ingrid, Diana-Luz Juárez-Flores, Mario Ezquerra, Raquel Fucho, Marc Catalán-García, Mariona Guitart-Mampel, Ester Tobías, et al. 2019. 'Mitochondrial and Autophagic Alterations in Skin Fibroblasts from Parkinson Disease Patients with Parkin Mutations'. *Aging (Albany NY)* 11 (11): 3750–67. https://doi.org/10.18632/aging.102014.

González-Rodríguez, Patricia, Enrico Zampese, Kristen A. Stout, Jaime N. Guzman, Ema Ilijic, Ben Yang, Tatiana Tkatch, et al. 2021. 'Disruption of Mitochondrial Complex I Induces Progressive Parkinsonism'. *Nature* 599 (7886): 650–56. https://doi.org/10.1038/s41586-021-04059-0.

Grünewald, Anne, Lisa Voges, Aleksandar Rakovic, Meike Kasten, Himesha Vandebona, Claudia Hemmelmann, Katja Lohmann, et al. 2010. 'Mutant Parkin Impairs Mitochondrial Function and Morphology in Human Fibroblasts'. *PLOS ONE* 5 (9): e12962. https://doi.org/10.1371/journal.pone.0012962.

Guillot, Thomas S., and Gary W. Miller. 2009. 'Protective Actions of the Vesicular Monoamine Transporter 2 (VMAT2) in Monoaminergic Neurons'. *Molecular Neurobiology* 39 (2): 149–70. https://doi.org/10.1007/s12035-009-8059-y.

Hammerling, Babette C., Sarah E. Shires, Leonardo J. Leon, Melissa Q. Cortez, and Åsa B. Gustafsson. 2020. 'Isolation of Rab5-Positive Endosomes Reveals a New Mitochondrial Degradation Pathway Utilized by BNIP3 and Parkin'. *Small GTPases* 11 (1): 69–76. https://doi.org/10.1080/21541248.2017.1342749.

Hattori, N., T. Kitada, H. Matsumine, S. Asakawa, Y. Yamamura, H. Yoshino, T. Kobayashi, et al. 1998. 'Molecular Genetic Analysis of a Novel Parkin Gene in Japanese Families with Autosomal Recessive Juvenile Parkinsonism: Evidence for Variable Homozygous Deletions in the Parkin Gene in Affected Individuals'. *Annals of Neurology* 44 (6): 935–41. https://doi.org/10.1002/ana.410440612.

Heikkila, Richard E., Arthur Hess, and Roger C. Duvoisin. 1984. 'Dopaminergic Neurotoxicity of 1-Methyl-4-Phenyl-1,2,5,6-Tetrahydropyridine in Mice'. *Science* 224 (4656): 1451–53. https://doi.org/10.1126/science.6610213.

Heikkila, Richard E., William J. Nicklas, Ivy Vyas, and Roger C. Duvoisin. 1985. 'Dopaminergic Toxicity of Rotenone and the 1-Methyl-4-Phenylpyridinium Ion after Their Stereotaxic Administration to Rats: Implication for the Mechanism of 1-Methyl-4-Phenyl-1,2,3,6-Tetrahydropyridine Toxicity'. *Neuroscience Letters* 62 (3): 389–94. https://doi.org/10.1016/0304-3940(85)90580-4.

Hell, Kai. 2008. 'The Erv1–Mia40 Disulfide Relay System in the Intermembrane Space of Mitochondria'. *Biochimica et Biophysica Acta (BBA) - Molecular Cell Research*, Redox regulation of protein folding, 1783 (4): 601–9. https://doi.org/10.1016/j.bbamcr.2007.12.005.

Hernansanz-Agustín, Pablo, and José Antonio Enríquez. 2021. 'Generation of Reactive Oxygen Species by Mitochondria'. *Antioxidants* 10 (3). https://doi.org/10.3390/antiox10030415.

Hertig, Damian, Andrea Felser, Gaëlle Diserens, Sandra Kurth, Peter Vermathen, and Jean-Marc Nuoffer. 2019. 'Selective Galactose Culture Condition Reveals Distinct Metabolic Signatures in Pyruvate Dehydrogenase and Complex I Deficient Human Skin Fibroblasts'. *Metabolomics: Official Journal of the Metabolomic Society* 15 (3): 32. https://doi.org/10.1007/s11306-019-1497-2.

Heytler, P. G., and W. W. Prichard. 1962. 'A New Class of Uncoupling Agents — Carbonyl Cyanide Phenylhydrazones'. *Biochemical and Biophysical Research Communications* 7 (4): 272–75. https://doi.org/10.1016/0006-291X(62)90189-4.

Hirata, Yoko, and Toshiharu Nagatsu. 2005. 'Rotenone and CCCP Inhibit Tyrosine Hydroxylation in Rat Striatal Tissue Slices'. *Toxicology* 216 (1): 9–14. https://doi.org/10.1016/j.tox.2005.07.010.

Hoffmann, Lavynia Ferreira, Alexandre Martins, Fernanda Majolo, Verônica Contini, Stefan Laufer, and Márcia Inês Goettert. 2022. 'Neural Regeneration Research Model to Be Explored: SH-SY5Y Human Neuroblastoma Cells'. *Neural Regeneration Research* 18 (6): 1265. https://doi.org/10.4103/1673-5374.358621.

Homma, Yuta, Shu Hiragi, and Mitsunori Fukuda. 2020. 'Rab Family of Small GTPases: An Updated View on Their Regulation and Functions'. *The Febs Journal* 288 (1): 36. https://doi.org/10.1111/febs.15453.

Homolak, Jan, Ana Babic Perhoc, Davor Virag, Ana Knezovic, Jelena Osmanovic Barilar, and Melita Salkovic-Petrisic. 2024. 'D-Galactose Might Mediate Some of the Skeletal Muscle Hypertrophy-Promoting Effects of Milk-A Nutrient to Consider for Sarcopenia?'

BioEssays: News and Reviews in Molecular, Cellular and Developmental Biology 46 (2): e2300061. https://doi.org/10.1002/bies.202300061.

Hsu, FoSheng, Stephanie Spannl, Charles Ferguson, Anthony A. Hyman, Robert G. Parton, and Marino Zerial. 2018. 'Rab5 and Alsin Regulate Stress-Activated Cytoprotective Signaling on Mitochondria'. eLife. eLife Sciences Publications Limited. 22 February 2018. https://doi.org/10.7554/eLife.32282.

Karbowski, Mariusz, Yumiko Oshima, and Nicolas Verhoeven. 2022. 'Mitochondrial Proteotoxicity: Implications and Ubiquitin-Dependent Quality Control Mechanisms'. *Cellular and Molecular Life Sciences* 79 (11): 574. https://doi.org/10.1007/s00018-022-04604-8.

Karpowicz, Richard J., Matthew Dunn, David Sulzer, and Dalibor Sames. 2013. 'APP+, a Fluorescent Analogue of the Neurotoxin MPP+, Is a Marker of Catecholamine Neurons in Brain Tissue, but Not a Fluorescent False Neurotransmitter'. *ACS Chemical Neuroscience* 4 (5): 858–69. https://doi.org/10.1021/cn400038u.

Keenan, Stacey N., Matthew J. Watt, and Magdalene K. Montgomery. 2020. 'Inter-Organelle Communication in the Pathogenesis of Mitochondrial Dysfunction and Insulin Resistance'. *Current Diabetes Reports* 20 (6): 20. https://doi.org/10.1007/s11892-020-01300-4.

Kitada, Tohru, Shuichi Asakawa, Nobutaka Hattori, Hiroto Matsumine, Yasuhiro Yamamura, Shinsei Minoshima, Masayuki Yokochi, Yoshikuni Mizuno, and Nobuyoshi Shimizu. 1998. 'Mutations in the Parkin Gene Cause Autosomal Recessive Juvenile Parkinsonism'. *Nature* 392 (6676): 605–8. https://doi.org/10.1038/33416.

König, Tim, and Heidi M. McBride. 2024. 'Mitochondrial-Derived Vesicles in Metabolism, Disease, and Aging'. *Cell Metabolism* 36 (1): 21–35. https://doi.org/10.1016/j.cmet.2023.11.014.

Koss, David J., Susanna Campesan, Flaviano Giorgini, and Tiago F. Outeiro. 2021. 'Dysfunction of RAB39B-Mediated Vesicular Trafficking in Lewy Body Diseases'. *Movement Disorders* 36 (8): 1744–58. https://doi.org/10.1002/mds.28605.

Kowalczyk, Paweł, Dorota Sulejczak, Patrycja Kleczkowska, Iwona Bukowska-Ośko, Marzena Kucia, Marta Popiel, Ewa Wietrak, Karol Kramkowski, Karol Wrzosek, and Katarzyna Kaczyńska. 2021. 'Mitochondrial Oxidative Stress—A Causative Factor and Therapeutic Target in Many Diseases'. *International Journal of Molecular Sciences* 22 (24). https://doi.org/10.3390/ijms222413384.

Koyano, Fumika, and Noriyuki Matsuda. 2015. 'Molecular Mechanisms Underlying PINK1 and Parkin Catalyzed Ubiquitylation of Substrates on Damaged Mitochondria'. *Biochimica et Biophysica Acta (BBA) - Molecular Cell Research*, Mitophagy, 1853 (10, Part B): 2791–96. https://doi.org/10.1016/j.bbamcr.2015.02.009.

Langston, J. W., P. Ballard, J. W. Tetrud, and I. Irwin. 1983. 'Chronic Parkinsonism in Humans Due to a Product of Meperidine-Analog Synthesis'. *Science (New York, N.Y.)* 219 (4587): 979–80. https://doi.org/10.1126/science.6823561.

Langston, J. William. 2017. 'The MPTP Story'. *Journal of Parkinson's Disease* 7 (s1): S11–19. https://doi.org/10.3233/JPD-179006.

Langston, J. William, Philip Ballard, James W. Tetrud, and Ian Irwin. 1983. 'Chronic Parkinsonism in Humans Due to a Product of Meperidine-Analog Synthesis'. *Science* 219 (4587): 979–80. https://doi.org/10.1126/science.6823561.

Li, Jeng-Lin, Tai-Yi Lin, Po-Lin Chen, Ting-Ni Guo, Shu-Yi Huang, Chun-Hong Chen, Chin-Hsien Lin, and Chih-Chiang Chan. 2021. 'Mitochondrial Function and Parkinson's Disease: From the Perspective of the Electron Transport Chain'. *Frontiers in Molecular Neuroscience* 14 (December):797833. https://doi.org/10.3389/fnmol.2021.797833.

Li, Mengqi, Yu Wang, Xiaoyan Wei, Wei-Feng Cai, Jianfeng Wu, Mingxia Zhu, Yongliang Wang, et al. 2024. 'AMPK Targets PDZD8 to Trigger Carbon Source Shift from Glucose to Glutamine'. *Cell Research*, June, 1–24. https://doi.org/10.1038/s41422-024-00985-6.

Liu, Raymond, and David C. Chan. 2017. 'OPA1 and Cardiolipin Team up for Mitochondrial Fusion'. *Nature Cell Biology* 19 (7): 760–62. https://doi.org/10.1038/ncb3565.

Ma, Hao-Jie, Cong Gai, Yuan Chai, Wan-Di Feng, Cui-Cui Cheng, Jin-Kun Zhang, Yu-Xin Zhang, et al. 2020. 'Bu-Yin-Qian-Zheng Formula Ameliorates MPP+-Induced Mitochondrial Dysfunction in Parkinson's Disease via Parkin'. *Frontiers in Pharmacology* 11 (December):577017. https://doi.org/10.3389/fphar.2020.577017.

Ma, Kaili, Guo Chen, Wenhui Li, Oliver Kepp, Yushan Zhu, and Quan Chen. 2020. 'Mitophagy, Mitochondrial Homeostasis, and Cell Fate'. *Frontiers in Cell and Developmental Biology* 8 (June):467. https://doi.org/10.3389/fcell.2020.00467.

Marcinko, Katarina, and Gregory R. Steinberg. 2014. 'The Role of AMPK in Controlling Metabolism and Mitochondrial Biogenesis during Exercise'. *Experimental Physiology* 99 (12): 1581–85. https://doi.org/10.1113/expphysiol.2014.082255.

Marella, Mathieu, Byoung Boo Seo, Takao Yagi, and Akemi Matsuno-Yagi. 2009. 'Parkinson's Disease and Mitochondrial Complex I: A Perspective on the Ndi1 Therapy'. *Journal of Bioenergetics and Biomembranes* 41 (6): 493–97. https://doi.org/10.1007/s10863-009-9249-z.

Matheoud, Diana, Ayumu Sugiura, Angélique Bellemare-Pelletier, Annie Laplante, Christiane Rondeau, Magali Chemali, Ali Fazel, et al. 2016. 'Parkinson's Disease-Related Proteins PINK1 and Parkin Repress Mitochondrial Antigen Presentation'. *Cell* 166 (2): 314–27. https://doi.org/10.1016/j.cell.2016.05.039.

Matsumine, H., M. Saito, S. Shimoda-Matsubayashi, H. Tanaka, A. Ishikawa, Y. Nakagawa-Hattori, M. Yokochi, et al. 1997. 'Localization of a Gene for an Autosomal Recessive Form of Juvenile Parkinsonism to Chromosome 6q25.2-27.' *American Journal of Human Genetics* 60 (3): 588.

Moon, Eun-Yi. 2008. 'Serum Deprivation Enhances Apoptotic Cell Death by Increasing Mitochondrial Enzyme Activity'. *Biomolecules & Therapeutics* 16 (1): 1–8. https://doi.org/10.4062/biomolther.2008.16.1.001.

Napolitano, Gaetana, Gianluca Fasciolo, and Paola Venditti. 2021. 'Mitochondrial Management of Reactive Oxygen Species'. *Antioxidants* 10 (11): 1824. https://doi.org/10.3390/antiox10111824.

Neuspiel, Margaret, Astrid C. Schauss, Emelie Braschi, Rodolfo Zunino, Peter Rippstein, Richard A. Rachubinski, Miguel A. Andrade-Navarro, and Heidi M. McBride. 2008. 'Cargo-Selected Transport from the Mitochondria to Peroxisomes Is Mediated by Vesicular Carriers'. *Current Biology* 18 (2): 102–8. https://doi.org/10.1016/j.cub.2007.12.038.

Niu, Mengxi, Naizhen Zheng, Zijie Wang, Yue Gao, Xianghua Luo, Zhicai Chen, Xing Fu, et al. 2020. 'RAB39B Deficiency Impairs Learning and Memory Partially Through Compromising Autophagy'. *Frontiers in Cell and Developmental Biology* 8:598622. https://doi.org/10.3389/fcell.2020.598622.

Okatsu, Kei, Toshihiko Oka, Masahiro Iguchi, Kenji Imamura, Hidetaka Kosako, Naoki Tani, Mayumi Kimura, et al. 2012. 'PINK1 Autophosphorylation upon Membrane Potential Dissipation Is Essential for Parkin Recruitment to Damaged Mitochondria'. *Nature Communications* 3 (1): 1016. https://doi.org/10.1038/ncomms2016.

Olesen, Margrethe A., Francisca Villavicencio-Tejo, and Rodrigo A. Quintanilla. 2022. 'The Use of Fibroblasts as a Valuable Strategy for Studying Mitochondrial Impairment in Neurological Disorders'. *Translational Neurodegeneration* 11 (1): 36. https://doi.org/10.1186/s40035-022-00308-y.

Orlicka-Płocka, Marta, Dorota Gurda-Wozna, Agnieszka Fedoruk-Wyszomirska, and Eliza Wyszko. 2020. 'Circumventing the Crabtree Effect: Forcing Oxidative Phosphorylation

(OXPHOS) via Galactose Medium Increases Sensitivity of HepG2 Cells to the Purine Derivative Kinetin Riboside'. *Apoptosis* 25 (11): 835–52. https://doi.org/10.1007/s10495-020-01637-x.

Pacelli, Consiglia, Domenico De Rasmo, Anna Signorile, Ignazio Grattagliano, Giuseppe di Tullio, Andria D'Orazio, Beatrice Nico, et al. 2011. 'Mitochondrial Defect and PGC-1α Dysfunction in *Parkin*-Associated Familial Parkinson's Disease'. *Biochimica et Biophysica Acta (BBA) - Molecular Basis of Disease*, Translating nuclear receptors from health to disease, 1812 (8): 1041–53. https://doi.org/10.1016/j.bbadis.2010.12.022.

Palikaras, Konstantinos, Eirini Lionaki, and Nektarios Tavernarakis. 2018. 'Mechanisms of Mitophagy in Cellular Homeostasis, Physiology and Pathology'. *Nature Cell Biology* 20 (9): 1013–22. https://doi.org/10.1038/s41556-018-0176-2.

Payne, Thomas, Toby Burgess, Stephen Bradley, Sarah Roscoe, Matilde Sassani, Mark J Dunning, Dena Hernandez, et al. 2024. 'Multimodal Assessment of Mitochondrial Function in Parkinson's Disease'. *Brain* 147 (1): 267–80. https://doi.org/10.1093/brain/awad364.

Peng, Wesley, Leonie F. Schröder, Pingping Song, Yvette C. Wong, and Dimitri Krainc. 2023. 'Parkin Regulates Amino Acid Homeostasis at Mitochondria-Lysosome (M/L) Contact Sites in Parkinson's Disease'. *Science Advances* 9 (29): eadh3347. https://doi.org/10.1126/sciadv.adh3347.

Picca, Anna, and Angela Maria Serena Lezza. 2015. 'Regulation of Mitochondrial Biogenesis through TFAM–Mitochondrial DNA Interactions: Useful Insights from Aging and Calorie Restriction Studies'. *Mitochondrion* 25 (November):67–75. https://doi.org/10.1016/j.mito.2015.10.001.

Pinho, Sónia A., Cláudio F. Costa, Cláudia M. Deus, Sonia L. C. Pinho, Inês Miranda-Santos, Gonçalo Afonso, Olivia Bagshaw, Jeffrey A. Stuart, Paulo J. Oliveira, and Teresa Cunha-Oliveira. 2022. 'Mitochondrial and Metabolic Remodelling in Human Skin Fibroblasts in Response to Glucose Availability'. *The FEBS Journal* 289 (17): 5198–5217. https://doi.org/10.1111/febs.16413.

Poewe, Werner, Klaus Seppi, Caroline M. Tanner, Glenda M. Halliday, Patrik Brundin, Jens Volkmann, Anette-Eleonore Schrag, and Anthony E. Lang. 2017. 'Parkinson Disease'. *Nature Reviews Disease Primers* 3 (1): 1–21. https://doi.org/10.1038/nrdp.2017.13.

Protasoni, Margherita, and Jan-Willem Taanman. 2023. 'Remodelling of the Mitochondrial Bioenergetic Pathways in Human Cultured Fibroblasts with Carbohydrates'. *Biology* 12 (7): 1002. https://doi.org/10.3390/biology12071002.

Przedborski, Serge, Kim Tieu, Celine Perier, and Miquel Vila. 2004. 'MPTP as a Mitochondrial Neurotoxic Model of Parkinson's Disease'. *Journal of Bioenergetics and Biomembranes* 36 (4): 375–79. https://doi.org/10.1023/B:JOBB.0000041771.66775.d5.

Purlyte, Elena, Herschel S Dhekne, Adil R Sarhan, Rachel Gomez, Pawel Lis, Melanie Wightman, Terina N Martinez, Francesca Tonelli, Suzanne R Pfeffer, and Dario R Alessi. 2018. 'Rab29 Activation of the Parkinson's Disease-associated LRRK2 Kinase'. *The EMBO Journal* 37 (1): 1–18. https://doi.org/10.15252/embj.201798099.

Raimi, Olawale G., Hina Ojha, Kenneth Ehses, Verena Dederer, Sven M. Lange, Cristian Polo Rivera, Tom D. Deegan, et al. 2024. 'Mechanism of Human PINK1 Activation at the TOM Complex in a Reconstituted System'. *Science Advances* 10 (23): eadn7191. https://doi.org/10.1126/sciadv.adn7191.

Rakshe, Pratik Shankar, Bhaskar Jyoti Dutta, Shivani Chib, Niyogita Maurya, and Sanjiv Singh. 2024. 'Unveiling the Interplay of AMPK/SIRT1/PGC-1α Axis in Brain Health: Promising Targets against Aging and NDDs'. *Ageing Research Reviews* 96 (April):102255. https://doi.org/10.1016/j.arr.2024.102255.

Rambold, Angelika S., Brenda Kostelecky, Natalie Elia, and Jennifer Lippincott-Schwartz. 2011. 'Tubular Network Formation Protects Mitochondria from Autophagosomal Degradation

during Nutrient Starvation'. *Proceedings of the National Academy of Sciences* 108 (25): 10190–95. https://doi.org/10.1073/pnas.1107402108.

Ramonet, D., C. Perier, A. Recasens, B. Dehay, J. Bové, V. Costa, L. Scorrano, and M. Vila. 2012. 'Optic Atrophy 1 Mediates Mitochondria Remodeling and Dopaminergic Neurodegeneration Linked to Complex I Deficiency'. *Cell Death and Differentiation* 20 (1): 77. https://doi.org/10.1038/cdd.2012.95.

Ramsay, Rona R., James I. Salach, Jahan Dadgar, and Thomas P. Singer. 1986. 'Inhibition of Mitochondrial NADH Dehydrogenase by Pyridine Derivatives and Its Possible Relation to Experimental and Idiopathic Parkinsonism'. *Biochemical and Biophysical Research Communications* 135 (1): 269–75. https://doi.org/10.1016/0006-291X(86)90972-1.

Rappold, Phillip M., Mei Cui, Adrianne S. Chesser, Jacqueline Tibbett, Jonathan C. Grima, Lihua Duan, Namita Sen, Jonathan A. Javitch, and Kim Tieu. 2011. 'Paraquat Neurotoxicity Is Mediated by the Dopamine Transporter and Organic Cation Transporter-3'. *Proceedings of the National Academy of Sciences of the United States of America* 108 (51): 20766–71. https://doi.org/10.1073/pnas.1115141108.

Reitzer, L. J., B. M. Wice, and D. Kennell. 1979. 'Evidence That Glutamine, Not Sugar, Is the Major Energy Source for Cultured HeLa Cells.' *Journal of Biological Chemistry* 254 (8): 2669–76. https://doi.org/10.1016/S0021-9258(17)30124-2.

Reyes-Galindo, Meztli, Roselia Suarez, Mercedes Esparza-Perusquía, Jaime de Lira-Sánchez, J. Pablo Pardo, Federico Martínez, and Oscar Flores-Herrera. 2019. 'Mitochondrial Respirasome Works as a Single Unit and the Cross-Talk between Complexes I, III2 and IV Stimulates NADH Dehydrogenase Activity'. *Biochimica Et Biophysica Acta. Bioenergetics* 1860 (8): 618–27. https://doi.org/10.1016/j.bbabio.2019.06.017.

Risiglione, Pierpaolo, Loredana Leggio, Salvatore A. M. Cubisino, Simona Reina, Greta Paternò, Bianca Marchetti, Andrea Magrì, Nunzio Iraci, and Angela Messina. 2020. 'High-Resolution Respirometry Reveals MPP+ Mitochondrial Toxicity Mechanism in a Cellular Model of Parkinson's Disease'. *International Journal of Molecular Sciences* 21 (21): 7809. https://doi.org/10.3390/ijms21217809.

Rossetti, M. Florencia, Cora Stoker, and Jorge G. Ramos. 2020. 'Agrochemicals and Neurogenesis'. *Molecular and Cellular Endocrinology* 510 (June):110820. https://doi.org/10.1016/j.mce.2020.110820.

Rossignol, Rodrigue, Robert Gilkerson, Robert Aggeler, Kunihiro Yamagata, S. James Remington, and Roderick A. Capaldi. 2004. 'Energy Substrate Modulates Mitochondrial Structure and Oxidative Capacity in Cancer Cells'. *Cancer Research* 64 (3): 985–93. https://doi.org/10.1158/0008-5472.CAN-03-1101.

Saito, Toshiro, Jihoon Nah, Shin-ichi Oka, Risa Mukai, Yoshiya Monden, Yasuhiro Maejima, Yoshiyuki Ikeda, et al. 2019. 'An Alternative Mitophagy Pathway Mediated by Rab9 Protects the Heart against Ischemia'. *The Journal of Clinical Investigation* 129 (2): 802–19. https://doi.org/10.1172/JCI122035.

Samangouei, Parisa, Gustavo E. Crespo-Avilan, Hector Cabrera-Fuentes, Sauri Hernández-Reséndiz, Nur Izzah Ismail, Khairunnisa Binte Katwadi, William A. Boisvert, and Derek J. Hausenloy. 2018. 'MiD49 and MiD51: New Mediators of Mitochondrial Fission and Novel Targets for Cardioprotection'. *Conditioning Medicine* 1 (5): 239–46.

Schapira, A. H. V., J. M. Cooper, D. Dexter, P. Jenner, J. B. Clark, and C. D. Marsden. 1989. 'MITOCHONDRIAL COMPLEX I DEFICIENCY IN PARKINSON'S DISEASE'. *The Lancet* 333 (8649): 1269. https://doi.org/10.1016/S0140-6736(89)92366-0.

Schapira, Anthony HV. 2004. 'Disease Modification in Parkinson's Disease'. *The Lancet Neurology* 3 (6): 362–68. https://doi.org/10.1016/S1474-4422(04)00769-0.

Schildknecht, Stefan, Regina Pape, Johannes Meiser, Christiaan Karreman, Tobias Strittmatter, Meike Odermatt, Erica Cirri, et al. 2015. 'Preferential Extracellular Generation of the Active Parkinsonian Toxin MPP+ by Transporter-Independent Export of the Intermediate

MPDP+'. *Antioxidants & Redox Signaling* 23 (13): 1001–16. https://doi.org/10.1089/ars.2015.6297.

Seirafi, Marjan, Guennadi Kozlov, and Kalle Gehring. 2015. 'Parkin Structure and Function'. *The Febs Journal* 282 (11): 2076–88. https://doi.org/10.1111/febs.13249.

Shafique, Adeena, Martina Brughera, Marta Lualdi, and Tiziana Alberio. 2023. 'The Role of Rab Proteins in Mitophagy: Insights into Neurodegenerative Diseases'. *International Journal of Molecular Sciences* 24 (7): 6268. https://doi.org/10.3390/ijms24076268.

Shimura, H., N. Hattori, S. i Kubo, Y. Mizuno, S. Asakawa, S. Minoshima, N. Shimizu, et al. 2000. 'Familial Parkinson Disease Gene Product, Parkin, Is a Ubiquitin-Protein Ligase'. *Nature Genetics* 25 (3): 302–5. https://doi.org/10.1038/77060.

Singh, Pawan Kishor, and Miratul M. K. Muqit. 2020. 'Parkinson's: A Disease of Aberrant Vesicle Trafficking'. *Annual Review of Cell and Developmental Biology* 36 (Volume 36, 2020): 237–64. https://doi.org/10.1146/annurev-cellbio-100818-125512.

Son, Geurim, and Jinju Han. 2018. 'Roles of Mitochondria in Neuronal Development'. *BMB Reports* 51 (11): 549. https://doi.org/10.5483/BMBRep.2018.51.11.226.

Soubannier, Vincent, Gian-Luca McLelland, Rodolfo Zunino, Emelie Braschi, Peter Rippstein, Edward A. Fon, and Heidi M. McBride. 2012. 'A Vesicular Transport Pathway Shuttles Cargo from Mitochondria to Lysosomes'. *Current Biology* 22 (2): 135–41. https://doi.org/10.1016/j.cub.2011.11.057.

Stenmark, Harald. 2009. 'Rab GTPases as Coordinators of Vesicle Traffic'. *Nature Reviews Molecular Cell Biology* 10 (8): 513–25. https://doi.org/10.1038/nrm2728.

Subrahmanian, Nitya, and Matthew J. LaVoie. 2021a. 'Is There a Special Relationship between Complex I Activity and Nigral Neuronal Loss in Parkinson's Disease? A Critical Reappraisal'. *Brain Research* 1767 (September):147434. https://doi.org/10.1016/j.brainres.2021.147434.

———. 2021b. 'Is There a Special Relationship between Complex I Activity and Nigral Neuronal Loss in Parkinson's Disease? A Critical Reappraisal'. *Brain Research* 1767 (September):147434. https://doi.org/10.1016/j.brainres.2021.147434.

Sung, Jee Young, Jongsun Kim, Seung R. Paik, Jeon Han Park, Young Soo Ahn, and Kwang Chul Chung. 2001. 'Induction of Neuronal Cell Death by Rab5A-Dependent Endocytosis of α-Synuclein*'. *Journal of Biological Chemistry* 276 (29): 27441–48. https://doi.org/10.1074/jbc.M101318200.

Tokuyama, Takeshi, and Shigeru Yanagi. 2023. 'Role of Mitochondrial Dynamics in Heart Diseases'. *Genes* 14 (10): 1876. https://doi.org/10.3390/genes14101876.

Valente, Andrew J., Lucas A. Maddalena, Ellen L. Robb, Fereshteh Moradi, and Jeffrey A. Stuart. 2017. 'A Simple ImageJ Macro Tool for Analyzing Mitochondrial Network Morphology in Mammalian Cell Culture'. *Acta Histochemica* 119 (3): 315–26. https://doi.org/10.1016/j.acthis.2017.03.001.

Valente, E. M., F. Brancati, V. Caputo, E. A. Graham, M. B. Davis, A. Ferraris, M. M. B. Breteler, et al. 2002. 'PARK6 Is a Common Cause of Familial Parkinsonism'. *Neurological Sciences: Official Journal of the Italian Neurological Society and of the Italian Society of Clinical Neurophysiology* 23 Suppl 2 (September):S117-118. https://doi.org/10.1007/s100720200097.

Varughese, Joyce T., Susan K. Buchanan, and Ashley S. Pitt. 2021. 'The Role of Voltage-Dependent Anion Channel in Mitochondrial Dysfunction and Human Disease'. *Cells* 10 (7): 1737. https://doi.org/10.3390/cells10071737.

Vercellino, Irene, and Leonid A. Sazanov. 2022. 'The Assembly, Regulation and Function of the Mitochondrial Respiratory Chain'. *Nature Reviews Molecular Cell Biology* 23 (2): 141–61. https://doi.org/10.1038/s41580-021-00415-0.

Wang, Shouliang, Haijiao Long, Lianjie Hou, Baorong Feng, Zihong Ma, Ying Wu, Yu Zeng, Jiahao Cai, Da-wei Zhang, and Guojun Zhao. 2023. 'The Mitophagy Pathway and Its

Implications in Human Diseases'. *Signal Transduction and Targeted Therapy* 8 (1): 1–28. https://doi.org/10.1038/s41392-023-01503-7.

Watanabe, Yu, Toshiki Himeda, and Tsutomu Araki. 2005. 'Mechanisms of MPTP Toxicity and Their Implications for Therapy of Parkinson's Disease.' *Medical Science Monitor* 11 (1): RA17–23.

Wilson, Gabrielle R., Joe C. H. Sim, Catriona McLean, Maila Giannandrea, Charles A. Galea, Jessica R. Riseley, Sarah E. M. Stephenson, et al. 2014. 'Mutations in RAB39B Cause X-Linked Intellectual Disability and Early-Onset Parkinson Disease with α-Synuclein Pathology'. *American Journal of Human Genetics* 95 (6): 729–35. https://doi.org/10.1016/j.ajhg.2014.10.015.

Wong, Yvette C., Daniel Ysselstein, and Dimitri Krainc. 2018. 'Mitochondria-Lysosome Contacts Regulate Mitochondrial Fission via Rab7 GTP Hydrolysis'. *Nature* 554 (7692): 382. https://doi.org/10.1038/nature25486.

Wu, Kelvin Ka Lok, KeKao Long, Huige Lin, Parco Ming Fai Siu, Ruby Lai Chong Hoo, Dewei Ye, Aimin Xu, and Kenneth King Yip Cheng. 2021. 'The APPL1-Rab5 Axis Restricts NLRP3 Inflammasome Activation through Early Endosomal-Dependent Mitophagy in Macrophages'. *Nature Communications* 12 (1): 6637. https://doi.org/10.1038/s41467-021-26987-1.

Xicoy, Helena, Bé Wieringa, and Gerard J.M. Martens. 2017a. 'The SH-SY5Y Cell Line in Parkinson's Disease Research: A Systematic Review'. *Molecular Neurodegeneration* 12 (January):10. https://doi.org/10.1186/s13024-017-0149-0.

———. 2017b. 'The SH-SY5Y Cell Line in Parkinson's Disease Research: A Systematic Review'. *Molecular Neurodegeneration* 12 (1): 10. https://doi.org/10.1186/s13024-017-0149-0.

Yamano, Koji, Adam I. Fogel, Chunxin Wang, Alexander M. van der Bliek, and Richard J. Youle. 2014. 'Mitochondrial Rab GAPs Govern Autophagosome Biogenesis during Mitophagy'. *eLife* 3 (February):e01612. https://doi.org/10.7554/eLife.01612.

Yamano, Koji, Chunxin Wang, Shireen A Sarraf, Christian Münch, Reika Kikuchi, Nobuo N Noda, Yohei Hizukuri, et al. 2018. 'Endosomal Rab Cycles Regulate Parkin-Mediated Mitophagy'. Edited by Ivan Dikic. *eLife* 7 (January):e31326. https://doi.org/10.7554/eLife.31326.

Yang, Jin-Yi, and Wei Yuan Yang. 2013. 'Bit-by-Bit Autophagic Removal of Parkin-Labelled Mitochondria'. *Nature Communications* 4 (1): 2428. https://doi.org/10.1038/ncomms3428.

Youle, Richard J., and Derek P. Narendra. 2011. 'Mechanisms of Mitophagy'. *Nature Reviews Molecular Cell Biology* 12 (1): 9–14. https://doi.org/10.1038/nrm3028.

Zanellati, Maria C., Valentina Monti, Chiara Barzaghi, Chiara Reale, Nardo Nardocci, Alberto Albanese, Enza M. Valente, Daniele Ghezzi, and Barbara Garavaglia. 2015. 'Mitochondrial Dysfunction in Parkinson Disease: Evidence in Mutant PARK2 Fibroblasts'. *Frontiers in Genetics* 6:78. https://doi.org/10.3389/fgene.2015.00078.

Zhao, Qiang, Zhixue Liu, Ping Song, Zuyi Yuan, and Ming-Hui Zou. 2023. 'Mitochondria-Derived Vesicle Packaging as a Novel Therapeutic Mechanism in Pulmonary Hypertension'. *American Journal of Respiratory Cell and Molecular Biology* 70 (1): 39. https://doi.org/10.1165/rcmb.2023-0010OC.

Zilocchi, Mara, Ilaria Colugnat, Marta Lualdi, Monica Meduri, Federica Marini, Victor Corasolla Carregari, Mohamed Taha Moutaoufik, et al. 2020. 'Exploring the Impact of PARK2 Mutations on the Total and Mitochondrial Proteome of Human Skin Fibroblasts'. *Frontiers in Cell and Developmental Biology* 8 (June):423. https://doi.org/10.3389/fcell.2020.00423.

Zilocchi, Mara, Giovanna Finzi, Marta Lualdi, Fausto Sessa, Mauro Fasano, and Tiziana Alberio. 2018. 'Mitochondrial Alterations in Parkinson's Disease Human Samples and Cellular

Models'. *Neurochemistry International* 118 (September):61–72. https://doi.org/10.1016/j.neuint.2018.04.013.

Review papers

Shafique A, **Brughera M**, Lualdi M, Alberio T. The Role of Rab Proteins in Mitophagy: Insights into Neurodegenerative Diseases. Int J Mol Sci. 2023;24(7):6268. doi:10.3390/ijms24076268

Alberio T, **Brughera M**, Lualdi M. Current Insights on Neurodegeneration by the Italian Proteomics Community. Biomedicines. 2022;10(9):2297. doi:10.3390/biomedicines10092297